NOVEL TECHNOLOGIES FOR ALGAE BIOFUEL PRODUCTION

by

Yen-Hsun Tseng

A dissertation submitted to the faculty of
The University of Utah
in partial fulfillment of the requirements for the degree of

Doctor of Philosophy

Department of Chemical Engineering

The University of Utah

August 2016

The University of Utah Graduate School

STATEMENT OF DISSERTATION APPROVAL

The dissertation of **Yen-Hsun Tseng**

has been approved by the following supervisory committee members:

Swomitra K. Mohanty	, Chair	**05/04/2016** Date Approved
Leonard F. Pease lll	, Member	**05/04/2016** Date Approved
John D. McLennan	, Member	**05/04/2016** Date Approved
Anthony E. Butterfield	, Member	**05/04/2016** Date Approved
Kathryn A. Peterson	, Member	**05/04/2016** Date Approved

and by **Milind Deo** , Chair/Dean of

the Department/College/School of **Chemical Engineering**

and by David B. Kieda, Dean of The Graduate School.

ABSTRACT

The processes of making biodiesel from algae include the following essential steps: the growth of algae in a photobioreactor, lipid extraction to harvest the biocrude, and transesterification to turn biocrude into biodiesel. The objective of this research project is to improve these steps of biodiesel production. First, we developed a new highly scalable Periodic Symmetry Defined Bioreactor (PSDB). We evaluated its scalability by comparing the algae growth rate of three different sized PSDBs (i.e., 1-cell, 7-cell, and 19-cell), and an algae growth model was proposed and used to evaluate the optimal height of the PSDBs. The theoretical energy requirement for PSDBs were assessed and compared to that for the traditional raceway pond. Second, we proposed using a confined impinging jet mixer (CIJM) to implement a liquid-liquid extraction process given that lipid harvest remains one of the most challenge problems in algal fuel production. The CIJM combined algae biomass pretreatment and lipid extraction into one single step. The high turbulent mixing in CIJM broke up the algae cell walls, which released the lipid inside the algae cells into the aqueous phase and decreased the diffusion distance between the lipid and the organic solvent. The CIJM extracted the algae biocrude directly from the algae suspension with the yield of 25.6±2.7% (lipid biocrude/algae biomass). The multistaged extraction of CIJM was performed, and the total yield after four stages was 38.8±7.7% (lipid biocrude/algae biomass). Theoretical

models were proposed to estimate the yield of biocrude. Third, we blended biodiesel with waxy crude oil to decrease the wax appearance temperature (WAT). Biodiesel is a potential diluent for the waxy crude oil produced in the east Utah. The performance was verified by using the Fourier transform infrared spectroscopy (FTIR) method. At the 30% weight-mixing ratio (diluent wt./total wt.), the WAT of waxy crude oils dropped from 45.1 to 42.4^{o}C for Yellow Wax and from 41.6 to 37.7^{o}C for Black Wax. The energy analysis for the whole processes of biodiesel production from algae was performed. By using the proposed technologies, the total energy requirement for algae biodiesel production is 44% less than the traditional processes.

TABLE OF CONTENTS

LIST OF TABLES

LIST OF FIGURES

LIST OF ACRONYMS

PSDB	Periodic Symmetry Defined Bioreactor
CIJM	Confined Impinging Jet Mixer
WAT	Wax Appearance Temperature
FTIR	Fourier Transform Infrared Spectroscopy
EIA	Energy Information Administration
LED	Light Emitting Diode
DAF	Dissolved Air Flotation
SAF	Suspended Air Flotation
PVC	Polyvinyl Chloride
DI	Deionized
UV-vis	Ultraviolet-Visible Spectroscopy
UROP	University of Utah Undergraduate Research Opportunities Program
GC/MS	Gas Chromatography/Mass Spectrometry
FAME	Fatty Acid Methyl Ester
HTGC	High Temperature Gas Chromatography
FID	Flame Ionization Detector
TAG	Triglyceride
PEEK	Polyether Ether Ketone

ACKNOWLEDGEMENTS

The author would like to acknowledge the support of his wife (Amy Chungmin Tang), and his family. The author gratefully acknowledges helpful advice with his advisers Dr. Swomitra Mohanty and Dr. Leonard Pease. The author acknowledges the enlightening conversations with Dr. John McLennan, Dr. Anthony Butterfield, and Dr. Richard Roehner.

CHAPTER 1

INTRODUCTION

Background

Algal fuel, one of the most promising alternative fuels, has generated increasing attention due to global warming, high fuel demand, and the world food crisis. Burning fossil fuels will produce greenhouse gases that lead to global warming. Unlike fossil fuels, Algal fuel is a carbon neutral fuel, which means the CO_2 emitted by burning algal fuel is the same CO_2 captured during cultivation. During cultivation, algae captures CO_2 and converts it into lipids by photosynthesis [1, 2]. We can connect the algae growing device (such as photobioreactor, and open pond system) to a CO_2 source (such as power plant, highway, and industrial factory). Several studies demonstrate that algae may be cultivated using flue gas exhausted from the power plants [3-5]. According to the forecast from the Energy Information Administration (EIA), the energy demands will increase 37.6% from 86.8 billion barrels per day in 2010 to 119.4 billion barrels per day in 2040 [6]. Renewable energy includes biofuel (including biomass to liquids) that has the highest increase rate (2.5% per year) compared to the other alternative energy source [7]. There are 7.3 billion people on the earth right now, which is predicted to be 9 billion people in 2040 [8]. These newborn populations will create massive food demand. Unlike first

generation biofuel which uses food crops like corn and vegetable oil as the fuel source, algae can be grown on nonarable land and with saline water, wastewater, and producewater [9, 10]. It means algae can be grown almost anywhere warmer than 20^{O}C even in the desert [11-13]. At the same time, unlike second-generation biofuel that uses the lignocellulose biomass and suffers from complicated harvest steps, algae has a more simple structure and produces more lipids per unit area. Microalgae (small phototropic cellular organisms; macroalgae are plants like kelp) containing 30% lipids of their dry biomass, some species can even reach 70% [14]. Microalgae can produce 97,800 liters biodiesel per hectare per year, which is significantly more than the other biodiesel sources like soybeans (446 L/ha/year), sunflowers (952 L/ha/year), palms (5950 L/ha/year), corns (172 L/ha/year) and rapeseeds (1190 L/ha/year) [15]. According to the U.S. Department of Energy, approximately $3.88 \cdot 10^{10}$ sq. m of land to grow the microalgae for the total replacement of petroleum [16, 17]. Furthermore, the growing cycle of microalgae is about 7-14 days, which is relatively short compared to the other annual crops [1].

Due to the highly unsaturated fatty acid, algal fuel is relatively unstable and biodegradable [12]. These features decrease the environmental impact if leaking or spilled [14]. Microalgae can be converted into a lot of different biofuels includes biodiesel, ethanol, butanol, acetone, biogasoline, and jet fuel [1, 18-21]. The flow chart of algae biodiesel production is shown in Figure 1.1.

The benefits of algal fuels include high productivity, noncompetitive with food crops, conservation of fresh water, biodegradable, carbon neutral, and the diversity of biofuels. These are essential features that minimize the impact on food production and the

environment, making microalgae one of only a few alternative fuel candidates that can potentially entirely replace fossil fuels for transportation fuel usage.

However, technological and economic barriers to industrial scale-up remain. The first problem is temperature control. The optimal growing temperature of microalgae varies from species to species, but it usually between 25-30^{o}C [11, 12, 22]. The growth rate will decrease when the temperature is too low (<16^{o}C) and microalgae will be killed when the temperature is too high (>35^{o}C) [23]. The temperature can be controlled by adding cooling flow or air conditioning, but it will increase the capital cost. The algae need fertilizer to provide nitrogen and phosphorus. But these fertilizers will create a lot of CO_2 emissions that neutralize the CO_2 absorbed during algae cultivation. A carbon neutral fertilizer or sufficient nitrogen source needs to be found to make the whole process environmentally friendly [24]. Algal fuel is still a relatively new technology. There are still a lot of processes steps that need to be optimized includes algae strain selection, cultivation, lipid extraction, biocrude purification. According to Table 1.1, the oil content varies from species to species and would also be affected by the culture condition such as nutrients concentrations. Different microalgae also has different growth rate. Therefore, we should try to find the species that grow fast and also accumulate more lipids. Once we can solve the problems mentioned above, we can start to produce the carbon neutral, sustainable fuel to replace the fossil fuel. Table 1.2 shows the advantages and disadvantages of algae biofuel.

Algae Cultivation Parameters

Growing microalgae mainly requires light, carbon sources, and nutrients. To build an artificial system for algae cultivation, we must reproduce the environment where wild algae live. The important factors that will affect algae growth include light intensity, carbon dioxide supply, medium mixing, oxygen and autoinhibitory removal, temperature, and the pH levels [25].

Light

Light provides the required energy for algae photosynthesis reaction. The source of light can be classified into two areas: light from the sun or other artificial devices likes a lamp, laser, LED, and so forth. Sunlight is free but suffers from diurnal cycle and seasonal effect. Artificial light is relatively stable but increases energy input dramatically. Both intensity and spectral quality should be considered when we are choosing a light source. The efficiency of algae photosynthesis vary with different spectral quality, as some algae favor red-yellow spectra more than the blue region [26]. Using the dye solution to absorb the certain range of spectrum or grating to block light can modify the light spectrum. Light intensity is also a critical factor for algae cultivation. The photosynthesis efficiency will increase when the light intensity increases, but when it reaches the saturation intensity the productivity will start to reach the steady state. If the light intensity is higher than a particular point, the photosynthesis efficiency will decrease dramatically due to photoinhibition [27].

Carbon Dioxide

Carbon is the essential element of photosynthesis reaction. It dissolves in water at about 0.03% (volume). But 0.03% is not enough for algae growth; so additional CO_2 should be supplied to the growing culture. The minimum and maximum limit of CO_2 is still unknown [28]. But it is commonly considered that the growth rate of algae will decrease when the CO_2 concentration is more than 1% [25]. Additional CO_2 can be supplied in the form of bubbles. The other more expensive way is using bicarbonate salt to increase the CO_2 concentration in the growing medium.

Mixing

Mixing can help algae cell suspension in the growing culture and prevent deposition on the bottom and side wall, increase light utilization efficiency, increase gas exchange include CO_2 dissolving and O_2 removing, enhance nutrient distribution, and improve temperature uniformity [25]. The two most common ways to mix the algae growing culture are: air bubble and hydrodynamic flow [29]. However, if the mixing is too fierce, the hydrodynamic stress will affect the algae growth or even destroy the cell [30]. The design of the mixing system is also the key factor of the construction cost and operation cost for the algae cultivation system.

Nutrient Supply

The nutrient is also the essential component for algae growth. The most important elements for algae growth include carbon, nitrogen, phosphorus, oxygen, hydrogen, sulfur, magnesium, sodium, calcium, chlorine, and potassium [25]. These elements are

estimated based on the algae composition [31]. Nitrogen is considered to be the critical factor that affects lipid accumulation; experiments show that nitrogen limitation helps lipid formation [32, 33]. When the primary nutrients are insufficient, algae may release the autoinhibitory as a self-defense mechanism [25]. The sources of the nutrients can be wastewater or directly support in the form of the salt, but it will increase the cost and also have carbon footprint issues [24]. Therefore, nutrient supply is still one of the barriers for algal fuel to scale-up that needs to be overcome.

Temperature

Just like most the other plants, the temperature is crucial to algae growth. Algae can be grown in a certain temperature range (15-40 ^{o}C) [25, 34]. Within this range, the algae growth rate increases until the ideal temperature is reached. But if the temperature lower or higher than this range the growth rate will drop dramatically [25, 33]. If the cultivation system is placed outside, the temperature control will be much harder than in the indoor system because it is affected by the diurnal cycle and seasonal effect. There are several ways to control the temperature includes the heat exchanger, greenhouse, and water spray, but they will also increase the cost [35]. Consequently, the temperature is also a technical barrier for algal fuel.

pH

The pH value of external culture medium will also affect the algae photosynthesis efficiency. The pH value will affect the CO_2 diffusivity, liquid chemistry, and the availability of nutrients [36]. The experiments show that the photosynthesis efficiency of

Coccochloris peniocystis optimally in the pH range between 7.0 and 10.0, but starts to decreases dramatically out of this range [37]. During cultivation, the pH value of the culture will gradually increases due to the consumption of carbon dioxide [38]. Therefore, one should monitor the pH value of the cultivation system to ensure the optimal growing condition.

Algae Cultivation Technologies

Open System

There are two primary types of algae cultivation, open systems and indoor/covered systems. The open system can be classified into two different types: the natural reservoir (lake and pond) and the artificial pond [39]. A commonly used open system is called raceway pond; because it is built like a racetrack. The water, algae, and nutrients were circulated by a paddlewheel. The fresh algae broth was introduced from one side, and the matured culture was pouring out from the other end. The gas sprayer can be installed to increase the CO_2 availability [40]. The continuous flow will keep algae suspended in the culture without extensive deposition on the bottom. The raceway pond system is usually shallow (between 0.2-0.5m) because sunlight can only penetrate to a certain depth [39]. This feature will increase the need for more lands. Because it uses sunlight as the light source, it will suffer from uneven light intensity due to diurnal cycle and seasonal effect. The raceway pond is usually made of concrete to save the construction cost. The open systems suffer from cold weather, wild microorganism invasion, evaporation losses, and contamination due to the coverless feature [29]. Temperature has a major effect on algae cultivation. If the temperature is not kept within

the certain range, the productivity of open ponds in winter will be affected [39]. To solve this problem, we can build a transparent cover on top of it, like a greenhouse, to enable temperature control and prevent contamination; however, it will increase the capital cost substantially. Contamination and wild microorganism are fatal defects for the open system. During the growing cycle, algae culture can be easily attacked by bacteria or other species algae [41]. Therefore, the open systems need to be built in a selective environment [42]. Multispecies algae can also increase the resistance of contamination. However, some people are still using the open monoculture system. For example, Lesley et al. [43], grow unicellular alga Dunaliella salina in Western Australia with extremely halophilic water. Table 1.3 shows that the annual production rates for open systems are between 10 to 25 $g \cdot m^{-2} day^{-1}$. Therefore, open systems are more scalable than close systems, but not as efficient as close systems.

Close System

Closed-loop systems include bubble columns, flat panels, tubular systems, and stirred tank photobioreactors, etc. [44]. Flat panel and tubular systems are usually placed in an outdoor environment. These outdoor-closed systems take advantage of the free sun light. Compare to the open systems, close systems provide a higher level of control for growing parameters (e.g., air flow rate, liquid flow rate, nutrient concentrations, pH, and evaporation loss) and remain free from contamination [45]. The closed systems permit monoculture microalgae cultivation [1]. A higher level of control for growing condition leads to a higher production rate and a higher biomass concentration, which will help decrease the harvest cost [25]. However, because these closed systems are placed in the

outdoor environment, they suffered from the outdoor conditions, such as temperature fluctuation and uneven light intensity. The indoor closed system, like bubble columns and stirred tank, are used to conquer these defects. Without using the sunlight, the indoor closed systems usually use artificial lights, such as LED, light tubes, or optical fibers [46-48]. By using the artificial lights, the light intensity, distribution, and spectral quality can be modified [49]. The temperature control for the indoor closed systems would be much easier in comparison with that for the outdoor systems. The indoor photobioreactors have the highest production efficiency, but they are also more expensive to construct and operate. They are not economically feasible to be used in biodiesel production processes. The biomass productivities for closed photobioreactors are shown in Table 1.4.

Bubble Column Reactor

The bubble column reactors are comprised of a cylindrical tube and the gas sprayer at the bottom (Figure 1.2a). The light sources can be placed externally or internally [50, 51]. The diameters of the columns would not exceed 0.2 m because light can only penetrate certain depth [52]. Due to the structural reasons and mutual shading problems, the heights of the bubble columns should below 4 m [52]. The critical operation parameter of bubble column is the aeration rate. The bubbles increase the gas exchange efficiency and it help to provide carbon dioxide and remove the oxygen produced by photosynthesis. The aeration rate has upper and lower limits, where the minimum aeration rate can prevent settlement, and the maximum aeration rate helps maintain the acceptable turbulent level without damaging the cell [53]. If the aeration rate is too high, it will generate microbubbles, which will accumulate and then block the light

penetration [52]. Bubble column photobioreactors have low capital cost, high surface-area-to-volume ratios, and no moving parts.

Flat Panel Reactor

The flat panel reactors were invented in the 1950s [54, 55]. It received a lot of attention and investigation due to the large illumination area and minimal light path. The shape of a flat panel reactor is cuboid (Figure 1.2b), and the algae cultures are trapped between the two transparent plates and are circulated by a gas sprayer at the bottom. The flat panel reactors can be placed horizontally or vertically. The largest wall of the vertical flat panel reactor is orientated north-south to increase the absorption of sunlight [56]. The light sources are placed on both sides of the vertical flat panel reactors when the artificial lights were used. Some commercial flat panel reactors also equipped temperature controller, pH monitor, and optical density detector, to control the growing parameters [57]. The transparent walls of flat panel reactors are usually made in plastic or glass. There is a new type of flat panel reactor was comprised of metal frame, and plastic bag that contain the algae culture [58]. This type of flat panel reactor is easy to replace if containment or leak. The flat panel bioreactors have the minimal light path. The mass productivity per unit volume of flat panel bioreactors is approximately 1.7 times higher than the bubble column bioreactors [59]. The amount of dissolved oxygen that produced by photosynthesis of algae in the flat panel reactors is lower than that in the tubular reactors [29]. However, compared with the tubular reactors, the flat panel reactors are relatively hard to scale-up due to the geometry restriction.

Tubular Reactor

Tubular reactor systems are comprised of two main parts: tubular array and gas exchanger (Figure 1.2c). Algae cultures are circulated by either a mechanical pump or an airlift pump, which is placed between the tubular array and the gas exchanger. The mechanical pumps are easy to install and operate, but the high stress caused by the circulating fluid might damage the algae cells [53, 60]. The airlift pumps are gentler than the mechanical pumps, and the gas bubbles can also facilitate the gas exchange [61-63]. The flow is maintained in highly turbulent to prevent algae settlement. The algae collect sunlight during the circulation in the tubular array. The diameter of the tubular array is usually 0.1 m or less because sunlight can only penetrate a certain depth. These tubes are made of transparent materials such as plastic or glass to allow sunlight penetration. To get maximum light energy utilized, the tubular array can be placed horizontally, or inclines toward the sun. In order to increase the reflection, a light reflective material (e.g., mirror) is placed on the bottom of the tubular array or the bottom of the array and it is painted in white [64]. However, some tubular systems with artificial illumination are placed in an indoor environment for the production of highly valuable algal products [35]. To maximize the density of the tubular array in an unit area, the tubular array is arranged like a fence [1]. The gas exchanger is used to remove the oxygen generated in the tubular array during the photosynthesis of algae. The gas-liquid separator is used to remove all the dissolved oxygen bubbles [65, 66]. If the oxygen level is too high (400% of air saturation value), it will inhibit the photosynthesis and produces photooxidative compounds, which will damage the algae cells [61]. Therefore, the tube length cannot exceed the certain length (usually 80 m), but it also depends on the other factors, such as

flow rate, tube diameter, and light intensity [1, 61]. Some tubular systems are equipped with carbon dioxide injectors, pH monitors, and heat exchangers in gas exchangers to improve the control of environmental parameters [64, 67].

Stirred Tank Reactor

The stirred tank reactors are comprised of a cylinder tank, motor powered impellers, the air sprayer, and the gas-liquid separator (Figure 1.2d). The air sprayer is place on the bottom and the gas-liquid separator is positioned on the top of the tank to remove the excess bubble and the oxygen produced by the photosynthesis of algae [44]. Due to the mechanical stirring, the stirred tank photobioreactors have better liquid-gas mixing [68], but the low surface-area-to-volume ratio decreases the light utilization [44]. To increase the light utilization, the internal illuminations are used in stirred tank reactors [69-71]. The temperature controller, pH controller, dissolved oxygen concentration monitors are installed in the reactors to control and monitor the growing parameters [72]. Due to the effective control of growing parameters, the stirred tank reactors have high production rates. However, the construction and operation costs are also greater than the other reactors.

Although each of the photobioreactor has advantages, challenges remain (Table 1.5). The open systems are cheaper and highly scalable, but not so productive in comparison with the close systems. The close systems have higher production rates, but it cost more due to the control of growing parameters. However, none of these photobioreactors can have high-energy efficiency, low construction cost, low operating cost, and high scalability simultaneously. Therefore, a new type of photobioreactor or

improved version of the reactors mention above should be invented to overcome these barriers.

Harvesting

After cultivation, the centralization of the algae biomass from the matured culture is another technical barrier. The mature algae culture produced from either open systems or close systems both contain more than 99% water in total mass [73]. Thus, dewatering is the critical steps in algae harvesting. The algae have low specific gravity and negative charges on the surface, which keep them suspended in the water [73, 74]. These features make them hard to separate from growing water. There are two ways to separate the algae from the water that increase gravity separation rate and neutralize the negative charges by adding coagulating agents [75, 76]. The harvesting steps can be classified into primary and secondary harvesting. Primary harvesting is the first dewatering step that is achieved by natural sedimentation or flotation technology [77, 78]. It will give an algal slurry with about 0.5-6% weight percent of algae biomass [73]. Secondary harvesting will concentrate algal slurry further more to get 10 to 20% weight percent of algae biomass [73]. It can be done by centrifuge or belt filter press [76, 79].

Gravity Sedimentation

The gravity sedimentation is trigger by gravitational force. The algae cells will settle at the bottom due to the higher specific gravity in comparison with growing culture. However, due to the specific gravity, difference between algae and water is quite small, the settlement time is very long. Due to the poor compaction of algae slurry, the weir

overflow rate should not be too high to prevent resuspension [80]. The gravity sedimentation also requires a lot of land, which make it unfavorable even it is a relatively inexpensive procedure [74].

Dissolved Air Flotation

The dissolved air flotation (DAF) uses air as a carrier to collect the algae cells from the culture. This process contains two steps: dissolve gas into algae culture and recover the air bubble with the algae adhered to it [73]. The matured algae biomass was first compressed in the saturator. Base on Henry's Law, the gas solubility will increase when the pressure increases. Therefore, a certain amount of gas will dissolve in the algae solution when the solutions were compressed. The compressed algae cultures are then released to the flotation cell which contains coagulating agents [73]. Due to the pressure drop between saturator and flotation cell, the dissolved gas is released back into the atmosphere in the form of small bubbles. During the release process, the algae cells will adhere to the bubbles and be carried to the surface [81, 82]. The algae cells accumulated on the surface are collected by the skimming mechanism with a part of recycle flow to repeat the process mention above [83]. The researchers have found the optimal operation parameters. The bubbles size should be between 10 and 100 μm [81, 83-85]. The pressure applied in the saturator can be used to control the bubbles sizes. The minimum pressure to achieve the optimal sizes of bubbles is about 390 kPa (56 psig) [81]. The DAF is reported to have 99% of algae removal efficiency [86]. However, it is suitable to be used in biofuel production due to the intensive energy consumption.

Suspended Air Flotation

The suspended air flotation (SAF) is similar to the DAF. The compressor in DAF consumes a lot of energy, which make DAF an energy intensive process. The SAF use surfactants that can produce gas bubbles to replace the compressor in DAF to solve this problem [73, 77]. The surfactants are selected to be positive charged, which will increase the aggregation rates of negative charged algae cells due to the electrostatic attraction force [77]. Unlike DAF that needs high-pressure saturator to dissolve gas into algae culture, the SAF only needs mixing vessel for the mixing of surfactants and algae culture. This feature will save a lot of energy for operation. The SAF also has higher loading rate and use about 60 times less flotation water in comparison with the DAF. The major drawback of SAF is that the surfactants will increase the carbon footprints for the whole process [73].

Electrocoagulation and Electroflotation

The electrocoagulation and electroflotation are the derivative from the flotation technology. The system contains metal electrode in the mixing vessel that is applied direct current to the algae culture [87-89]. It uses consumable metal electrodes (usually aluminum and iron) to generate cation, which will hydrolyze into aluminum or polymeric iron that can be utilized as coagulating species [88, 90, 91]. During the electrochemical reaction, the hydrogen and oxygen are generated at anode and cathode [89]. These bubbles will carry the adhered algae cells to the surface just like the DAF and the SAF. The algae cell accumulated on the surface will be collected by a skimming mechanism [89]. The size of bubbles and the concentration of cation in the solution can be controlled

by the current density applied [73]. The adequate size of bubbles for this system is between 17 to 40 μm [92]. This technology combines dissolving air and adding coagulate agents in one step, which will save the operation cost and reduce the complexity of the process. However, there are not enough research data to support that electrocoagulation and electroflotation is suitable for algae harvesting presently [73, 93].

Centrifugation

Centrifugation uses centrifugal force to speed up the separation between the algae cells and the growing culture. It is the most common harvesting method being used in the laboratory. It can concentrate algae to into slurry with 10 to 22 weight percent [79, 94]. Centrifugation is fast and efficient, but it costs a lot of energy for operation. Some authors argue that centrifugation can be used in secondary harvesting to avoid the pre-concentration cost [73]. The power rate of centrifugation is approximately 3000 kWh per unit ton of dry algae biomass [95].

Belt Filter Press

The belt filter press process is a dewatering technology commonly used in industry. It uses gravitational force and a mechanical press to remove the water from the algae slurry [96]. The algae slurry is fed between two moving filter cloths, and the rolling belt carried the algae slurry will first passed a gravity section where the liquid is extracted by gravity [97]. Afterward, it will enter the low-pressure section where the slurry will be squeezed by the rollers to remove the liquid inside [97]. Belt filter press can generate algae biomass with about 18% weight percent [79]. It's a relatively energy efficient

technology in comparison with the centrifuge [73]. However, the disadvantages of the belt filter press are leaking and preconcentrated algae biomass needed. The input algae slurry of the belt filter press should be treated by primary harvesting first [73]. The belt filter press can only be used in some large algae species given that some small algae cells will leak through the pores on the belt during the process [76].

Drying

Some further processes require extremely dried algae biomass [98]. Drying microalgae require a lot of energy because of the high latent heat of water (336 kJ kg^{-1}) [99]. There are several ways to dry the algae biomass: solar drying, spray drying, and freeze drying [98]. Solar drying is the most inexpensive method because it does not need any charged energy input but just free solar energy [39]. However, solar drying requires a large land field, and the drying rate depends on the weather condition [98]. The spray method has been successfully used in drying Dunaliella [76]. But the energy requirement of spray method is more than solar drying method [39]. Freeze drying method is widely used in the laboratory, but it's too expensive for large scale process [100].

After all, none of the technologies mentioned above are perfect (Table 1.6). The decision of dewatering methods depends on the next steps of the process. Take making biodiesel as an example; the next step is lipid extraction. If one chooses a mechanical press method to extract lipid, then the further concentrated algae biomass will be needed. If one uses chemical solution extraction, then it only requires concentrated algae solution. Therefore, a comprehensive evaluation is needed when we choose the harvesting technology.

Algae Lipid Extraction

Lipid harvest is the key barrier of biofuel production. Lipid extraction may be accomplished by mechanical or chemical methods [2]. The mechanical methods usually use mechanic force to break up the algae cell walls to release the lipid inside. The chemical methods often use intermediate solvents to extract lipid by diffusion, which is driven by concentration gradient [101]. Some harvest technologies require wet concentrated inputs and some require dry algae powder. Drying processes remove the free water before extraction, but are very energy intensive. The mechanical methods include expeller, ultrasonic, and microwave method [102]. The chemical methods include the chemical solvent, supercritical carbon dioxide, and ionic liquid extraction method [103].

Lipid Composition of Microalgae

The lipid composition of microalgae may vary from cell to cell and between species, but not all lipids can be converted into biodiesel. Lipids may be classified as polar or neutral, based on the polarity of the molecular head group [104]. Neutral lipids include acylglycerols and fatty acids. Some neutral lipids do not contain fatty acids including sterols, ketones, and chlorophylls. Polar lipid can be classified into phospholipids and glycolipids [105]. Among lipids, acylglycerols including triacylglycerols, diacylglycerols, and monoacylglycerols, may be converted into biodiesel. Other lipids are not readily convertible to biodiesel. The lipid composition may also be affected by the growing condition, just like temperature, light intensity,

nutrient composition, and pH [101]. The lipids contain in microalgae have carbon train length between 12 and 22 [2].

Expeller Pressing

Expeller pressing is widely used in food industry to extract oil from nuts and seeds [106]. It uses mechanical press to break up the algae cell walls to release the lipid inside [101]. Expeller can extract about 75% of lipid and still some lipid left in the pressed cake [107]. It is easy to operate and conserve the purity of biomass without adding chemical solvents. But it is a slow process and requires a lot of dry algae biomass, which will cost substantial energy for drying [108]. Expeller pressing is not suitable for biofuel production process due to the low efficiency and high-energy consumption.

Ultrasound Assisted Extraction of Oil

Ultrasonic-assisted extraction uses cavitation to destroy the cell wall [103]. Cavitation is caused by the bubbles explosion where the bubbles were generated by intense sonication (higher than 20 kHz) [109]. When the bubbles exploded near the algae cells, the shock wave and shear force created by high-speed liquid jet will damage the cell walls and release the lipid inside [101, 110]. Ultrasound-assisted extraction is fast, effective, and solvents free [103]. The most significant advantage is that it works for wet algae culture, which will save a lot of energy for drying. However, it still requires certain energy to generate the ultrasonic wave. The impact of oil quality and stability of ultrasound-assisted method is still undetermined [103]. Overall, this technology is not the primary lipid extraction method for algae.

Microwave Assisted Extraction of Oil

Microwave assisted extraction method uses heat to increases the mass transfer of lipids from algae cells to the bulk solvent [111]. Microwave heating is noncontact heating, which the microwave can penetrate the cell walls to interact with polar molecules [101]. The whole cells are heated simultaneously and uniformly [111]. The mass transfer and heat transfer have the same direction from inside of algae cells to bulk solvent [112]. Microwave assisted extraction can speed up the process and increases the yield of the traditional chemical solvent methods [111]. But is still use toxic solvents and energy intensive, thus, it is hard to scale up for the biofuel production processes.

Solvent Extraction Method

Among chemical methods, organic solvent extraction is the most common chemical method used to extract lipids from algae. In this method, the lipid held in the algae cellular matrices migrates into the organic solvent phase due to a concentration gradient between them. Extraction may be performed near room temperature or at elevated temperatures [113]. These processes usually require a few minutes to a few hours and extract about 6.3% to 28.6% of lipid on a dry mass basis [109, 114]. To shorten the process time, increasing temperature (20 to 200^{o}C) and pressure (10 to 15 MPa) have been used [101, 115]. The high temperature will help to increase the diffusion rate, and the high pressure will keep the solvent in the liquid state for safe and fast extraction [101]. Usually, the combination of polar (i.e., methanol and ethanol) and nonpolar (i.e., hexane and chloroform) solvents are used to extract both neutral and polar lipids [2]. The polar and nonpolar solvent ratio will affect the extraction efficiency. The most widely

used recipe is chloroform/methanol (1/2 v/v) [101, 116]. To minimal the cost for downstream purification, the selected solvent should have high levels of specificity towards target component like triacylglycerols [101]. The solvent boiling point should also be as low as possible to reduce the distillation cost [101]. Because the chemical solvent method is driving by diffusion, when the concentration of lipid in the bulk solvent reach the same level as inside the algae cell the diffusion will reach steady state and the concentration would not change anymore. The continuous solvent extraction like Soxhlet reactor is used to conquer this problem [2]. The other way is using mechanical assistance to break the cell wall like ultrasound and blender [101, 117]. The main disadvantages of organic solvent extraction are its heating cost, the toxicity of solvents used, and the long residence time required for lipid diffusion or low yield [118]. The advantages include consuming minimal amounts of energy and bypassing the algae drying process because it operates in wet environments.

Supercritical CO_2 Extraction

Supercritical fluid extraction is another emerging chemical method. By adjusting the extraction pressure and temperature, the solubility may be easily tuned. The partial liquid and partial gas characteristics of supercritical fluid accelerate the lipid extraction process [119]. Supercritical carbon dioxide remains the most commonly used solvent for supercritical extraction. Its low critical temperature (31.1^{o}C) decreases the cost and prevents the lipid degradation. However, due to the relatively nonpolar attributes of the solvent, supercritical carbon dioxide cannot extract the entire lipid in the algae. Some polar cosolvents (like methanol and dichloromethane) may be added to enhance the lipid

yield [120]. The operation parameters like temperature, pressure, flow rate, and cosolvents will affect the efficiency of lipid extraction [101]. Higher pressure and density of CO2 will extract more unsaturated compounds [101, 121, 122]. Supercritical carbon dioxide extraction features low toxicity, low flammability, better lipid selectivity, and lack of reactivity [123]. But the high construction costs make it challenging to scale up.

Ionic Liquid Extraction

Ionic liquids are just like salt, which comprised of cations and anions. But ionic liquid stay liquid under moderate temperature (0-140^{o}C) [124]. The polarity and solubility can be varied by changing the cations or anions [125]. The cations are usually nitrogen-containing ring structure and the anions can be single halogen or complex ions groups [126]. Due to the strong self-association, ionic liquids have low vapor pressure that can reduce the leaking problems during the process [127]. Due to the features of non-volatile, thermal stability, synthetic flexibility, and easily tuned solubility, ionic liquids are treated as a replacement of organic solvents [101, 128]. The limitations of the ionic liquid are the high material cost and toxicity [129].

Overall, the lipid extraction technologies mentioned above still have some technical barriers. The advantages and disadvantages are summarized in Table 1.7.

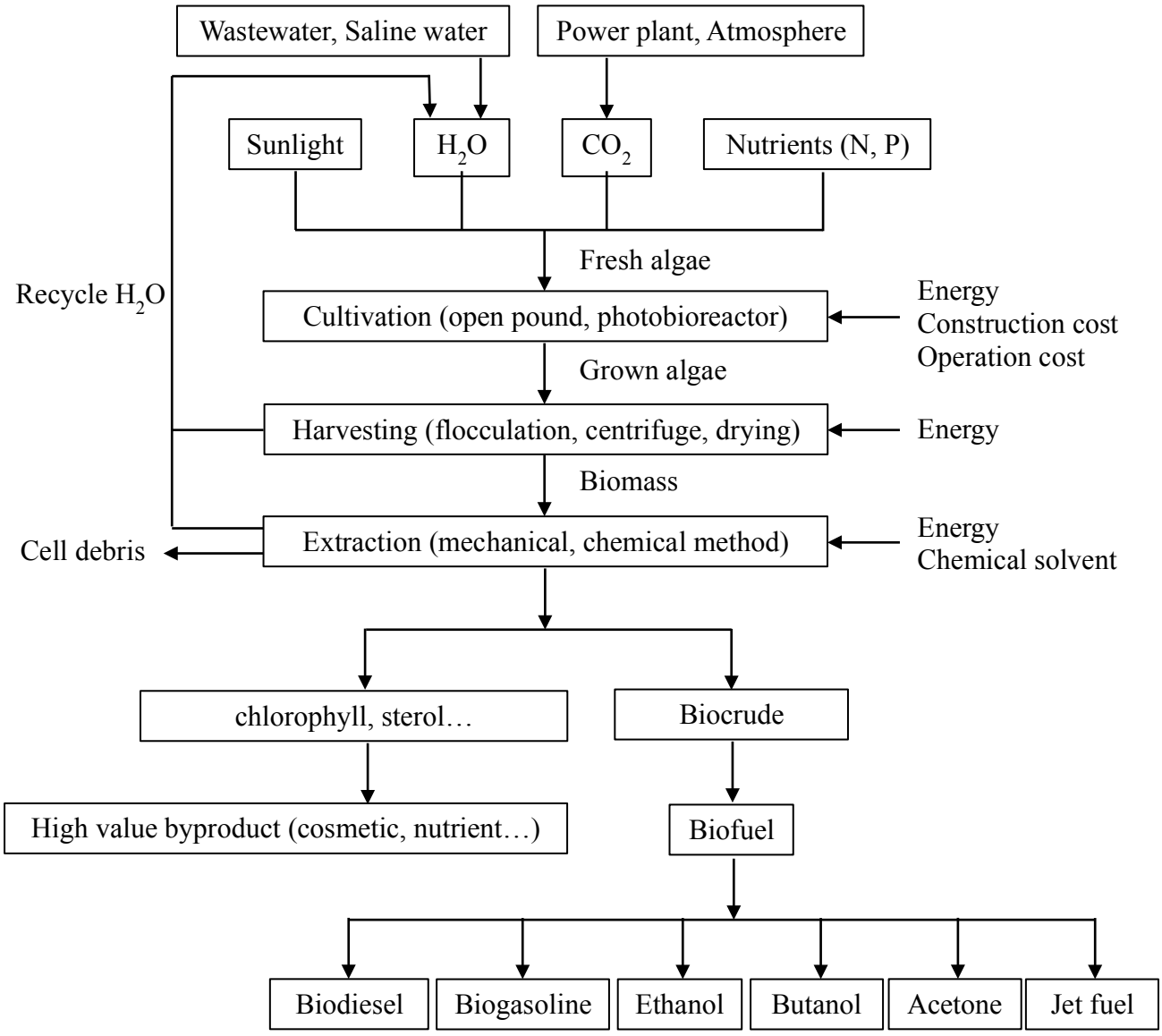

Figure 1.1. The flow chart of algae biodiesel production.

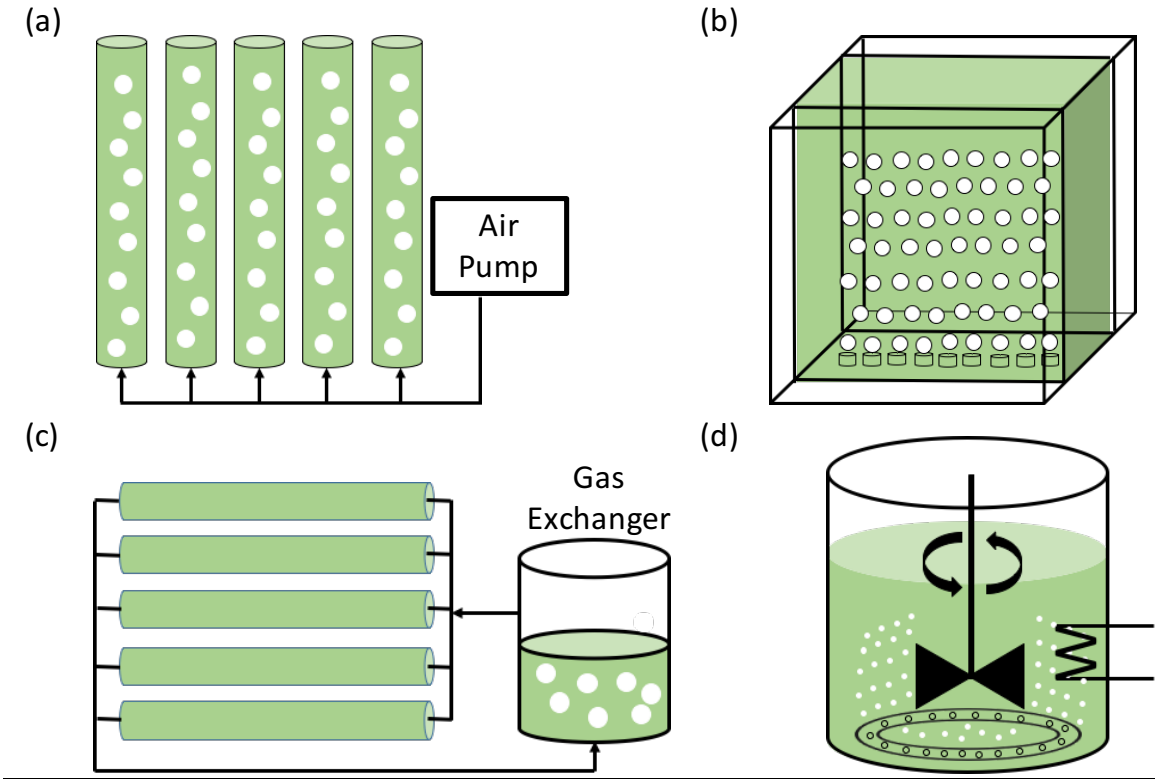

Figure 1.2. Exemplary photobioreactors: (a) bubble column reactor, (b) flat panel photobioreactor, (c) horizontal tubular photobioreactor, and (d) stirred tank photobioreactor. Courtesy of R. N. Singh [44].

Table 1.1. Oil content of some microalgae (% dry weight)

Species	Oil content	Reference
Ankistrodesmus TR-87	28-40	[130]
Botryococcus braunii	29-75	[17, 131, 132]
Chlorella sp	28.32	[17]
Cyclotella DI-35	42	[17]
Cylindrotheca sp.	16-37	[1]
Dunaliella tertiolecta	36-42	[133, 134]
Hantzschia DI-160	66	[17]
Isochrysis sp.	7-33	[17, 135]
Nannochloris	20-63	[1, 4, 130]
Nannochloropsis	31-68	[1, 136]
Nitzschia sp.	45-47	[1]
Nitzschia TR-114	28-50	[137]
Phaeodactylum tricornutum	31	[17]
Scenedesmus TR-84	45	[17]
Schizochytrium sp.	50-77	[1]
Stichococcus	33 (9-59)	[102]
Tetraselmis suecica	15-32	[138]
Thalassiosira pseudonana	21-31	[139]

Source: Adapted from 2011 Demirbas table 2.

Table 1.2. The pros and cons for algal fuel

Advantages	Disadvantages
Carbon neutral fuel	Required temperature control
Reduce CO2 emission	Fertilizer needed (increase CO2 emission)
Fast growth rate	Relatively new technology
High oil% of biomass	Hard to scale up
High lipid yield per unit area	
Not competitive with food source	
Conserve of fresh water	
Can be grow on non-arable land	
Biodegradable	
Diversity of fuel production	

Table 1.3. Biomass productivity figures for open pond production systems

Algae species	X_{max} (gl^{-1})	P_{aerial} (gm^{-2} day^{-1})	P_{volume}($gl^{-1}day^{-1}$)	Reference
Chlorella sp.	10	25	-	[140]
Chlorella sp.	40	23.5	-	[141]
Chlorella sp.	40	11.1	-	[141]
Chlorella sp.	40	18.1	-	[141]
Spirulina platensis	-	-	0.18	[142]
Spirulina platensis	0.47	14	0.05	[143, 144]
Haematococcus pluvialis	0.202	15.1	-	[145]
Various	-	19	-	[146]
Spirulina platensis	0.9	12.2	0.15	[147]
Spirulina platensis	1.6	19.4	0.32	[147]
Anabaena sp.	0.23	23.5	0.24	[148]

Table 1.4. Biomass productivities for closed photobioreactors.

Species	Reactor type	P_{volume} ($gl^{-1}day^{-1}$)	Reference
Porphyridium cruentum	Airlift tubular	1.5	[38]
Phaeodactylum tricornutum	Airlift tubular	1.2	[62]
Phaeodactylum tricornutum	Airlift tubular	1.9	[61]
Chlorella sorokiniana	Inclined tubular	1.47	[149]
Arthrospira platensis	Undular row tubular	2.7	[150]
Phaeodactylum tricornutum	Outdoor helical tubular	1.4	[151]
Haematococcus pluvialis	Parallel tubular (AGM)	0.05	[152]
Haematococcus pluvialis	Bubble column	0.06	[153]
Haematococcus pluvialis	Airlift tubular	0.41	[153]
Nannochloropsis sp.	Flat plate	0.27	[154]
Haematococcus pluvialis	Flat plate	-	[145]
Spirulina platensis	Tubular	0.42	[155]
Arthrospira	Tubular	1.15	[156]
Chlorella	Flat plate	3.8	[3]
Chlorella	Flat plate	3.2	[3]
Tetraselmis	Column	0.42	[138]
Chlorococcum	Parabola	0.09	[157]
Chlorococcum	Dome	0.1	[157]

Table 1.5. Advantages and limitations of open ponds and photobioreactors.

System	Advantages	Limitations
Raceway pond	Relatively cheap Easy to clean Utilizes non-agricultural land Low energy inputs Easy maintenance	Poor biomass productivity Large area of land required Limited to a few strains of algae Poor mixing Cultures are easily contaminated
Tubular	Large illumination area Suitable for outdoor cultures Relatively cheap Good biomass productivities	Some degree of wall growth Fouling Requires large land space
Flat plate	High biomass productivities Easy to sterilize Low oxygen build-up Readily tempered Good light path Large illumination surface area	Difficult scale-up Difficult temperature control Small degree of hydrodynamic stress Some degree of wall growth
Column	Compact High mass transfer Low energy consumption Good mixing with low shear stress Easy to sterilize Reduced photoinhibition and photo-oxidation	Small illumination area Expensive compared to open ponds Shear stress Sophisticated construction
Stirred tank	High gas-liquid mixing High biomass productivities High level control of growing parameters	Low surface to volume ratio Expensive to construct and operate

Table 1.6. Pros. and cons. of harvesting technologies.

Harvesting	Advantages	Limitations	Final Conc.
Sedimentation	Low cost Easy to operate	Require large area Low final concentration Slow	0.5-3%
DAF	High efficiency	High energy input High capital cost	3-5%
SAF	Energy efficient High loading rate	Require chemical supply	3-5%
EC/EF	High efficiency Simple process	Lack of experiment data	3-5%
Belt filter press	Fast Matured technology	Require pre-concentration Can't use small algae	18%
Centrifuge	Fast and effective	High energy input Small loading	10-22%
Solar Drying	Low cost Free solar energy	Require large area Slow	-

Source: Adapted from 2011 Patrick table 2.

Table 1.7. Advantages and disadvantages of lipid extraction technologies.

Production system	Advantages	Limitations
Expeller Pressing	Solvent free Easy to operated	Slow Low efficiency Large amount of biomass required
Ultrasound Assisted	Speed up the process Reduce solvent usage High yield	Energy intensive Hard to scale up
Microwave Assisted	High yield Fast Reduce solvent usage	Energy intensive Hard to scale up
Solvent Extraction	Relatively cheap Easy to operated Easy to scale up	Slow Toxic solvent used Cost energy for solvent recovery
Supercritical CO_2	Fast Selectivity for target lipid Green solvent used	Energy intensive Hard to scale up
Ionic Liquid Extraction	Tunable solubility Low vapor pressure High yield	Toxicity Expansive Hard to scale up

CHAPTER 2

PERIODIC SYMMETRY DEFINED BIOREACTORS ENHANCE ALGAE GROWTH

Abstract

Here we explore a new, highly scalable bioreactor design for photosynthetic, lipid producing organisms. Microalgae derived oils have the potential to become an important source of transportation fuels, but current photobioreactor designs are not readily scalable. Here we evaluate the productivity of periodic designs that use repeated unit cells defined by fluid dynamically driven recirculation profiles so that scale up may be achieved simply by increasing (massively) the number of unit cells. We construct photobioreactors with one, seven, and nineteen unit cells containing 13.2, 92.4, and 251 gal, respectively, to demonstrate scalability. Development of a kinetic growth model accounting for variations in photo intensity versus depth predicts approximately linear (instead of exponential) growth as observed in the first week of productivity. This design decreases the required power per volume by over 80% compared to paddlewheel designs, and material costs per unit cell decrease with increasing reactor size, because flow symmetry defines the boundaries of the unit cells in the absence of internal material walls. These results provide a more efficient path to scale up to commercially relevant acreage.

Introduction

Although renewable energy sources play a significant role in stationary energy production, generating high energy density transportation fuels from renewable sources that do not compete with the food supply remains challenging. Photosynthetic microorganisms (e.g., microalgae) have been investigated over past decades as a potential solution. Yet, critical engineering challenges remain that limit the economic viability of transportation fuel production from these sources. For example, state-of-the-art reactors remain difficult to scale up. Although more productive than large stagnant pools, paddlewheel driven raceways are inherently limited in their scalability, have moving parts, and remain significantly more expensive than open ponds. Therefore, demonstrating scalable photobioreactor designs remains critical to the future of microalgae as a potential fuel source, although microalgae are used commercially already for higher values pharmaceutical and nutriceutical products.

Here we evaluate a new photobioreactor design that is inherently scalable. Inspired by the periodic fluid recirculation patterns of the well-known Rayleigh-Benard instability (i.e., thermally driven recirculation patterns that develop when a lower surface is heated) [158], we use forced flow from pumps to guide fluid recirculation within unit cells as seen in Figures 2.1-2.2.

Each unit cell, as in the instability, is defined by the fluid flow profile. Fluid, initially entering the unit cell vertically (downward), impinges on the floor of the reactor before flowing laterally as required by the continuity equation. Lateral flow then collides with flow from neighboring cells at planes of symmetry, where continuity again demands that the fluid move upward before being picked up by a fluid intake. The pump re-

pressurizes the fluid before sending it back into the reactor. This process retains the symmetry of the inlet/outlet system, here hexagonal, and allows the internal walls to be completely removed because the fluid forces alone preserve the hexagonal symmetry.

In the remainder of this article, we first evaluate the scalability of this photobioreactor by considering algal biomass productivity from reactors with consecutive rings containing one, seven, and nineteen unit cells (Figure 2.1b). We then evaluate the influence of fluid depth and present a growth model that varies the photon availability as a function of depth and algae concentration to explain the approximately linear growth observed in the first week of productivity. We finally compare the energy consumption of these reactors to paddlewheel systems.

Materials and Methods

Reactor Configuration

Each reactor (Figure 2.1c) was composed of multiple unit cells with hexagonal sides (0.225 m long, 0.495 m depth) selected to be characteristic of typical paddlewheel photobioreactors. Hexagons were chosen because they are the lowest energy solution to the unbounded Rayleigh-Benard problem that remains space filling [158-160]. Three reactor sizes were constructed consisting of 1, 7, or 19 unit cells in consecutive rings for culture volumes of 50 L, 350 L, and 950 L, respectively, when filled to 0.38 m (Figure 2.1b). The outer edges and floor of the reactor (bold in Figure 2.1b) were constructed out of acrylic due to facilitate visual observation. For the 19 unit cell reactor, flat sheets (7 ft by 3 ft by 0.25 inch) of acrylic were joined using number three acrylic binder (Smarter

Adhesive Solutions, IPS, CA) with external shims (7 ft by 0.5 ft by 0.25 inch) to prevent junction leaks.

The structure of the flow was governed by strategic placement of the inlet and outlet tubes (see Figure 2.1). Each unit cell included an inlet tube (inner diameter 0.50 inches=0.0127 m) placed at the center of each hexagon 0.05 m above the floor with a flow rate governed by control valves upstream of the inlet tube. An outlet tube (also 0.50 inches in inner diameter) was placed immediately next to the inlet tube but raised to 0.10 m below the liquid level of the reactor regardless of vessel fill level.

For the single unit cell reactor, circulatory flow was driven by a 45 W pump (NH-50PX-X, Pan World Co., Japan). For larger reactors, one (7 cell) or two (19 cell) 250 W pumps (K55MYJDH-9025, US motors) were used to drive flow into manifolds connected to multiple inlet tubes. A similar manifold collected outlet flows for recycle. Pump flow rates were determined by connecting the pump outlet to a 5 gal water container (Home Depot, Model # 05GLHD2, Atlanta, GA) via a flexible tube and determining the volume increase over 30 s. Because 18 L/min per nozzle was the maximum flow rate achieved by the pumps driving the 19 cell reactor, the pumps for the single and seven-cell reactors were turned down to match flow rates of the 19 cell reactors by tuning the fraction of the pump flow that loops directly back to the pump bypassing the reactor (see Figure 2.2c). Energy consumption was recorded using a power meter (P4400.01, Intertek, London, UK).

The reactors were lit by 48 W artificial fluorescent light bulbs placed on top of the reactors (Philips, Andover, MA). Surface light intensities of four points around each unit cell were measured using a lux meter (LX1330B, Dr. Meter, PA). The average light

intensities at the fluid surface for 1, 7, and 19-cell reactors were 3975, 4421, and 3685 lux. All of the reactors were set in the indoor environment at ambient temperature (set to 24^{o}C), whereas the reactor temperature fluctuated between 26^{o}C and 29^{o}C due to pump generated heat. Three reactor fluid depths 20 cm, 29, and 38 cm (default), suggested by typical paddlewheel driven raceway depths of 10-40 cm [161-164] were tested in single cell reactors at otherwise constant conditions including liquid circulation rate, the initial concentration of algae seed culture, nutrient concentrations, light intensity, and temperature. Each case was repeated in triplicate. Due to the coverless design, water evaporated from the reactor at an average rate of approximately 1.3 L/day/unit cell. To maintain constant culture volume, fresh water was added to each reactor each day prior to sampling over each two week test for all photobioreactors.

Microalgae

Microalgae (*Synechococcus Elongatus*) were derived from stock provided by Utah State University, courtesy of Lance Seefeldt [165]. At the beginning of each run, concentrated seed algae culture (1.40 L/unit cell at 0.404±0.007 g/L for net concentration of 0.015±0.006 g/mL after dilution)) from prior runs with an optical density (OD) of 15.5±0.5 measured using a spectrometer (Spectronic 21D, Bausch & Lomb, Rochester, NY) at 650 nm with a 1.00 cm path length was transferred to the reactor with nutrient culture consisting of Miracle Gro® water soluble all purpose plant food 24-8-16 (Marysville, OH) in fresh local tap water at a concentration of 400 mg/L containing 24% nitrogen and 8% phosphate in weight. This composition provided better growth of this

species than more traditional formulations considered. Nutrients were added at the beginning of each run and were not supplemented during the two-week long runs.

The optical density, dry biomass, and cell number were tracked to determine algae growth rates. Three 50 mL centrifuge tubes samples were taken from the middle (laterally and vertically) of each reactor each day and stored at 4^{o}C. Algae adhering to reactor sidewalls were scraped off before sampling. The optical density of these algae suspensions was measured using the same spectrometer and settings as above. Dry biomass was obtained by weighing after the algae samples were first centrifuge at 7400 rpm with rotor F-35-6-30 (Eppendorf 5430R, Hauppauge, NY) for 1 h. The supernatant clear phase was discarded and the bottom paste was collected and dried (Thermo Scientific, Model 6263) overnight at 60^{o}C. The weight after drying was divided by the original sample volume to determine the algae dry biomass concentration.

Modeling Aspects

Model for Microalgae Growth

For phototropic organisms in well mixed nutrient suspensions, the photon intensity governs cell growth and varies as a function of photobioreactor depth. If well mixed algae, sample photons from the entire reactor depth, and receive light only from the top surface, then the Beer-Lambert law,

$$I = I_o e^{-\varepsilon c z}, \tag{2.1}$$

determines how the photon intensity I varies with vertical position z, where I_o is the upper surface intensity, c is algae suspension concentration in grams per liter, and ε is an

attenuation coefficient determined from UV-vis absorbance, A, using $A=\varepsilon c l$ with l as the spectrophotometer's path length. The average intensity may be determined by integration

$$\bar{I} = \frac{1}{\tau}\int_{t=0}^{t=\tau}\frac{1}{H}\int_{l=0}^{l=H} I_o e^{-\varepsilon c z} dz dt, \tag{2.2}$$

where τ is the time over which the average is taken and H is the depth of fluid in the photobioreactor. In a laboratory environment, the photon intensity remains time invariant, so only averaging over the reactor depth remains necessary. Integrating then finds

$$\frac{\bar{I}}{I_o} = \frac{1-e^{-\varepsilon c H}}{\varepsilon c H}. \tag{2.3}$$

In the initial phase of algae growth, the growth rate is linearly proportional to both the average light intensity and concentration as

$$\frac{dc}{dt} = k\bar{I}c, \tag{2.4}$$

where k is a constant of proportionality, and $k\bar{I}$ becomes the effective rate constant now that depends on reactor depth [166]. Substituting the average light intensity and integrating finds

$$c = \frac{1}{\varepsilon H} ln[1 + (e^{\varepsilon c_o H} - 1)e^{k I_o t}], \tag{2.5}$$

with $c = c_o$ at $t = 0$ s. In the limit of thin reactors where H vanishes, L'Hospital's rule recovers

$$c = c_o e^{k I_o t}. \tag{2.6}$$

The biomass productivity may be estimated from this concentration. The total dry biomass production rate per unit area, $(dm/dt)/A$, becomes

$$\frac{1}{A}\frac{dm}{dt} = \frac{V}{A}\frac{dc}{dt} = \frac{k I_o}{\varepsilon}\frac{(e^{\varepsilon c_o H}-1)e^{k I_o t}}{1+(e^{\varepsilon c_o H}-1)e^{k I_o t}}, \tag{2.7}$$

after some algebra, where A is the bottom area of reactor and V is the volume of reactor. The second fraction ranges between 0 and 1, showing that the growth rate saturates at large depths and times, and the production rate becomes linear in photointensity.

Power Consumption

Conceptually, the electrical power consumption of the pump may be calculated as

$$\dot{P} = \frac{Q\rho g h_L}{\eta}, \tag{2.8}$$

where Q is the volumetric flow rate through the reactor, ρ is the liquid density of algae culture, h_L is the total head loss, g is earth's gravitational acceleration, and η is the pump efficiency (assumed to be 70% [167]). The head loss may be divided into friction losses in the piping system, h_f, and friction losses in the reactor, h_R, as

$$h = h_f + h_R. \tag{2.9}$$

The friction loss in the pipe system may be calculate by Darcy-Weisbach Equation,

$$h_f = \frac{f_D L v^2}{2Dg}, \tag{2.10}$$

where L is the length of pipe, d is the inner diameter of pipe, v is the fluid velocity, and f is Darcy's friction factor calculated by the Colebrook-White equation [168, 169],

$$\frac{1}{{f_D}^{0.5}} = -2\log_{10}\left(\frac{2.51}{\mathrm{Re}{f_D}^{0.5}} + \frac{k_r}{3.7 d_p}\right), \tag{2.11}$$

where Re is the pipe Reynolds number, k_r is roughness of pipe, and d_p is the inner diameter of the pipe. The pressure drop cause by collisions of the algae with the surface of the pipe may be neglect safely due to the sufficiently dilute concentration. The energy losses in bends and fittings were combined into h_f using an equivalent length

approximation (e.g., a one inch 90° elbow bend is equivalent to 5.2 in. of one inch pipe) [170, 171].

The friction loss in the reactor includes friction due to jet flow across the floor and sidewalls. The friction loss along the bottom can be calculated by

$$W_S = \int_S (\boldsymbol{\tau} \cdot \boldsymbol{n}) \cdot \boldsymbol{v} dS \tag{2.12}$$

where dS is the differential surface area, $\boldsymbol{v}$ is the velocity vector, $\boldsymbol{n}$ is the normal to the surface, and $\boldsymbol{\tau}$ is the deviatoric stress tensor. In cylindrical coordinates, the normal vector points in the vertical z direction as is $\boldsymbol{n} = \boldsymbol{e}_z$ and the relevant shear stress is $\boldsymbol{\tau} = \tau_{rz}\boldsymbol{e}_r\boldsymbol{e}_z$, where $\boldsymbol{e}_i$ is the unit vector in the i^{th} direction. Then

$$W_S = \int_S \tau_{rz} v_r dS, \tag{2.13}$$

where v_r is the velocity in the radial direction and integration proceeds over each hexagon. The shear stress may be written in terms of a skin coefficient, c_f, as

$$\tau_{rz} = \frac{1}{2} c_f \rho v_{r,m}^2, \tag{2.14}$$

where $v_{r,m}$ is the maximum velocity in the vertical profile of the radial direction given as

$$v_{r,m} = \frac{h_r U_o d_o}{r}, \tag{2.15}$$

where h_r is a velocity-decay constant. Beltaos asserts h_r = 1.1 and gives the skin coefficient of friction for radial wall jets as [172, 173]:

$$c_f = 0.098 \mathrm{Re}_o^{-1/5}. \tag{2.16}$$

This jet Reynolds number, Re_o, is given by

$$\mathrm{Re}_o = \frac{\rho U_o d_o}{\mu}, \tag{2.17}$$

where U_o is the nozzle velocity, d_o is the nozzle diameter, and μ is the suspension viscosity. Each hexagonal area of integration may be divided into 12 symmetric triangles

such that the radial limit of integration depends on θ with

$$W_S = 6c_f \rho h_r^3 U_o^3 d_o^3 \int_0^{\pi/6} \int_{d_o/2}^{s/cos\theta} \frac{1}{r^3} r dr d\theta, \tag{2.18}$$

where s is the shortest distance between the center of the hexagon and the nearest edge. Here v_r is evaluated as $v_{r,m}$ (an overestimate) and radial integration begins at the $d_o/2$ (a smaller underestimate) so that the radial velocity does not exceed the nozzle velocity. Integrating twice gives

$$W_S = 6c_f \rho h_r^3 U_o^3 d_o^3 \left[\frac{\pi}{3d_o} - \frac{1}{2s}\right]. \tag{2.19}$$

For N unit cells after substitution of the skin coefficient of friction, the rate of energy loss as a positive value is

$$W_S = 0.588 N \mu^{0.2} \rho^{0.8} h_r^3 U_o^{2.8} d_o^{2.8} \left[\frac{\pi}{3d_o} - \frac{1}{2s}\right] \tag{2.20}$$

for N unit cells. The head loss due to the friction loss in the reactor then becomes

$$h_R = \frac{W_S}{Q\rho g}. \tag{2.21}$$

In the limit of large reactors where the reactor height remains much smaller than the reactor area, only the bottom friction remains.

Power Consumption for Raceway

For comparison, Ketheesan and Nirmalakhandan estimate the power required for the paddlewheel driven raceway operation as

$$\dot{P}_p = \frac{C_D \rho A_p v_p^3}{2}. \tag{2.22}$$

where C_D is the paddlewheel drag coefficient (typically 1.2 to 1.8), A_p is the paddlewheel projected area in the direction of motion, and v_p is the velocity of paddlewheel relative to

water (assumed to be 0.3 by Ketheesan and Nirmalakhandan) [174, 175].

Results and Discussion

The essential feature of this photobioreactor is its periodic design defined by fluid dynamic symmetries instead of physical walls (see Figures 2.1-2.2). Figure 2.1c considers an algae suspension flowing downward from the inlet tube and spreading out along the floor of the reactor until flow approaches a midpoint between two adjacent inlet tubes where continuity forces the fluid up and the along the symmetry boundary to the upper interface. In this manner, a frictionless symmetry boundary replaces an internal wall. An outlet tube then conveys the suspension through a pump, which then drives the suspension back into the photobioreactor. Because convection exceeds diffusion for these cellular suspensions (i.e., the Peclet number is large), each unit cell is effectively isolated from adjacent unit cells (except in the manifold and pump) so that each acts as an independent (but synchronized) constantly stirred tank reactor (CSTR) and scale up proceeds by numbering up, similar to microfluidic systems. However, our reactors remain much larger with unit cells O (10^{-1}-10^{1} m) in characteristic length, facilitating rapid scale up to industrially relevant areas and volumes. In this manner, symmetry defined photobioreactors naturally overcome perennial scale up challenges associated with scale dependent flow regimes and mixing.

This design was inspired by the well-known Rayleigh-Bérnard convection cells [158]. This flow pattern develops from heating a surface below a fluid layer so that fluid adjacent to the surface becomes less dense than fluid above. The fluid is unstable to periodic disturbances that allow less dense fluid to rise with the periodicity defining the

length of the convection cell. In three dimensions, the unit cells adopt a hexagonal configuration to minimize energy [158-160, 176, 177]. Here we replace thermally driven natural convection with pump driven forced convection, retaining the hexagonal arrangement to minimize the energy required.

In the remainder of this article, we first evaluate the hypothesis that this reactor design is scalable simply by increasing the number of unit cells. To evaluate this hypothesis, we compare algal biomass productivity from reactors with consecutive rings containing one, seven, and nineteen unit cells (Figure 2.1). Development of a phototropic growth model that accounts for variations in photo-intensity facilitates comparison and permits prediction of optimum photoreactor depths for various light conditions. We finally compare the power required to operate these photoreactors to traditional paddlewheel designs.

Scalability

We now evaluate this hypothesis qualitatively and quantitatively. Figure 2.3a presents the algae biomass concentration versus time for photobioreactors containing one, seven, and nineteen unit cells. In each case, the initial concentration of biomass begins at 0.015±0.006 g/L and increases over time with constant light exposure. Qualitatively, the growth curves for each reactor size overlap substantially. The panel presents measurements in triplicate with error bars as one standard deviation. Table 2.1 further evaluates whether the average biomass concentrations from the three reactors arise statistically from the same population through the use of a single factor (one-way) ANOVA test. If the populations are different then we must reject the null hypothesis (H_o:

$\mu_1=\mu_7=\mu_{19}$, where μ_i represents the sample mean and i represents the number of unit cells, and H_1: at least one mean remains different from the others). The hypothesis is rejected when our p-value remains less than a significance value of $\alpha=0.05$. This interpretation of this approach is from engineering perspective and may not be consistent with interpretation as statistic analysis. Therefore, other method should be utilized to analysis this data.

Review of Table 2.1 shows that each p-value remains larger than 0.05 (except for day 10, which remains close to this value), confirming that the populations are indeed the same within the available data. Therefore, this analysis affirms that the productivity per unit cell is essentially the same for each of the three reactor sizes in support of our governing hypothesis that this photobioreactor design is scalable simply by increasing the number of unit cells.

Model for Microalgae Growth

Careful review, however, shows that within this variation, the productivity does rise marginally faster for the seven cell reactor (circles in Figure 2.3a). This may be due to a somewhat higher average light intensity in the seven unit cell reactor. The photon intensity measured at the fluid surface is $3.9 \cdot 10^3 \pm 2.4 \cdot 10^3$, $4.4 \cdot 10^3 \pm 1.4 \cdot 10^3$, and $3.7 \cdot 10^3 \pm 1.3 \cdot 10^3$ lux for the three reactors from smallest to largest, respectively (sidewall intensities are an order of magnitude smaller). To evaluate the influence of variations in photon intensity across reactors, we constructed a model that accounts explicitly for photon intensity as a function of depth. Our model averages variations in photon intensity described by the Beer-Lambert law, because the algae sample photon intensities across

the vertical depth of the reactor as they circulate through the volume of the unit cell. Our model employs the traditional first order rate law but partitions the rate constant into contributions from the average photon intensity and other sources. Without this partitioning, the model simply returns the exponential or so called log growth expected of photobioreactors. However, with this partitioning, the growth rate more closely follows linear growth than exponential growth (see Equation 2.6). This unexpected consequence results because increases in concentration decrease the average light intensity, which in turn lowers the growth rate. Remarkably, the experimental data in Figure 2.3 observe the same approximately linear growth predicted by the model until the end of the growth phase between days seven and ten, when growth tapers off.

We hasten to note that many smaller photobioreactors would not observe this decrement in growth rate. Indeed, in the limit of very thin reactors, our model returns the traditional exponential growth usually anticipated (see Equation 2.7). We also recognize that these results for *S. Elongatus* were not optimized for either biomass or lipid production but were collected to evaluate scalability. Other algae species, nutrient compositions, and environments may provide different growth rates than the ones presented here. For example, optimizing the algae species may improve the value of k and performing the experiments in outdoor solar radiation could substantially increase the productivity levels through an increase in I_o (at least until photon saturation). Indeed, the photobioreactor presented herein provides a scalable platform that may be used to optimize the productivity of a variety of traditional and emerging algae strains.

Effect of Reactor Depth

Because variations in photon intensity as a function of depth comprise a key feature of our phototropic growth model, we further evaluate productivity at three fill levels of 20, 29, and 38 cm in the single cell photobioreactor. By comparison, typical depths of paddlewheel driven raceways range from 10-40 cm [161-164]. Figure 2.3b displays the biomass concentration as a function of time for each of the three heights. The figure shows that reactors with shorter light paths increase in biomass concentration more quickly. This observation in isolation motivates development of ever thinner photobioreactors.

However, the biomass produced is the product of both the concentration and the volume, which increases linearly with the reactor depth. These competing effects are evaluated in Figure 2.4, which considers the rate of biomass produced as a function of time. Figure 2.4a shows that the rate of biomass production increases monotonically with reactor height indicating that volume increases trump concentration increases. This finding gives new impetus to the development of deeper photobioreactors operating on more concentrated algal suspensions instead of shallower systems anticipated from concentration alone. However, the optimal reactor height quickly asymptotes suggesting that reactor depths much larger than approximately one meter may not lead to additional biomass productivity. Essentially light only penetrates so far such that increases in reactor height lead to ever smaller decreasing marginal returns. Figure 2.4b considers the additional productivity anticipated at typical solar photon intensities of approximately 25000 lux. The figure shows that the biomass production rate is nearly an order of magnitude larger out of doors than in doors. The model also indicates that at very high

photon intensities the biomass growth rate becomes linear in time, photon intensity, and rate constant, and the influence of reactor depth vanishes as a governing factor.

In this limit, the rate of change in biomass concentration remains inversely proportion to reactor depth but the biomass growth rate per area depends linearly on reactor depth so that this factor cancels in the absence of photon saturation effects outside the scope of this article. Given the push to intensify biomass production to achieve energy parity for biofuels derived from microalgae sources, deeper reactors operating at higher concentrations remain increasingly likely in practice, making this approximately linear model more useful than simple exponentials achieved by rather small reactors.

Power Consumption

Finally, we compare the energy required to operate these reactors versus paddlewheel systems. Table 2.2 presents a comparison of the energy required for the two systems. The energy requirements for the paddlewheel systems parallel those presented by Ketheesan and Nirmalakhandan accounting for paddlewheel losses.

We estimate the energy consumption based on a typical 70% pump efficiency accounting for frictional losses in the piping and in the photobioreactor. Measurements from our experiments found that the single cell photobioreactor consumes much more power (108 W) per unit cell than the seven (83.6W) and nineteen (59.5W) cell photobioreactors. This is in large measure due to the low pump efficiencies of 2.1% and 16.2% for the pumps for the single cell and larger cells photobioreactors, respectively. In industrial practice a 70% pump efficiency remains quite reasonable and on this basis, our photobioreactors consume at least 80% less than the traditional paddlewheel driven

raceway. That our photobioreactors may be more optimal is not particularly surprising given that typically higher efficiencies of pumping systems and the direct elimination of interior walls using symmetry boundaries instead.

Acknowledgements

We recognize support from the University of Utah Undergraduate Research Opportunities Program (UROP). We acknowledge Rete Browning, Ian Walton, Mason Burger, Anthony Oyler, Brad Wahlen, and Lance Seefeldt for enlightening conversations and Drew Hugentobler, Anna Carter, and Chad Hunsaker for assistance with preliminary prototypes.

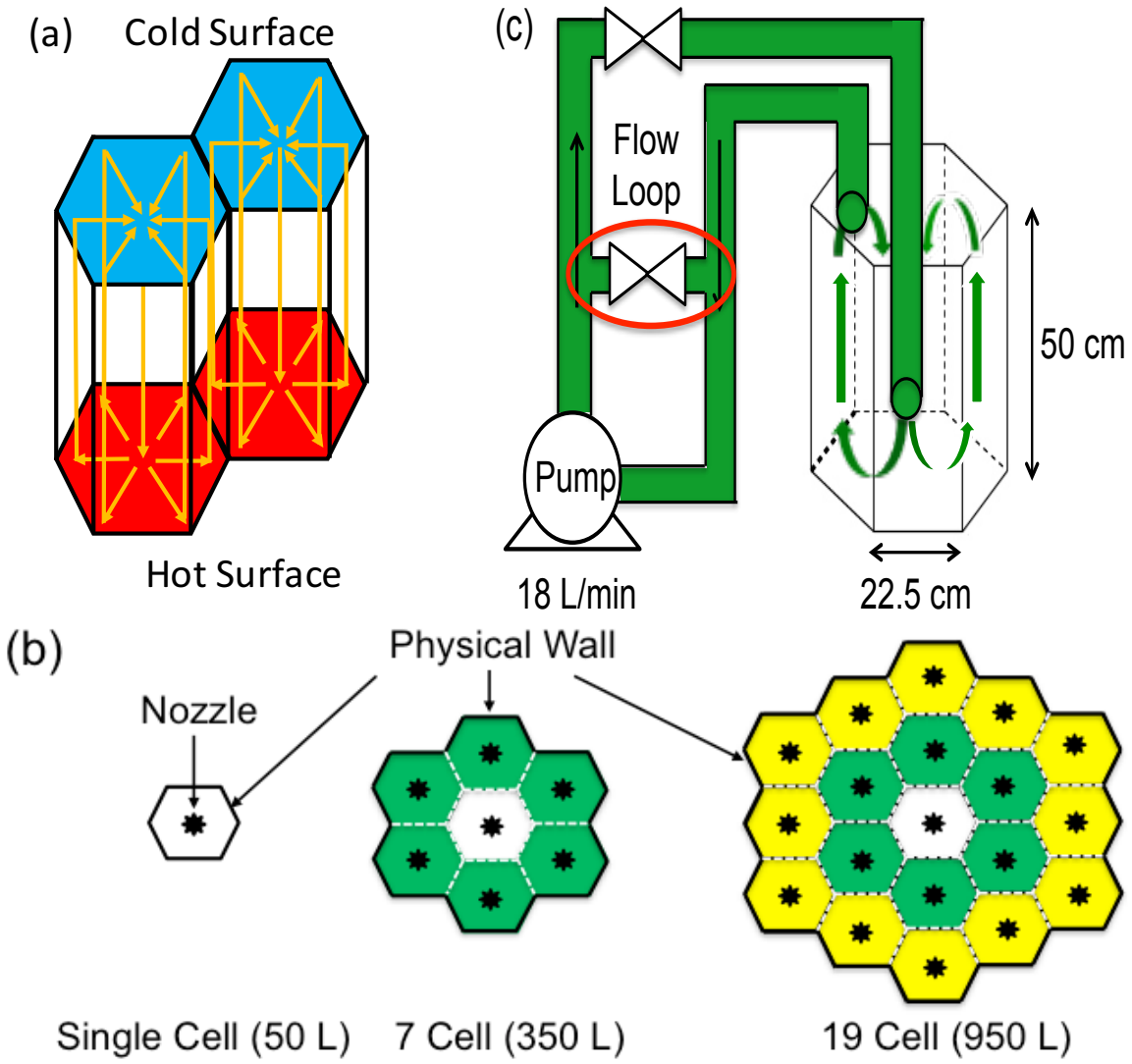

Figure 2.1. (a) Rayleigh-Bérnard natural convection cells form by heating the bottom plate to generate a density gradient that induces periodic turnover of fluid. Adapted with permission of Yehao Deng et. al [178].(b) Top-view of photobioreactor containing consecutive rings of one, seven and nineteen unit cells inspired by Rayleigh-Bérnard convection and evaluated herein. Nozzles are represented by stars, internal symmetry boundaries are dashed and external walls are solid and black. (c) Diagram of single unit cell photobioreactor with pump and flow loop.

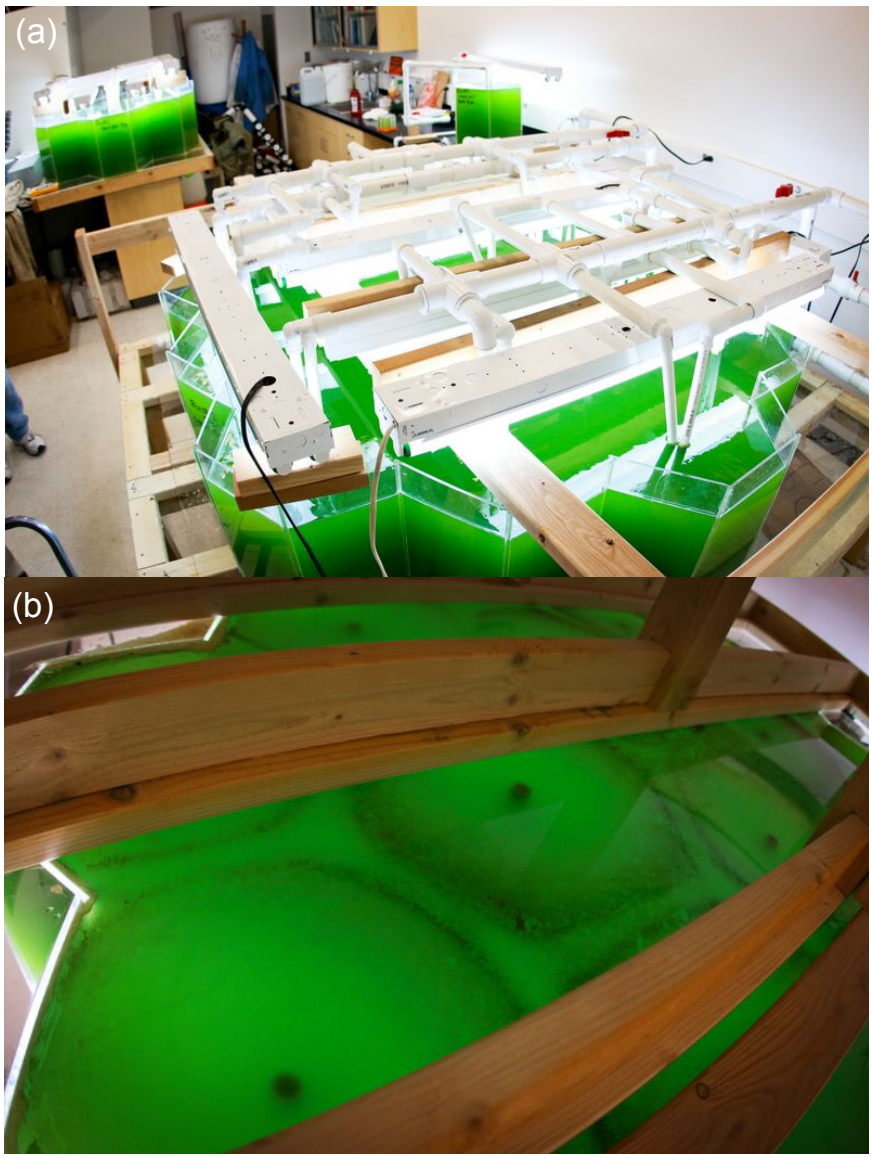

Figure 2.2. (a) Digital image of PSDBs with a single cell reactor at the top center right, a seven cell reactor at the top left, and a nineteen-cell reactor at the bottom. The piping system and light are placed on the top of reactors. There is no internal wall in seven and nineteen reactor as shown in the picture. (b) Under view of nineteen cell photobioreactor and wooden supports with outer wall in white. The algae settled near stagnation zones associated with planes of symmetry, forming hexagon deposition patterns in the absence of internal material walls. Images courtesy of Dan Hixom, University of Utah College of Engineering.

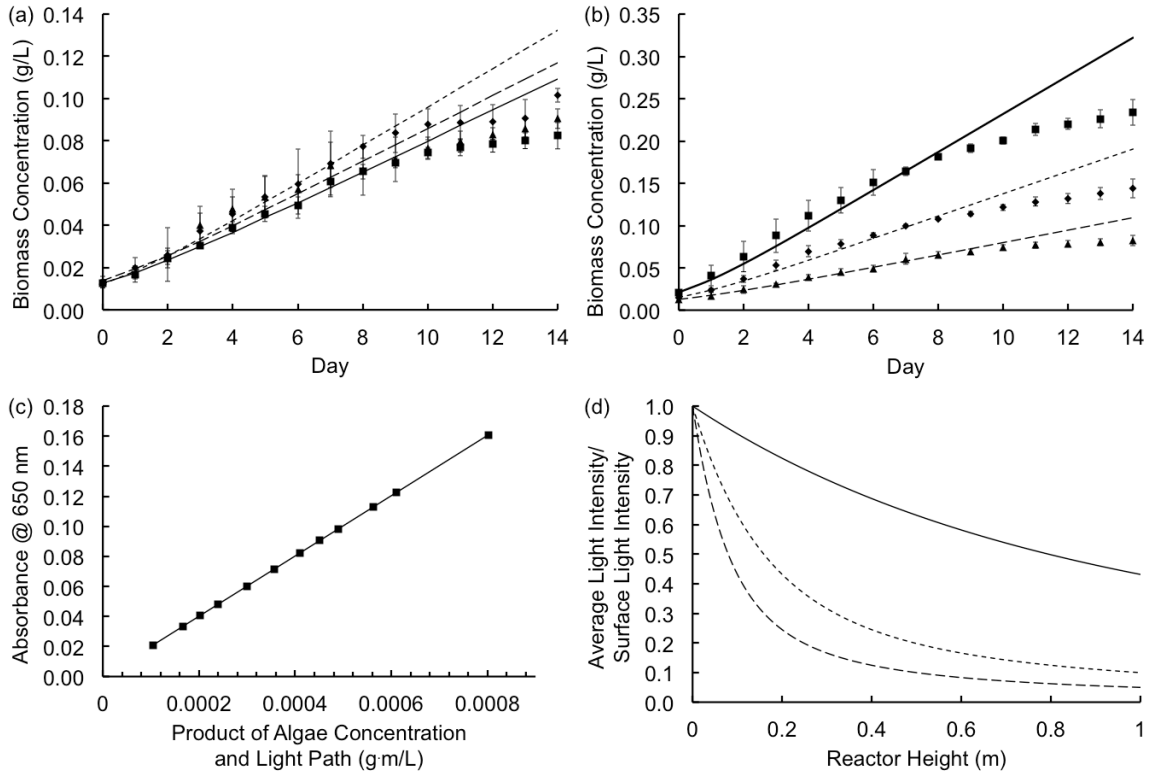

Figure 2.3. (a) Biomass concentration versus time for single unit cell (square, solid), seven cell (diamond, short dash), and nineteen cell (triangle, long dash). Data fit with growth model over the first nine days using Equation 6 with H = 0.38 m; c_o = 0.013 (single cell), 0.012 (seven cell), or 0.014 (nineteen cell) g/L; ε = 200.6 m^2/kg as in panel c; I_o = 3975 (single cell), 4421 (seven cell), or 3685 (nineteen cell) lux, and $k = 1.41 \cdot 10^{-4}$ (single cell), $1.56 \cdot 10^{-4}$ (seven cell), or $1.61 \cdot 10^{-4}$ (nineteen cell) 1/(s·lux) using only k as a fitting parameter. Error bars represent one standard deviation. (b) Biomass concentration versus time in the single cell filled to 0.38 (triangle, long dash), 0.29 (diamond, short dash), or 0.20 m (square, solid). Data fit with growth model over the first nine days using Equation 6 with c_o = 0.021 (H = 0.20 m), 0.015 (H = 0.29 m), or 0.013 (H = 0.38 m) g/L; ε = 200.6 m^2/kg as in panel c; I_o = 3975; and $k = 2.26 \cdot 10^{-4}$ (H = 0.20 m), $1.92 \cdot 10^{-4}$ (H = 0.29 m), or $1.41 \cdot 10^{-4}$ (H = 0.38 m) 1/(s·lux) using only k as a fitting parameter. Error bars represent one standard deviation. (c) Absorbance versus product of algae concentration and light path (1.00 cm) so that slope returns ε = 200.6 m^2/kg with R^2 = 1.000 from Equation 2. (d) Ratio of average light intensity to surface light intensity versus reactor height for three algae concentrations of 0.01 (solid), 0.05 (short dash) and 0.10 g/L (long dash) with ε = 200.6 m^2/kg from fit of panel c.

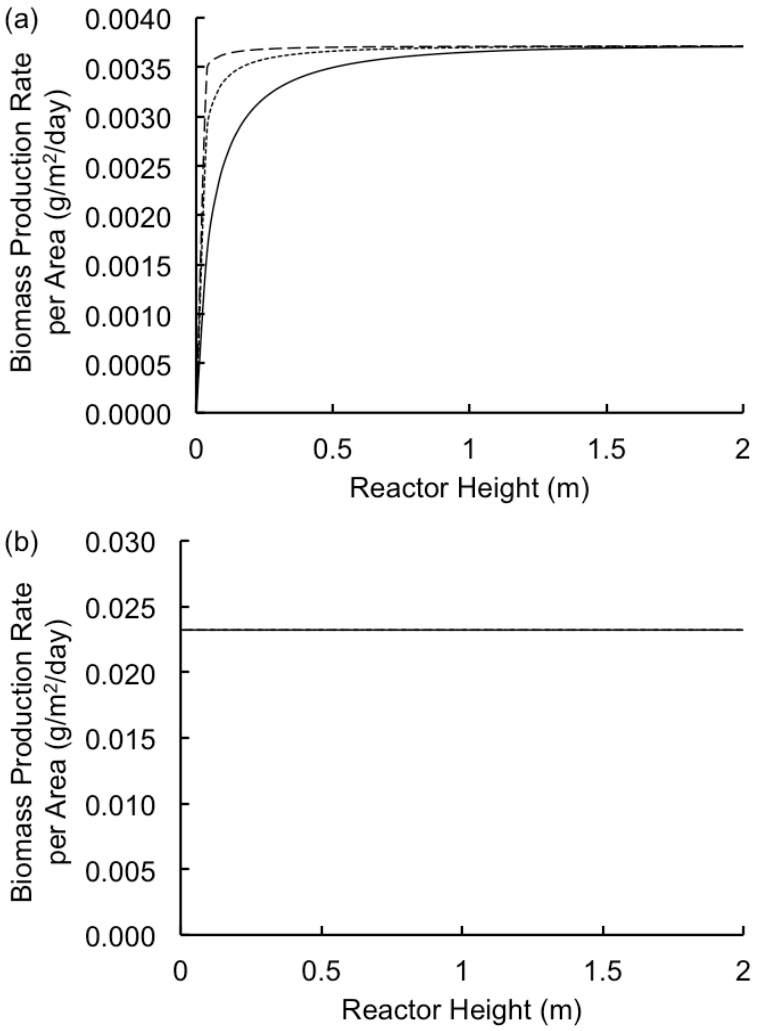

Figure 2.4. Algal biomass production rate (at days 3 (solid), 7 (short dash), and 10 (long dash)) at surface photon intensities of (a) 4000 lux and (b) 25000 lux versus reactor height predicted by growth model for $\varepsilon = 200.6$ m^2/kg, $c_o = 1.00 \cdot 10^{-2}$ g/L, and $k = 1.86 \cdot 10^{-4}$ lux^{-1}day^{-1}. All three curves in panel b overlap and start from zero.

Table 2.1. Statistical evaluation of biomass production.

Day	*p*-value
1	0.596
2	0.963
3	0.298
4	0.368
5	0.440
6	0.503
7	0.736
8	0.195
9	0.155
10	0.046
11	0.104
12	0.139
13	0.203
14	0.067

Table 2.2. Theoretical power consumption of symmetry defined bioreactors versus and raceways.

Energy required of symmetry defined bioreactor (W/L)[1]	0.0375
Energy required of raceway (W/L)[2]	0.230-0.345
Energy savings (%)	83.7-89.1

1. For 50.0 L/unit cell with side length of 0.225 m and H = 0.380 m without material sidewalls. Piping system includes 0.500 m of one inch tubing, 0.700 m of half inch tubing, and two 90^o elbow fittings all of PVC with $k_r = 5{\cdot}10^{-6}$ [179]. Each one in. 90^o elbow bend equivalent to 5.2 ft of one inch pipe. [13][14]. Pumping system operates at Q = 1.08 m^3/h, h_L = 0.477 m, and h = 70.0%.
2. Paddlewheel raceway volume of 21.2 L from depth of 0.150 m and area of 0.131 m^2. Power loss calculation from C_D = 1.20-1.80, A_p = 0.080 m^2 from Ketheesan and Nirmalakhandan, $V_{raceway}$ = 0.200 m/s, n = 0.0008, L_R = 1.34 m, R = 0.0569 m.

CHAPTER 3

ALGAL LIPID EXTRACTION USING CONFINED IMPINGING JET MIXERS

Abstract

Here we show that confined impinging jet mixers (CIJMs) improve lipid extraction from microalgae. CIJMs turbulently mix organic solvent into algae suspensions driven by gear pumps pairs to create linear pulse-free impinging flow ($160 \leq Q \leq 1280$ mL/min). The highly turbulent flow ($0.7 \cdot 10^4 \leq \mathrm{Re} \leq 5.4 \cdot 10^4$) shrinks the Kolmogorov length between algae cells and organic solvent down to ≥0.70 μm, facilitating lipid diffusion and increasing lipid yield. CIJM extraction operates at room temperature and completes rapidly (residence time ≥0.0079 s). Lipid extraction from *Synechococcus Elongatus* into hexane obtains yields of 25.6±2.7% (lipid biocrude/biomass) by weight similar to the performance of Bligh and Dyer methods using stronger chloroform and methanol solvent cocktails (25.7±1.3%) but much faster. Experiments show that the lipid yield does not vary with the concentration of algae feedstock in the tested algae concentration range (3.6-13.3 g/L), which implies that matured algae culture from photobioreactors may be used directly as feedstock to CIJM without intervening dewatering steps. Algal biocrude obtained from CIJM converts successfully into biodiesel, and cascades of CIJMs may be used to increase the net lipid

production. CIJMs provide fast and high yield lipid extraction, suggesting compelling opportunities to use CIJMs for extraction generally.

Significance Statement

Confined impinging jet mixers (CIJMs) extract lipid from microalgae rapidly and continuously. The algae suspension and organic solvent turbulently mix due to confined impingement at high speed. Lipid mass transfer between cells and the organic solvent is unusually rapid because turbulent shear cleaves cell walls and membranes, and the turbulence reduces the characteristic length scale for diffusion to the Kolmogorov length scale. Lipid extraction is accomplished in less than a second. These results demonstrate the potential to use these mixers as an essential element in multistage unit operations as an essential step in algae biofuel production.

Introduction

Algae derived fuel, one of the most promising alternative fuels, has generated increasing attention due to elevated fuel and food demand and persistent air pollution. As algae grow, they capture photons and CO_2 and convert them into lipid via photosynthesis [1, 2]. Unlike fossil fuel, algal biofuel may be nearly carbon neutral (i.e., CO_2 emitted by burning algal fuel may approximate CO_2 captured during the cultivation). Unlike first generation biofuels, which use food crops as fuel sources (e.g., corn), algae may be grown on nonarable land and with saline water, wastewater, or/and produced water from mineral and petroleum extraction [9, 10]. Furthermore, unlike second-generation biofuels, which use lignocellulose biomass and suffer from complicate harvest steps,

algae have simpler cell structures and produce more lipids per harvestable area. Additionally, the growing cycle of microalgae is at most 7-14 days, short compare to other annual crops [1]. These features make algae a competitive candidate as a biofuel source.

However, technological and economic barriers to industrial scale-up remain. Algae harvesting ranks among the main challenges. Traditional organic solvent methods remain slow and suffer from the low yields and production rates [103]. Supercritical carbon dioxide methods require elevated operating temperatures and pressures, which translate into substantial energy requirements and challenge scale up [103]. Furthermore, dewatering poses another challenge to algae harvesting. Traditional algae harvesting methods usually require dry algae powers or at minimum highly concentrated algae suspensions, which introduces additional energy intensive steps into the algae processing flow sheet, a significant drawback for algal fuel production [180]. Therefore, the need for better lipid extraction technology remains.

Where mass transfer limits the rate at which lipids transfer, confined impinging jet mixers (CIJM) show promise. These devices drive two or more turbulent jets coaxially into a confined mixing chamber (see Figure 3.1) [181, 182]. Although microscale devices, they do not suffer from the slow laminar mixing of microfluidics, because rapid turbulent energy dissipation promotes microscale mixing to accelerate molecular scale processes [183, 184]. Due to the high inlet flow rate and relatively small mixing chamber, the residence time within CIJMs remains small yet the flow structure ensures that feed streams mingle intimately [181]. Furthermore, CIJMs have been used

in continuous processing of nanoprecipitation, nanomedicine, and nanoparticles production at industrially relevant scales and rates [185-188].

Here we critically evaluate the potential of CIJMs for lipid extraction. The inlet flows consist of a concentrated algae suspension (0.03-0.13 wt% biomass) and a modest organic solvent (hexane). As the streams turbulently mix, the algae distort and shear permitting lipid release, and the highly turbulent energy dissipation shrinks the Kolmogorov length [181], dramatically decreasing the time scale required for lipid diffusion from algae cells to the organic solvent (see Figure 3.1). In the remainder of this article, we explore the parameters that govern lipid extraction in CIJMs. We evaluate the influence of inlet flow rates and solvent-to-algae-biomass ratios. We propose a mathematical model for algal lipid extraction based on Kolmogorov length scale reduction. Yields from the CIJM using hexane, a weak solvent, are compared to a modified Bligh and Dyer method using a stronger solvent cocktail, and yields with and without ultrasonic pretreatment (which may open cell membranes) are evaluated. Finally, biodiesel generated from the extract is characterized and multistage extraction cascades are considered.

Results and Discussion

Here we evaluate the performance of CIJMs (see Figure 3.1) as a lipid extraction tool. We explore inlet flow rates, algae suspension concentrations, and multistage operations. Biocrude yields are compared to a Bligh and Dyer method and to those obtained with an ultrasonic pretreatment known to disrupt cell membranes. Predictions from our mathematical model are compared to experiment data for both single and multi-

stage operations. Because the biocrude yield varies somewhat with each batch of algae, we use the same batch of algae for each group of experiments to ensure comparability within all panels.

Figure 3.2a shows the biocrude yield expressed as a weight percent as a function of the inlet flow rate. As the volumetric flow rate increases, the biocrude yield rises smartly before attenuating after 480 mL/min. The largest biocrude yield in our experiments is 25.6±2.7%, similar to the yield obtained from a Bligh and Dyer method (25.7±1.3%) for this algae species and culture condition. Conventionally, the extraction yield from the Bligh and Dyer method is thought to be the most lipid or biocrude extractible from algae in a single pass extraction method, although this assertion has recently been called into question [9, 189-191]. Either way, yields from the CIJM and the Bligh and Dyer methods remain similar. However, in contrast to Bligh and Dyer methods that extracts lipids from dried and powderized algae, our extraction process completes within a fraction of a second without any drying or dewatering required. Furthermore, our method uses hexane, which is a moderate solvent for algal extraction [189], whereas the Bligh and Dyer method in this comparison uses a chloroform and methanol cocktail known to be a better solvent [2]. These differences are substantial because they translate into significant energy and capital cost reductions to proposed algae flowsheets.

The essential mechanism responsible for these improvements is a dramatically faster mass transfer process due to the small mass transfer length scales generated by confined turbulence. Within the CIJM, lipids release from the cells either due to thermodynamic equilibrium with the surrounding aqueous media enhanced by local

changes in cell curvature from membrane distortion due to turbulent shear or due to cell breakup [192, 193]. The shear forces present are clearly sufficient to break up the cells. Analysis by Morshed, et al., considers the shear stresses on red blood cells in plasma by balancing the power dissipated within an eddy and the cell-free fluid (plasma in their analysis) within that eddy. In the limit of small concentrations (concentrated algae solutions remain more dilute than physiological blood), their expression for the shear stresses applied to the cells reduces to $\tau=\mu^2/(\rho\eta^2)$. For typical viscosities ($\mu=10^{-3}$ Pa·s), densities ($\rho=10^3$ kg/m^3), and Komolgorov length scales (10^{-6} m), the shear stress applied to the cells is on the order of 1 kPa, whereas Michels, et al. [194], have shown microalgae viability to be adversely affected by shear stresses above 1 Pa, clearly indicating that shear forces are sufficient to cleave the cell membrane and wall. Furthermore, in contrast to traditional methods, the distance over which these lipids must transport to reach the organic lamina approximates the Kolmogorov length scale. Figure 3.2b shows that the Kolmogorov length decreases with volumetric flow rate through the CIJM. Therefore, the distance that lipid molecules must transfer between algae cells to organic solvent decreases as the flow rate increases. Shorter distances reduce the timescale required so that high biocrude yields may be obtained within the residence time of the CIJM mixer. This time is remarkably short on the order of 10 ms. Inserting the Kolmogorov length scale into the concentration profile for self-similar diffusion provides an approximate expression for lipid accumulation within the organic phase, also termed lipid yield. Figure 3.2a shows that this expression fits the data remarkably well. Additionally, our experiments (see Figure 3.3a) confirm that pretreating the algae suspension to ultrasound

beyond conditions reported to break open cells does not improve the efficacy of CIJM, consistent with the high shear stresses induced within the mixing chamber.

We also evaluated the biocrude yield as a function of the algae suspension concentration. This is important because algal lipid extraction techniques typically require high entering concentrations to be effective [2]. However, Figure 3.4a finds the biocrude yield to be essentially independent of algae inlet concentration holding the inlet volumetric flow rate constant (960 mL/min). Across all conditions explored in this set, the average biocrude yield is 22.7±2.3% (1σ). This indicates that the lipid extraction process is all but independent of algae suspension concentration in the experimental concentration range (3.6-13.3 g/L). This range covers typical harvest concentrations from photobioreactors [195-197], which suggests that matured algae suspension may be fed directly into the CIJM from photobioreactors without intervening concentrating or dewatering processes. This is a significant feature because dewatering and drying rank among the most energy intensive and, therefore, expensive processes in algae harvesting. This finding is not particularly surprising in light of our model that suggests the dimensionless concentration in the aqueous phase depends on entering composition through at most the kinematic viscosity. Yet because these concentrations are relatively dilute in terms of algae volume fraction, corrections to the kinematic viscosity remain rather small, leaving the yield all but independent of entering algae concentration.

The effect of solvent ratio for CIJM is shown in Figure 3.4b. The result shows that solvent ratios have negligible effect on biocrude yields in the domain explored. This result suggests that decreasing the solvent flow rate by a factor of two is clearly feasible

without significant loss in productivity. Further decreases may be possible with suitable control over the flow rates and relative pressure drops.

Figure 3.3b compares the composition of biodiesel made from the biocrude extracted using the CIJM to biodiesel prepared from biocrude extracted in the traditional manner. The traditional manner is directly mixed algae suspension and methanol for transesterification. The panel shows that the major components of our biodiesel include C-16 and C-18, similar to typical biodiesel compositions [198]. However, the biodiesel productivity of the control sample was inferior to the CIJM processed sample. These results demonstrate that the CIJM facilitates algal biocrude and lipid extraction so as to enhance the net biodiesel productivity.

Figure 3.5 considers the potential of extraction cascades. Figure 3.5a shows an example of a multistage cross current extraction process, here with four stages. Figure 3.5b shows that that the second and subsequent stages each extract biocrude, albeit in successively decreasing amounts. However, the total extracted biocrude consecutively increases. After four cycles, the total yield of biocrude is 38.8%, which is about 2.5 times more than first extraction cycle alone and substantially higher than the single pass yield with the Bligh and Dyer method. This finding demonstrates the potential value of arranging multiple CIJM in series to obtain better extraction performance. A simple mass balance (see Equation 3.18) reasonably predicts the extraction obtained experimentally. Further optimization using a counter-current extraction process may be possible [199]. Nevertheless, it is clear that a multiple stage extraction process may be used with CIJMs as the essential element in a mixer-settler configuration.

Remarkably, CIJM processes approach the maximum lipid loading per unit surface area. The surface area available for lipid absorption is approximately the volume of the mixing chamber (~$1.7 \cdot 10^{-7}$ m^3) divided by Kolmogorov length scale (1-$5 \cdot 10^{-6}$ m). For each residence time, the number of lipid molecules absorbed is approximately the surface area divided by the area of the lipid head (~$1 \cdot 10^{-18}$ m^2), and the number of residence times is equal to the process time (4.8-37.5 s) divided by the residence time (0.4-$3.2 \cdot 10^{-2}$ s). With a lipid molecular weight range of 848-932 g/mol (triglyceride with C16-C18 carbon chain), 0.57-3.16 g/L (dry/wet) may be extractable from 0.100 L of algae suspension. Experimentally, we find 1.5-3.7 g/L (dry/wet) biocrude (not lipid alone) is extracted. Therefore, the CIJM may have driven lipid to saturate the surface area available.

Materials and Methods

Confined Impinging Jet Mixer Configuration

The design of the confined impinging jet mixer evaluated herein followed that of Siddiqui, et al. (2009) with dimensions given in Figure 3.1b [183]. The mixer was machined in house out of clear, transparent acrylic (McMASTER-CARR, IL) to facilitate visualization of the mixing process. Swagelok tube fittings (male connector with ½" OD, Salt Lake City, UT) were used to connect the 3/8" tubing (Laboratory Tygon PVC Tubing for Chemical, McMaster Carr) between gear pumps and the CIJM (see Figure 3.1a). A small port at the top of the reactor used to facilitate machining of the chamber and exit lines was joined with screws and sealed with number three acrylic binder (Scigrip, Durham NC).

Two gear pumps (Reglo-Z, IDEX Corporation, Lake Forest, IL) were selected to provide constant, pulse-free flows. The two pumps operated at the same flow rate unless noted below to sustain impinging jet mixing. Algae suspension was fed through one inlet, and hexane was fed through the other inlet (see Figure 3.1a). Hexane was chosen as the representative organic solvent because it remains one of the most commonly used, albeit less effective, lipid extraction solvents [189]. For each experiment, 100 mL of each fluid was used at flow rates of 160-1280 mL/min. Prior to mixing, the inlet tubes were prefilled with fluid (algae suspension and hexane) at 100 mL/min. The mixer outlet flow (left open to atmosphere pressure) containing the extraction products was collected in a beaker for further analysis.

Algae Suspension

The algae (*Synechococcus Elongatus*) used in these experiments were cultivated in periodic symmetry defined bioreactors described in detail elsewhere [165]. The algae were cultivated for two weeks under artificial light (~4000 lux at the liquid surface) in the absence of supplemental CO_2, nitrogen restriction, or temperature control. The algae suspensions were then concentrated in an Eppendorf 5430R centrifuge (Hauppauge NY) at 7400 rpm for 10 min in 50 mL centrifuge tubes. A portion of the concentrated algae suspension was then taken to total dryness in the oven (60^{o}C) to obtain a starting concentration (algae dry biomass/volume of algae suspension). Lower concentration algae suspensions used in these experiments were prepared by simple dilution of the concentrated algae suspension to the desired weight fraction.

Algae Biocrude

The product from the confined impinging jet mixer was centrifuged (Eppendorf 5430 R, Hauppauge NY) for 30 min at 7400 rpm in 50 mL centrifuge tubes. After centrifugation, four distinct layers appear with the translucent hexane on the top, a cloudy emulsion as the second layer, transparent water in the third layer, and the opaque algae cell debris at the bottom. The emulsion layer, which contains the lipid extract, was transfer into beaker by pipette and dried completely in an oven (Thermo Scientific, Lab-line, Waltham, MA) at 60^{o}C under atmospheric pressure. The final weight was record for the biocrude yield (biocrude/initial algae dry biomass) calculation.

Bligh And Dyer Method

Yields obtained using the CIPM were compared to those obtained using a modified Bligh and Dyer method as described elsewhere [191]. Briefly, algae suspension was dried to completion in an oven (Thermo Scientific, Lab line, Waltham, MA) at 60^{o}C under atmospheric pressure for 48 h and ground into powder. One half gram of dried algae power was mixed with 100 mL of methanol and 50 mL of chloroform and then mixed in a blender (Blendtec Inc., Orem UT) at 14,700 rpm (speed 5) for 5 min to induce lipid/biocrude extraction. An additional 50 mL chloroform and 90 mL DI water (Milli Q grade, resistivity of 18.2 MΩ·cm) were added to the blender and mixed for another 2 min at the same speed to induce phase separation. The algae cell debris in the final product was removed by No. 4 filter paper (Whatman, GE Healthcare Bio-Sciences, Marlborough MA). The organic portion of the filtered suspension was dried in the oven (60^{o}C) and

weighted to calculate the lipid yield. Following common practice, the terms biocrude yield and lipid yield are used interchangeably herein [200, 201].

Biodiesel Conversion

The biocrude extracted from the CIJM was convert into biodiesel by transesterification. Biocrude (0.3 g) was added to 100 mL of methanol (10 wt% NaOH) and placed on a hot plate (Corning, P420D, Corning, NY) at 80^{o}C for 2 h. A control experiment used 100 mL of raw, unprocessed algae suspension (13.3 g/mL) directly mixed with 100 mL of methanol (10 wt% NaOH) and heated on a hot plate (Corning, P420D, Corning, NY) at 80^{o}C for 2 h. Products were analyzed by gas chromatography/mass spectrometry (GC/MS) (HP6890, an MSD HP5973 detector, and a Zebron ZB-5MSi Guardian (30 m x 0.25 mm ID, 0.25 μm film thickness; Phenomenex) column). Biodiesel samples were injected using a HP7682 injector maintained at 250^{o}C with a volume of 1.0 μL and 10:1 split ratio with helium as a carrier gas. The oven was maintained at 95°C for 1.5 min then increased to 118°C under a rate of 40°C/min and maintained for 1.0 min. After that, the temperature was increased to 250°C at a rate of 5°C/min and to 330°C at a rate of 25°C/min and then maintained for 12.3 min. Results were compared to well-established standards to determine the FAME composition (Figure 3.3b). The MS scan rate was 16 scans/s with the MS quad temperature 150^{o}C and source temperature 230^{o}C.

Effect of Different Flow Rates

To investigate the influence of volumetric flow rate on extraction efficiency, six flow rates (160, 320, 480, 640, 960, 1280 mL/min) were tested. The algae feed concentration (13.33 g/L) and the organic-solvent-volume-to-dry-algae-biomass ratio (75 mL/g) used in these experiments were held constant, and the algae were from the same batch to minimize variability. In total, 100 mL each of algae suspension and hexane were fed to the CIJM in each test. The biocrude from the CIJM was collected and quantified as described above. Each flow rate was tested in triplicate.

Effect of Different Concentration of Algae Suspension

To investigate the influence of algae concentration on extraction efficiency, five algae concentrations from 3.63 g/L to 13.3 g/L were tested. The flow rates for these experiments were held constant (960 mL/min). In total, 100 mL each of algae suspension and hexane were fed to the CIJM in each test. The biocrude from the CIJM was collected and quantified as indicated above. Each flow rate was tested in triplicate.

Effect of Multistage Extraction

To evaluate whether additional CIJM cycles may be used to extract additional lipid with each cycle and, thereby increase the total yield from one starting suspension, the same algae suspension was run through the CIJM multiple times to mimic multiple stage cross-current extraction. The algae concentration used in this experiment was 13.3 g/L with an inlet flow rate of 960 mL/min. The suspension was processed as described above, and the product recovered from the CIJM the first time was centrifuged as

described above. The organic and emulsion layers were recovered for biocrude assay and their yield reported. The algae slurry (i.e., the fourth and bottom layer as indicated above) was resuspend in 100 mL DI water (Milli Q grade, 18.2 MΩ·cm resistivity) and sent through the CIJM again. A total of four stages or cycles was evaluated.

Effect of Solvent Ratio

The ratio of solvent to algae inlet flow rates may affect the usage of organic solvent. Three ratios (1.00, 0.75, and 0.50) were achieved by varying the inlet flow rate of organic solvent, maintaining the algae suspension inlet flow rate at 1024 mL/min. The volume of algae suspension for each test is 100 mL with biomass concentration 13.33 g/L. The biocrude yield was determined as described above and tested in triplicate.

Ultrasonic Pretreatment

To evaluate the influence of otherwise intact cell walls, an ultrasonic pretreatment step was implemented. The concentrated algae suspension (100 mL, about 13.3 g/L) was placed in a sonicator (Branson 1800, Danbury, CT) for 30 min at a power setting of 40 W. These conditions were selected to exceed conditions reported in the literature known to breakup cell walls and release lipids [202-204]. The ultrasonic treated algae suspensions were run through the CIJM with inlet flow rate at 960 mL/min. A set of experiments using algae suspension directly sent to CIJM at the same inlet flow rate of 960 mL/min without ultrasonic treatment was evaluated as a control.

Model of Lipid Extraction

A simple model to estimate the lipid or biocrude yield may be constructed as follows. The term biocrude is used below as the more general term. As described elsewhere, shortening the distance over which mass transfer occurs to the Kolmogorov length scale is essential to CIJM [184]. During high speed turbulent mixing, the thickness of lamina of algae suspension between lamina of organic solvent narrows, as described by a Kolmogorov length scale (the smallest of turbulent length scales). This length scale is given as

$$\eta = \left(\frac{\upsilon^3}{\varepsilon}\right)^{1/4}, \tag{3.1}$$

where υ is the kinematic viscosity of the fluid and ε is the average rate of dissipation of turbulent kinetic energy per unit mass describe by

$$\varepsilon = \frac{u^3}{L}, \tag{3.2}$$

where u is the macroscale velocity of entering fluid and L is the characteristic dimension of mixing chamber that restricts the size of turbulent eddies [205]. The average velocity of fluid may be obtained from the volumetric flow, Q, and the cross sectional area of the inlet tube as

$$u = \frac{4Q}{\pi d_o^2}, \tag{3.3}$$

where d_o is the diameter of inlet tube. Combined,

$$\eta = \frac{\nu^{3/4} L^{1/4} \pi^{3/4} d_o^{3/2}}{4^{3/4} Q^{3/4}}, \tag{3.4}$$

which shows that the Kolmogorov length scale decreases as the volumetric flow rate increases.

Diffusion of biocrude from the cell to the organic layer through the water layer is a transient process that may be approximated using well-known self-similar concentration profiles. Then the dimensionless concentration, θ, profile is given by

$$\theta = \frac{C}{C_a K_1} = Erfc\left(\frac{x}{2\sqrt{Dt}}\right), \tag{3.5}$$

where C is the biocrude concentration anywhere in aqueous phase, C_a is the biocrude concentration in the algae, $K_1 = C_a/C(x = 0)$ is the partition coefficient of biocrude between algae and water at the cellular interface (i.e., $x = 0$), x is the distance over which diffusion occurs here approximately the Kolmogorov length scale, D is the diffusion coefficient, and t is the residence time in the confined impinging jet mixer [205]. We recognized the erfc function to be only approximate because the concentration does not fully decay to zero but is bounded by the Kolmogorov length scale. The diffusion coefficient may be approximated by the Stokes-Einstein equation as

$$D = \frac{k_b T}{3\pi\mu_w d}, \tag{3.6}$$

where k_b is Boltzmann constant ($1.38 \cdot 10^{-23}$ J/K), T is the absolute temperature, μ is the dynamic viscosity of water (0.001 Pa·s), d is the characteristic dimension of the lipid molecule (approximately 4 nm for C16-C18 from end-to-end, radius of gyration, and Kuhn length considerations and as estimated from the carbon-carbon bond lengths 0.154 nm) [206, 207].

The residence time within the confined impinging jet mixer and, therefore, the characteristic time scale for diffusion may be estimated from

$$t = \frac{V}{2Q}, \tag{3.7}$$

where Q is the volumetric flow rate of each of the inlet flows feeding the round chamber volume V of diameter 4.76 mm (see Figure 3.1b). Combining Eqs. 3.5-3.7 finds

$$\theta = Erfc\left(\sqrt{\frac{\eta^2 Q}{2DV}}\right). \tag{3.8}$$

Substituting in the Komogorov length scale yields

$$\theta = Erfc\left[\frac{1}{Q^{1/4}}\left(\frac{v^{3/4}L^{1/4}\pi^{3/4}d_o^{3/2}}{4D^{1/2}V^{1/2}}\right)\right]. \tag{3.9}$$

Please note that of all the contributing variables, Q remains the only variable that varies during a test (the others are largely fluid properties or CIJM dimensions) and that θ is a clear function of Q.

The dimensionless concentration may be converted into the lipid or biocrude yield by determining the concentration at the aqueous-organic interface, C_h. There the partition coefficient, K_2, is defined as

$$C_h = \frac{C(x=\eta)}{K_2} = \frac{K_1 C_a \theta(x=\eta)}{K_2} \tag{3.10}$$

with substitution. The measured yield, Y, is defined as the mass of lipid (or biocrude) extracted divided by the lipid (or biocrude) in the initial biomass, $m_{biomass}$. The mass of lipid extracted may be expressed as the volume of hexane, V_h, multiplied by the concentration of lipid (or biocrude) in the hexane, C_h, both including that trapped in the emulsion layer. Then

$$Y = \frac{V_h C_h}{m_{biomass}} = \frac{V_h K_1 C_a \theta(x=\eta)}{m_{biomass} K_2} \tag{3.11}$$

after substitution. Recognizing that although V_h and $m_{biomass}$ may be known, the partition coefficients and concentration of lipid within the cell remain unknown, suggesting a

lumped constant defined as $\kappa = V_h C_a K_1/(m_{biomass} K_2)$. This fitting constant is species and solvent specific. Then

$$Y = \kappa \, Erfc\left[\frac{1}{Q^{1/4}}\left(\frac{v^{3/4}L^{1/4}\pi^{3/4}d_o^{3/2}}{4D^{1/2}V^{1/2}}\right)\right]. \tag{3.12}$$

This expression is compared to the experimentally obtained yield as a function of flow rate in Figure 3.2a.

Model of Multistage Extraction

For multiple stage extraction in a cross flow cascade, the entering solvent streams are devoid of biocrude. Figure 3.5a and species balances represent the solvent as S, the extract as E, and the raffinate as R, which is the aqueous stream containing algae and remaining lipids. Following the nomenclature of Seader, streams coming off the same stage are given the same subscript, and the entering algae stream is labeled as R_o for notational simplicity, though technically not a raffinate stream. In this scenario, the flow rates of the entering and exit streams are approximately equal in the experiments above, immediately satisfying the overall mass balances. The species mass balances then become

$$x_i^R + x_i^E = x_{i-1}^R \tag{3.13}$$

for $i \geq 0$, where x_i is a mass fraction of wet material. In traditional form, we define $x_i^E = k_i x_i^R$ with k_i positive definite so that

$$x_i^R = \frac{x_{i-1}^R}{1+k_i} \quad \text{and} \quad x_i^E = \frac{k_i x_{i-1}^R}{1+k_i}. \tag{3.14}$$

When $k = k_i$ for all i (true within uncertainty here),

$$\frac{x_i^R}{x_o^R} = \frac{1}{(1+k)^i} \quad \text{and} \quad \frac{x_i^E}{x_o^R} = \left(\frac{k}{1+k}\right)^i \tag{3.15}$$

and the total amount extracted in multiple stages is

$$x_{total}^{E} = \sum_i x_i^E = x_o^R \sum_i \left(\frac{k}{1+k}\right)^i. \quad (3.16)$$

The final term contains a geometric series such that

$$\frac{x_{total}^{E}}{x_o^R} = k\left[1 - \left(\frac{k}{1+k}\right)^n\right], \quad (3.17)$$

where n is the number of stages, which shows that in the limit of a large number of stages only a fraction k of all of the entering biocrude may be captured. The experimental observable is the ratio of the dry biocrude mass extracted to dry algae mass entering. The dry biocrude mass is $x_i^E E_i f_{DB}$, where f_{DB} is the ratio of the mass of dry biocrude to the mass of wet biocrude, differing in the degree of hydration. The dry algae mass is $x_o^R R_i f_{DA}$, where f_{DA} is the ratio of the dry algae mass to the mass of wet algae suspension. Where E_i=R_i, we plot

$$B_i = \frac{x_i^E}{x_o^R}\frac{f_{DB}}{f_{DA}} = f\left(\frac{k}{1+k}\right)^i \quad \text{and} \quad S_i = \frac{x_{total}^E}{x_o^R}\frac{f_{DB}}{f_{DA}} = fk\left[1 - \left(\frac{k}{1+k}\right)^n\right], \quad (3.18)$$

where f=f_{DB}/f_{DA}. The ratio of B_2/B_1 may be used to determine k as $(B_2/B_1)/(1\text{-}B_2/B_1)$. Then f may be determined as B_1^2/B_2.

Acknowledgements

The authors gratefully acknowledge helpful conversations with Anthony Butterfield, Robert Prud'homme, and Chris Macosko.

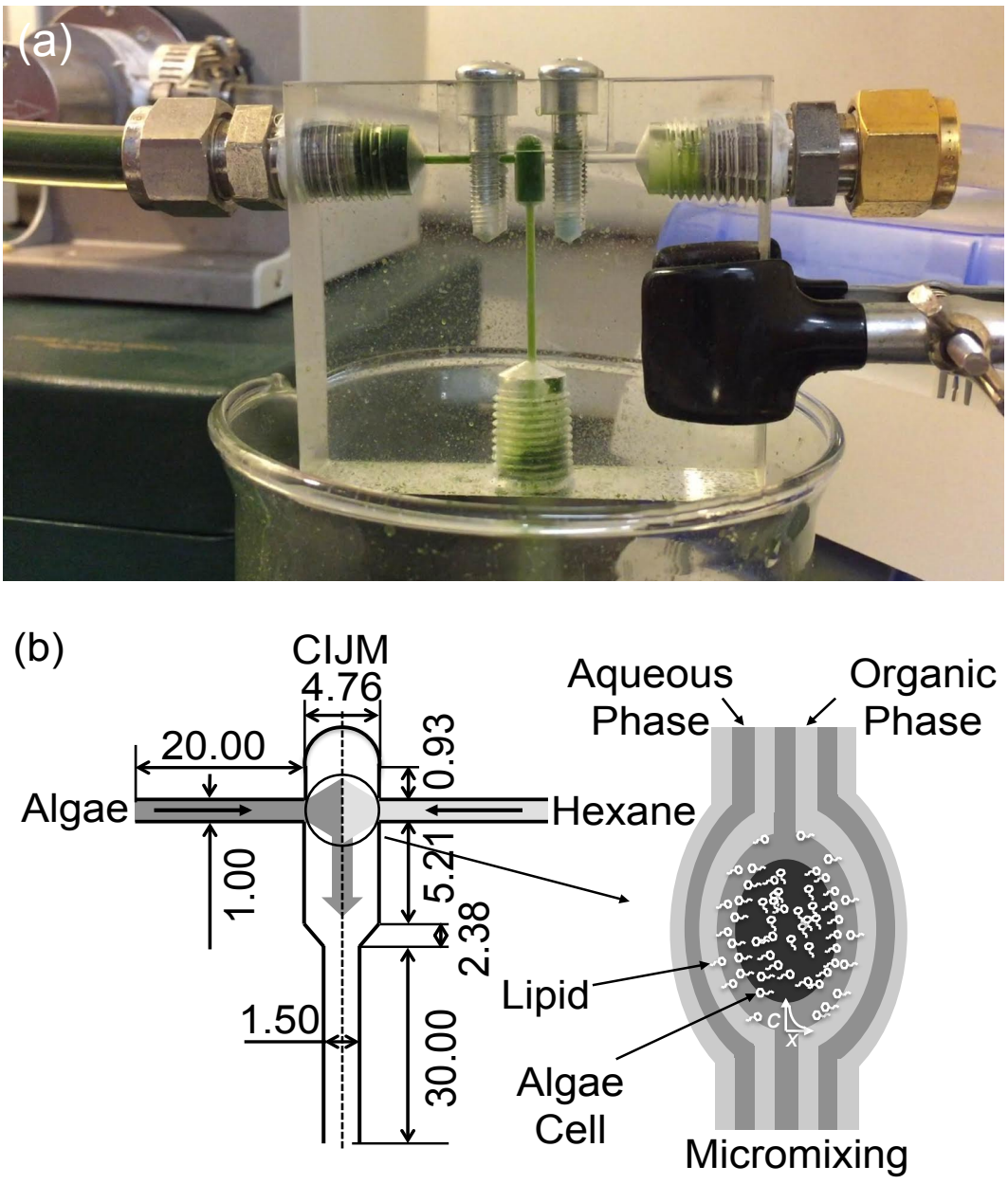

Figure 3.1. Confined impinging jet mixer (CIJM). (a) Digital image of confined impinging jet mixer showing algae (from left) and solvent (from right) streams impinging in a central chamber with exit towards the bottom. (b) As designed impinging jet mixer (lengths and diameters in millimeters) with representation of the lipid transfer process at the Kolmogorov length scale.

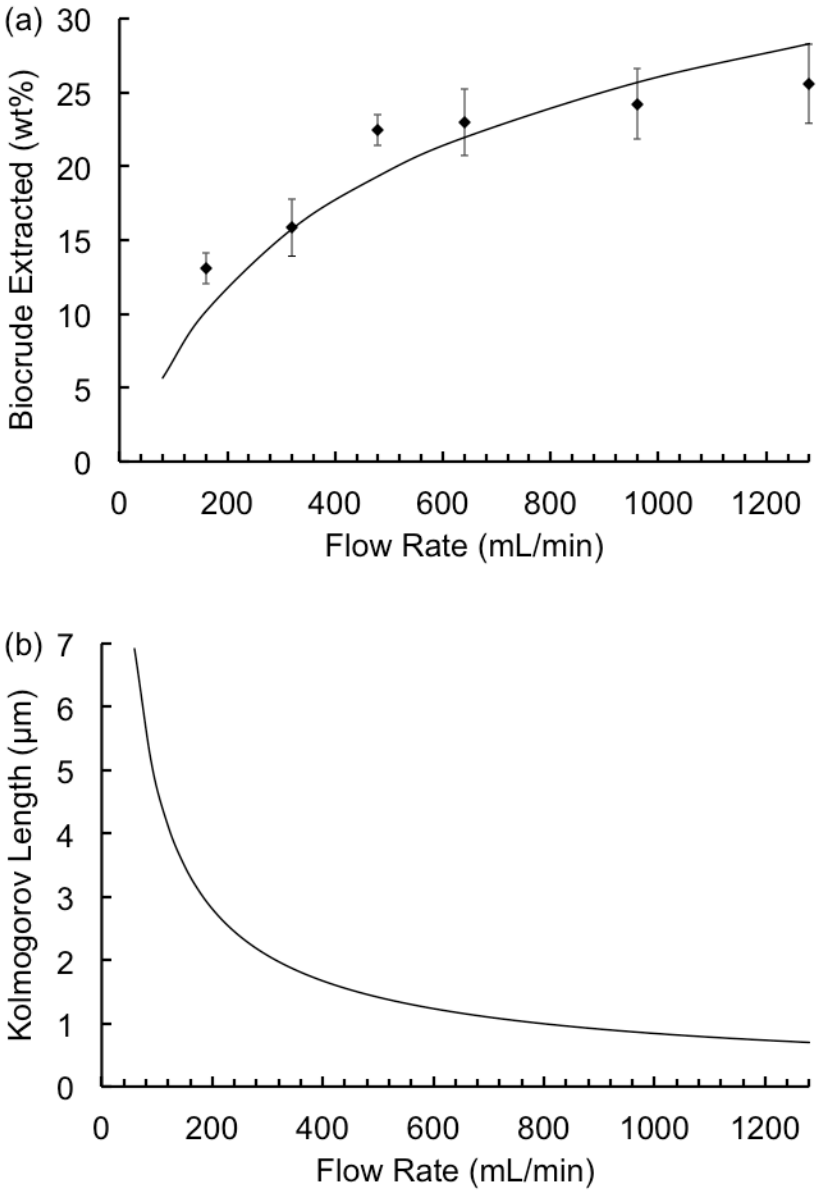

Figure 3.2. Biocrude extraction and Kolmogrov length scale versus flow rate. (a) Biocrude extract versus flow rate comparing experimental data (diamonds) with model predictions (curve, Equation 3.12). Error bars represent one standard deviation. (b) Kolmogorov length versus volumetric flow rate. Both panels use $n = 1.00 \cdot 10^{-6}$ m^2/s, $L =$ 4.76 mm, $d_o =$ 1.00 mm, $V = 1.7 \cdot 10^{-7}$ m^3, $\kappa = 0.76$, and $D = 1.46 \cdot 10^{-10}$ m^2/s (from $k_b =$ $1.38 \cdot 10^{-23}$ J/K, $T =$ 298 K, $\mu = 1.00 \cdot 10^{-3}$ Pa·s, $d =$ 4.0 nm).

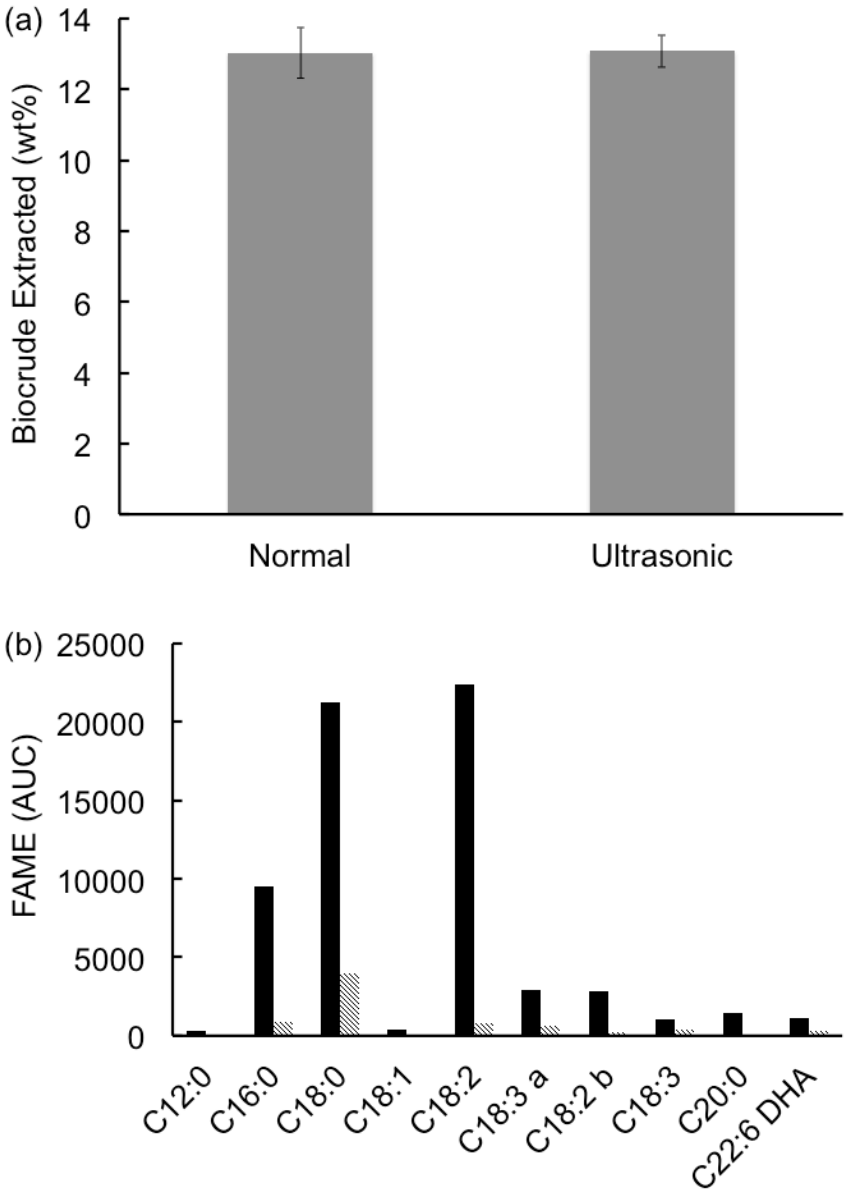

Figure 3.3. Biocrude extract and biodiesel composition. (a) Comparison of biocrude yield with and without ultrasonic pretreatment. (b) Biodiesel composition of fatty acid methyl ester (FAME) via a unit of area under curve (AUC) method comparing the biodiesel made from CIJM (black) with the one without running through the CIJM (gray). Error bars represent one standard deviation.

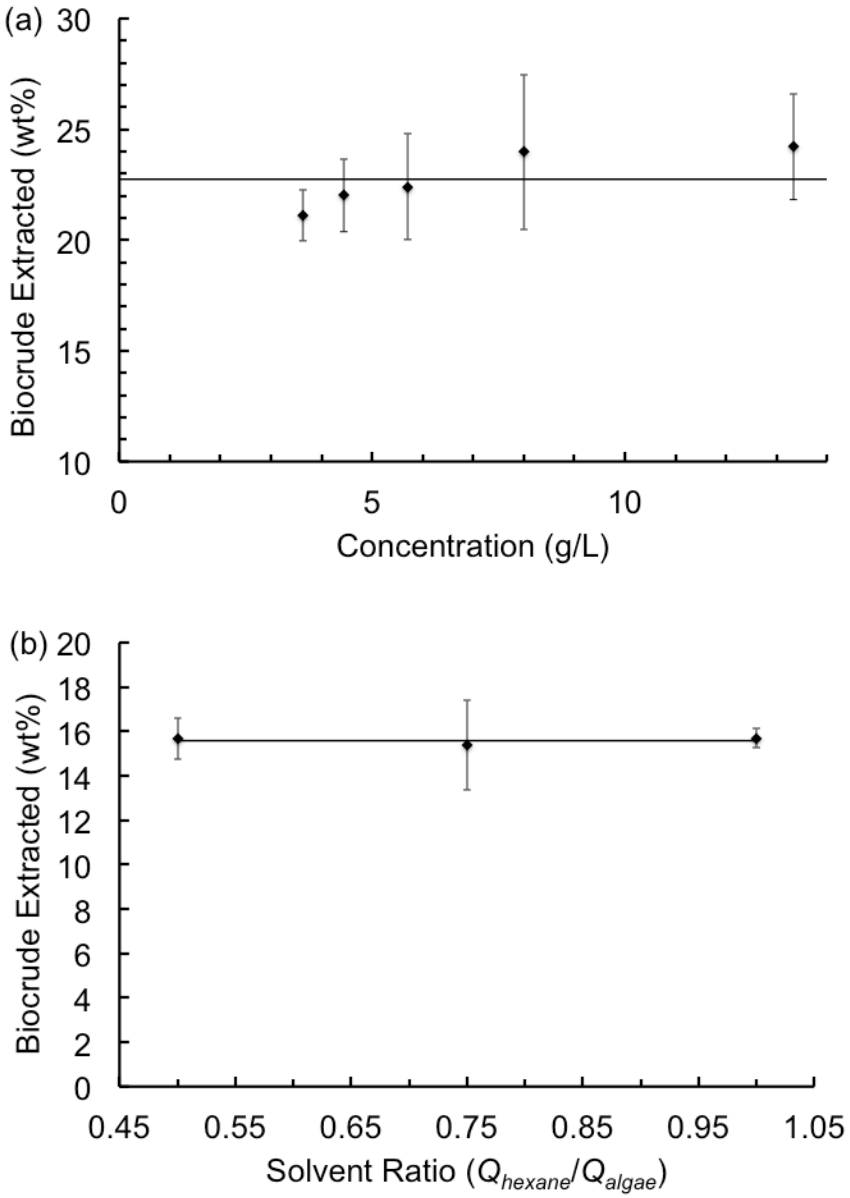

Figure 3.4. Biocrude extraction versus feed characteristics. (a) Biocrude yield versus algae suspension concentration. (b) Biocrude crude yield versus solvent ratio (Q_{hexane}/Q_{algae}). Amount extracted for one cycle varies between but not within panels because different algae stock was used for each panel, but the same stock was used for all points within a panel. Lines represent the average across all experiments, and error bars represent one standard deviation across all data.

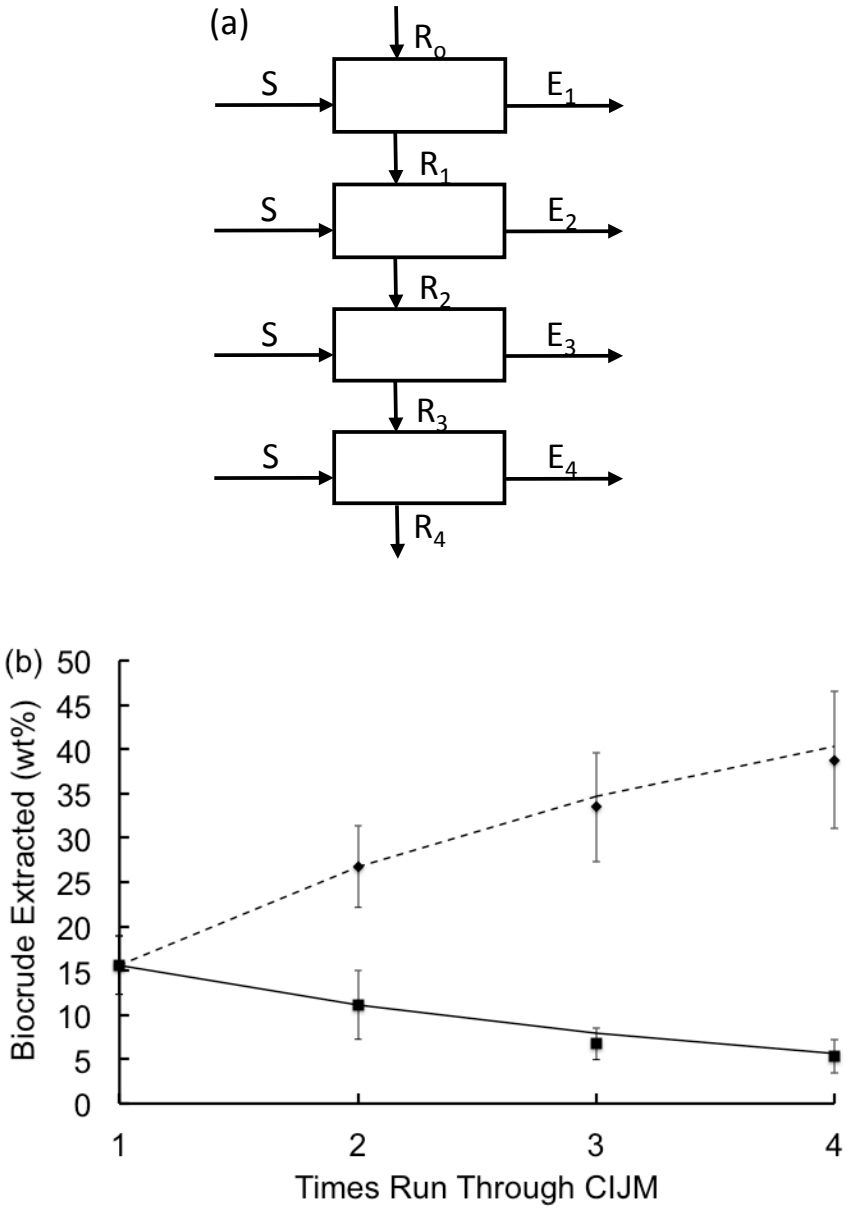

Figure 3.5. Multiple-stage crosscurrent extraction. (a) Block diagram identifying multiple lipid extraction steps. (b) Biocrude yield versus number of times or cycles that same algae is processed by the CIJM. Yield for each step (square, solid) and accumulated yield (diamond, dash). Curves from Eq. 18 with $f = 21.9$ and $k = 2.48$.

CHAPTER 4

WAX PRECIPITATION IN UINTAH BASIN CRUDE OILS AND BLENDS

Abstract

Wax precipitation curves for Uintah Basin crude oils and blends anticipated for pipeline transport have been determined using a FT-IR method. Prospective pipeline blends of Uintah Basin crude oils with 30% by weight local gas condensate, Bakken crude oil, and biodiesel produced from canola oils show reductions in precipitated wax for given oil temperatures. The thirty percent by weight blend of gas condensate into Uintah Basin waxy crude oil is approaching behavior which can be effectively pour point depressed, or "flow improved" using chemical additives to allow conventional pipeline transport.

Introduction

Wax precipitation in crude oils induces fouling and plugging in petroleum production and transportation operations. Uintah basin crude oils have historically been labeled as waxy in character, with associated transport pipelines plagued by flow disruptions and shutdowns [215]. While these crude oils are commercially produced, transported, and refined, wax precipitation in these crude oils and relevant blends has not

been documented in the literature. This study uses Fourier Transform Infrared Spectroscopy (FT-IR) with a previously documented method to investigate wax precipitation in black wax and yellow wax crude oils produced from the Uintah basin [216], as well as possible blends for future pipeline transport. Blend stocks include gas condensate from related gas processing in the Uintah Basin, Bakken crude oil, and biodiesel produced from canola oils. Bakken crude is a low-wax intermediate type crude oil, which is transported by rail through the Uintah Basin. The biodiesel has been investigated as a renewable feedstock, which may be produced in the intermountain west of the United States [217].

Background

Experimental determination of wax precipitation has been well summarized in the literature [218], with primary methods involving differential scanning calorimetry (DSC), viscometry, centrifugation of cold oil, and nuclear magnetic resonance (NMR) spectroscopy. As described by Roehner and Hanson [216], FT-IR can be used to monitor the absorbance at approximately 720 cm^{-1}, which is indicative of long chain paraffin rocking vibrations. Increases in absorbance at this wave number with decreasing temperature are related to formation of solid paraffin waxes in crude oil below the wax precipitation temperature (WPT). The WPT is then identified by the change in the slope of absorbance versus oil temperature, which occurs at the WPT. This allows for construction of a solid wax precipitation curve for a given crude oil, with the advantage of not having to determine the paraffin distribution present in the crude oil liquid and solid phases. Unlike alternative techniques, this method is insensitive to cooling rates.

The Uintah basin waxy crude oils contain high percentages of normal paraffin with carbon numbers above C_{18} as measured using high temperature gas chromatography (HTGC) based on ASTM D7169-11 [219]. This is shown in Table 4.1 for black wax and yellow wax crude oils respectively. Table 4.2 summarizes the source and measured physical properties for the samples of black wax and yellow wax crude oils analyzed in this study. Table 4.3 shows the compositions of gas condensate obtained from traditional gas chromatography.

Experimental Section

The FT-IR procedure used is summarized here, along with details of sample procurement, handling, blending, and characterization.

FT-IR Instrumentation

All analyses were conducted on a Nicolet iS50 FT-IR Spectrometer, with Omnic 9.2 107 software. The spectra were collected from 4000-400 cm^{-1} over a temperature range (15-70^{o}C). A Spectra Tech HC-32 temperature controlled liquid FT-IR cell (modified by replacement of stainless steel coolant loop with ¼" copper tubing for increased coolant flow) with 32 mm NaCl windows and a 0.1 mm lead spacer was used. A Julabo F25 bath was used to control the temperature with a general cooling rate approximating 0.07^{o}C/min. A micro-thermocouple placed in the liquid cell and connected to Omega HH-147U digital thermometer was used to represent the sample temperature.

Sampling and Blending

Two samples (duplicates) were prepared and tested using FT-IR for each crude oil or blend analyzed. All the crude oil and diluents were preheated in the oven under 60^{o}C for 6 h before blending. For blend preparation, the preheated crude oil was transfered by glass syringe from the original glass container (40 mL Pyrex bottle with Teflon cap) to the sample container (40 mL Pyrex bottle with Teflon cap) which was used for final weight determination. The selected thirty percent by weight diluent was then also added to the sample container by glass syringe. All the sealed samples were placed in a convection oven at 60^{o}C for 6 h before testing. Samples are transferred by preheated syringe to the Spectra Tech HC-32 liquid cell.

Calculations

Peak areas for absorbance attributed to rocking vibrations of long chain methylene groups for each temperature were obtained by integration of the spectral data from 735 cm^{-1} to 715 cm^{-1}. To eliminate any shift of baseline that might occur during analysis, the corrected peak area collected for each temperature was added to the same base area obtain from the first high temperature measurement. The WPT was obtained from the intersection of the liquid absorbance versus temperature line and the liquid-solid absorbance versus temperature line. The solid weight percent precipitated wax for crude oil temperatures below the WPT was calculated by using previously derived Equation 4.1 with constant *C* again assigned a value of 1.0 [216].

$$\text{Wt \% Solid} = C * [(A_{total} - A_{ext.liq})/A_{total}] * 100\% \quad (4.1)$$

In Equation 4.1, A_{total} is the integrated total observed absorbance a given oil temperature below the WPT, and $A_{ext.liq}$ is the extrapolated integrated liquid phase absorbance at the same oil temperature.

Model Oil Validation

In the previous publication by Roehner and Hanson [216], a model oil of known composition and solid-liquid equilibrium was used to validate the FT-IR method. In the current work, analysis of the same model oil system was used to validate a revised testing procedure modified to account for an upgraded spectrometer and software in the FT-IR system. The same repeatability for the revised FT-IR procedure was observed with determination of the wax precipitation temperature within ±1.0^{o}C.

Oil Composition by High Temperature Gas Chromatography

The Uintah Basin crude oils (black wax and yellow wax crude oils) were characterized by high temperature gas chromatography (HTGC). All analyses were conducted using a modified version of ASTM D-7169 and an Agilent 6890N chromatograph equipped with a HP-1 capillary column (5 m x 0.53 mm x 0.15 microns) and a flame ionization detector (FID). Ultra-high purity grade helium was used as carrier gas [219]. The injector inlet used was a cool-on-column with injection volume of 0.5 microliter. Samples were diluted to 2% (m/m) in CS_2. The initial oven temperature is held at -20^{o}C, the temperature is then heated to 425^{o}C with a heating rate of 15^{o}C/min. The final hold time is 10 min.

Biodiesel Generation

Biodiesel (fatty acid alkyl esters) was produced from triglyceride (lipid) and alcohol by transesterification. Although, the lipid may come from any feedstock such as corn, soybean, canola, palm, and microalgae, commercial canola oil was chosen as lipid source for this experiment due to its purity and stability. The lipids were mixed with methanol containing 10% NaOH at 80^{o}C for 2 h to produce the biodiesel. The sample was analyzed by the GS/MS with a Zebron ZB-5MSi Guardian (30 m x 0.25 mm ID, 0.25 μm film thickness; Phenomenex) column. The resulting chromatogram is provided in Table 4.4. The cloud point of canola biodiesel was about -3^{o}C with a density is 870 kg/m^{3} [208]. Biodiesel produced from canola oil contains hydrocarbons within the single carbon number range of C16 to C20 as shown in Table 4.4, and the average density base on the GC data was about 309.9 g/mol.

Results of Analyses

Figures 4.1 and 4.2 show the wax precipitation curves created from FT-IR analysis of black wax and yellow wax crude oils and their blends. Each figure shows wax precipitation for the identified neat oil, and thirty percent by weight blends with biodiesel, Bakken crude oil, and gas condensate. It is important to note the large slope of the wax precipitation curves for the neat oils, with less than 5^{o}C between the observed WPT and an oil temperature where there is two weight percent precipitated solid. The amount of two weight percent solid is often used as a common rule of thumb for the temperature where the crude oil will have sufficient gel character to be identified as having reached the “pour point temperature” typically defined by ASTM D5853 [220].

This matches well with the measured pour point temperatures for black wax and yellow wax crude oils given in summary Table 4.2.

Figure 4.3 provides the IR spectra for different temperatures overlaid into a common plot, and shows how the long chain methylene rocking vibrations change with temperature. The peak grows and even splits indicating high paraffin content, which is confirmed from HTGC results summarized in Tables 4.1, 4.2.

Conclusion

Wax precipitation curves for Uintah Basin crude oils and blends thought to be relevant for pipeline transport have been determined using a novel FT-IR method. The results for temperatures where neat black wax and yellow wax crude oils approximate 2% by weight precipitated solid relate well to measured crude oil pour point temperatures. Prospective pipeline blends of these Uintah Basin crude oils with 30% by weight local gas condensate, Bakken crude oil, and biodiesel produced from canola oils show reductions in precipitated wax for given oil temperatures. Of note, the 30% weight blend with gas condensate is approaching behavior which can be effectively pour point depressed / flow improved using chemical additives to allow conventional pipeline transport. This study suggests that with additional study of non-Newtonian rheology of these blends, additional evaluations of flow improvers and wax crystal modifiers may be merited.

Acknowledgments

The authors would like to acknowledge the support of the State of Utah, Office of Energy Development for this work. The HTGC analyses were performed by Intertek Westport Technology Center, Houston, Texas.

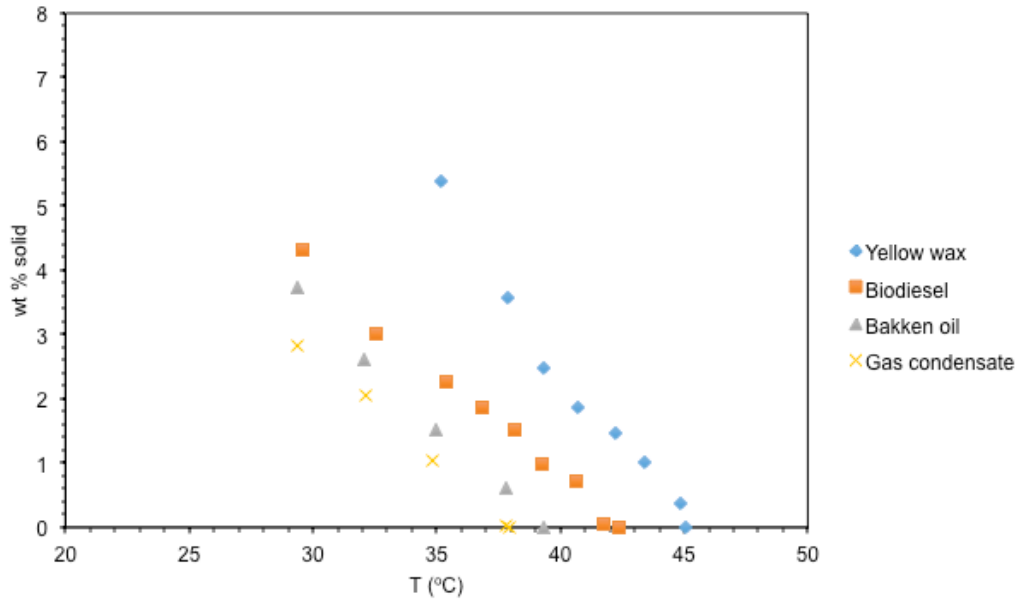

Figure 4.1. Wax precipitation in yellow wax crude oil and blends (30% Wt. Biodiesel, bakken oil, gas condensate)

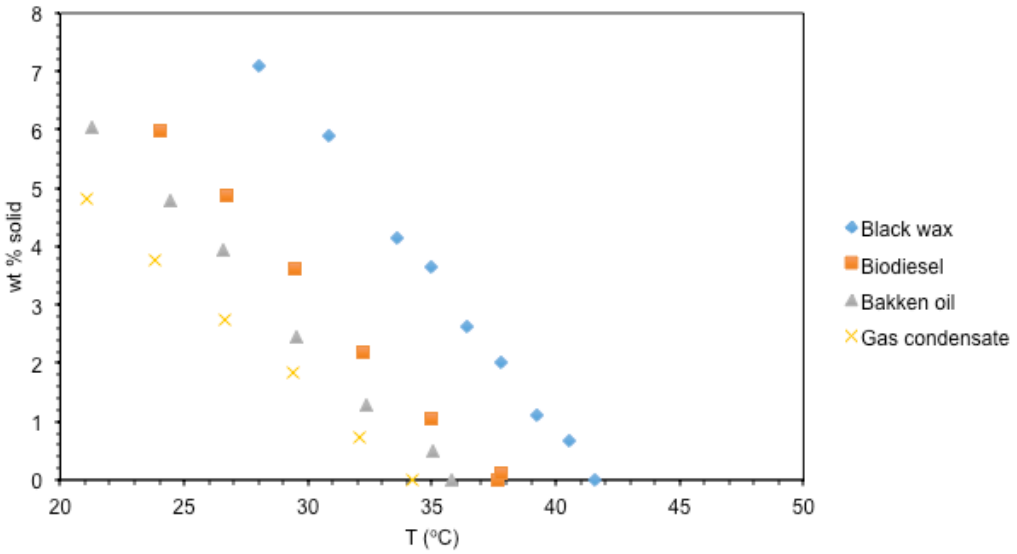

Figure 4.2. Wax precipitation in black wax crude oil and blends (30% Wt. Biodiesel, bakken oil, gas condensate)

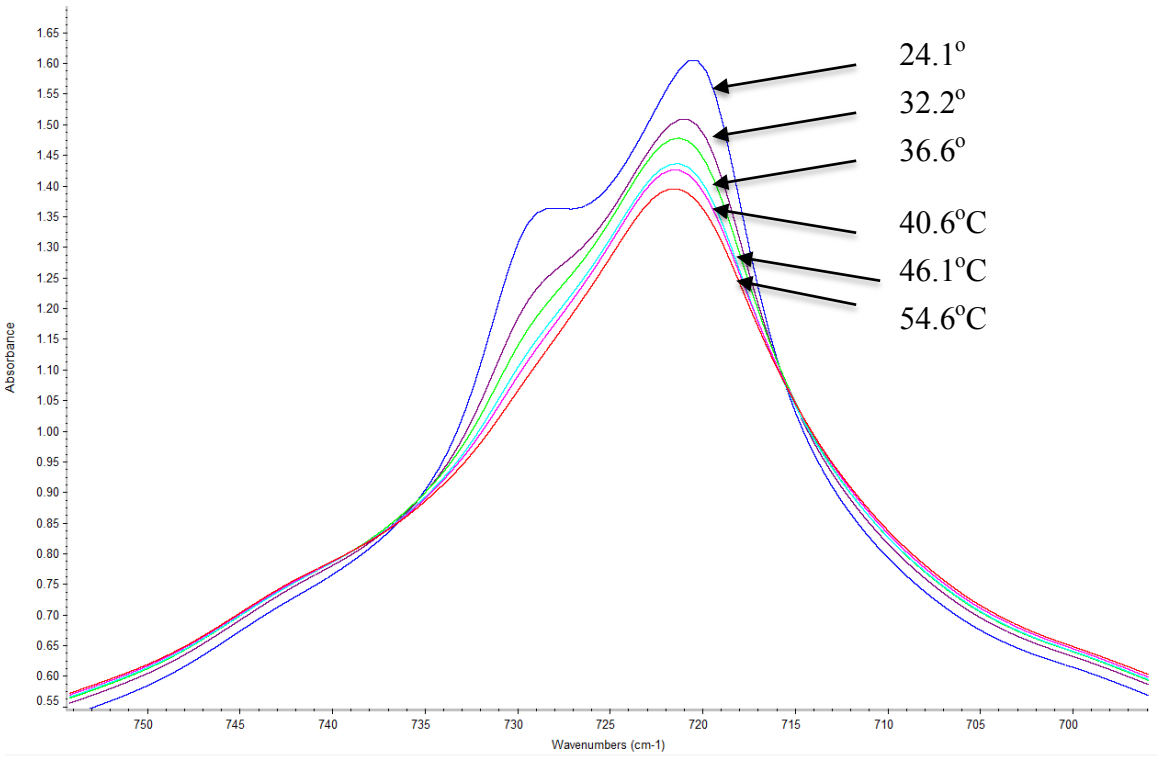

Figure 4.3. FTIR spectra for black wax crude oil with 30% wt. biodiesel

Table 4.1. Composition of Uintah Basin crude oils by GC.

(a)

Black Wax Wt. (%)								
C No.	Total	n-$C_{18\sim80}$	C No.	Total	n-$C_{18\sim80}$	C No.	Total	n-$C_{18\sim80}$
C1	0.000		C39	1.248	0.107	C79	0.268	0.000
C2	0.000		C40	1.213	0.097	C80	0.221	0.000
C3	0.050		C41	1.180	0.077	Total	100.000	13.569
iC4	0.030		C42	1.079	0.058			
nC4	0.090		C43	1.047	0.075			
iC5	0.080		C44	0.972	0.062			
nC5	0.120		C45	0.952	0.082			
C6	0.297		C46	0.992	0.067			
C7	1.281		C47	0.924	0.081			
C8	1.932		C48	0.913	0.061			
C9	2.408		C49	0.924	0.067			
C10	2.418		C50	0.839	0.047			
C11	2.122		C51	0.834	0.060			
C12	2.007		C52	0.783	0.051			
C13	2.714		C53	0.795	0.063			
C14	2.577		C54	0.740	0.049			
C15	2.580		C55	0.808	0.063			
C16	2.103		C56	0.777	0.040			
C17	2.740		C57	0.767	0.041			
C18	2.512	1.097	C58	0.688	0.028			
C19	2.596	1.183	C59	0.687	0.031			
C20	2.421	0.963	C60	0.669	0.012			
C21	2.405	0.928	C61	0.697	0.022			
C22	2.370	0.928	C62	0.606	0.021			
C23	2.561	0.997	C63	0.541	0.017			
C24	2.332	0.936	C64	0.577	0.016			
C25	2.555	1.004	C65	0.492	0.014			
C26	2.397	0.910	C66	0.453	0.013			
C27	2.776	0.972	C67	0.421	0.012			
C28	2.731	0.754	C68	0.403	0.007			
C29	2.818	0.718	C69	0.414	0.006			
C30	2.526	0.554	C70	0.428	0.005			
C31	2.286	0.440	C71	0.374	0.004			
C32	1.919	0.277	C72	0.361	0.003			
C33	1.636	0.222	C73	0.368	0.001			
C34	1.566	0.166	C74	0.388	0.001			
C35	1.494	0.130	C75	0.360	0.000			
C36	1.507	0.094	C76	0.375	0.000			
C37	1.465	0.094	C77	0.346	0.000			
C38	1.332	0.093	C78	0.317	0.000			

Table 4.1. Continued.

(b)

Yellow Wax Wt. (%)								
C No.	Total	n-$C_{18\sim80}$	C No.	Total	n-$C_{18\sim80}$	C No.	Total	n-$C_{18\sim80}$
C1	0.000		C39	1.081	0.151	C79	0.119	0.000
C2	0.010		C40	1.038	0.140	C80	0.100	0.000
C3	0.060		C41	0.884	0.132	Total	100.000	18.784
iC4	0.030		C42	0.832	0.125			
nC4	0.160		C43	0.790	0.121			
iC5	0.120		C44	0.737	0.111			
nC5	0.320		C45	0.751	0.104			
C6	0.787		C46	0.720	0.095			
C7	1.626		C47	0.704	0.096			
C8	3.573		C48	0.739	0.088			
C9	3.322		C49	0.665	0.076			
C10	3.158		C50	0.675	0.066			
C11	2.896		C51	0.662	0.063			
C12	3.018		C52	0.584	0.060			
C13	3.192		C53	0.599	0.057			
C14	3.219		C54	0.607	0.045			
C15	3.111		C55	0.530	0.048			
C16	3.098		C56	0.566	0.045			
C17	2.949		C57	0.500	0.047			
C18	2.933	1.523	C58	0.482	0.034			
C19	2.785	1.531	C59	0.480	0.037			
C20	2.667	1.423	C60	0.459	0.032			
C21	2.587	1.367	C61	0.438	0.027			
C22	2.627	1.384	C62	0.450	0.024			
C23	2.669	1.376	C63	0.443	0.023			
C24	2.517	1.299	C64	0.373	0.022			
C25	2.526	1.267	C65	0.355	0.016			
C26	2.532	1.169	C66	0.348	0.015			
C27	2.537	1.112	C67	0.365	0.012			
C28	2.504	1.014	C68	0.343	0.007			
C29	2.435	0.925	C69	0.324	0.004			
C30	2.228	0.721	C70	0.291	0.003			
C31	2.005	0.607	C71	0.210	0.002			
C32	1.718	0.479	C72	0.151	0.001			
C33	1.630	0.409	C73	0.148	0.001			
C34	1.536	0.311	C74	0.138	0.001			
C35	1.226	0.228	C75	0.155	0.000			
C36	1.191	0.180	C76	0.119	0.001			
C37	1.172	0.161	C77	0.117	0.001			
C38	1.118	0.148	C78	0.133	0.000			

Table 4.2. Physical properties of Uintah Basin crude oils.

Crude Oil Sample	Density (g/m^3)	Pour Point (^oC)	Reid Vapor Press. (psig)
Black Wax (Pariette)	0.8436	33	1.5
YellowWax (Thorne)	0.7853	39	1.3

Table 4.3. Gas condensate composition by GC.

Components	wt %	MW (g/mol)
C2	0.01	
C3	0.06	
iC4	0.11	
nC4	0.24	
iC5	0.51	
nC5	0.57	
C6	2.65	
C7+	95.85	
Total	100.00	130.8

Table 4.4. The composition of biodiesel.

Lipid	Wt %
C8:0	0.009
C10:0	0.018
C11:0	0.001
C12:0	0.019
C13:0	0.000
C14:0	0.096
C15:0	0.038
C16:0	10.7
C16:1	0.110
C17:0	0.085
C18:0	29.5
C18:1n9c	26.0
C18:2n6c	19.2
C18:3n3	11.4
C20:0	1.399
C20:1	0.693
C20:2	0.039
C20:3n3	0.003
C21:0	0.009
C22:0	0.325
C22:1	0.027
C22:2	0.008
C23:0	0.019
C24:0	0.152
C24:1	0.103
C25:0	0.008
C26:0	0.011
C28:0	0.002

CHAPTER 5

ENERGY ANALYSIS FOR BIODIESEL PRODUCTION

Figure 5.1 shows the flow chart of biodiesel production from microalgae with the comparison between the traditional method and the new technologies proposed in this dissertation. In the typical process, the algae were first cultivated in the raceway pond then sent to the dewatering step after matured. The flocculation was used to concentrate the grown algae biomass to get about 1-2 % dry biomass weight to solvent ratio. The concentrated algae suspension will further concentrate by centrifuging to reach about 10-25 % weight ratio [209]. Then, the dense algae slurry will be treated by high-pressure homogenization to break up the cell wall that can facilitate the oil extraction efficiency. The broken algae slurry will send to mixed with hexane for oil extraction. The biocrude extracted from solvent extraction will be converted into the final product biodiesel. The proposed method used the PSDB mentioned in Chapter 2 for algae cultivation and the CIJM mention in Chapter 3 for lipid extraction. The CIJM combined two steps: cell disruption and oil extraction in the traditional process into one single step.

Since we produce biodiesel for energy purposes, the most important thing is the energy requirement for the process. The energy requirement for each step of the process is shown in Table 5.1. The energy requirement is present in the unit of the energy

required for the process (MJ) divided by the energy of the equivalent amount of biodiesel produced (MJ). The combustion heat of biodiesel is assumed to be 37.5 ($MJ/kg_{biodiesel}$), and the transesterification efficiency is assumed to be 90% (TAG to biodiesel) [210]. In this analysis, the TAG concentration in algae biomass is estimated to be 20% (w/w).

For algae cultivation, the energy comparison between PSDBs and raceway pond has been made in Chapter 2. The energy requirement analysis for raceway pond was done by Stephenson et al. [167], are chosen to be the standard for this analysis. We here assume the algae growing condition and production rate are the same as the raceway pond standard condition. Then the energy requirement per unit weight of biomass for PSDBs is about 11.6% of raceway pond system. The detail energy requirement for dewatering can be found in elsewhere [211]. The energy required for flocculation and centrifugation are assumed to be 0.015 and 0.059 $MJ/MJ_{bodiesel}$ in this analysis [167]. The algae weight percent came out from centrifugation is assumed to be 25%. The homogenization pressure is estimated to be 150 MPa for a near complete cell disruption [210]. The energy required for the homogenization operated with 150 MPa is 0.095 $MJ/MJ_{bodiesel}$ and the detailed analysis can be found in elsewhere [212]. The pumping energy is assumed to be the only energy requirement of CIJM. The operating parameters are summarized in Table 5.2.

The pumping energy of CIJM can be calculated by Equation 5.1:

$$P_{CIJM} = \frac{Q_L \rho_L h g}{\eta}, \tag{5.1}$$

where Q_L is the volumetric flow rate of the inlet of CIJM, ρ_L is the liquid density of inlet fluid, h is the total head loss in the tube, g is gravitational acceleration, and η is the pump efficiency of CIJM (η was assumed to be 70% in this experiment). The mixing energy for

the traditional method can be evaluated as a function of algae concentration, TAG concentration, residence time, mixing intensity, and solvent to algae ratio (Equation 5.2) [210].

$$\Phi_{mix} = \frac{I_{mix} t_{res}}{x_{TAG} \rho_{mix} \Delta H^{o}_{c\ biodiesel} \eta_{transest}}, \tag{5.2}$$

where I_{mix} is the mixing intensity, t_{res} is the residence time in CIJM, x_{TAG} is the concentration of TAG, ρ_{mix} is the density of the mixture, $\Delta H^{o}_{c\ biodiesel}$ is the combustion heat of biodiesel, and $\eta_{transest}$is the biodiesel conversion efficiency. The energy required for phase separation can be spited into three parts: separation by centrifuge (Φ_{sep}), solvent evaporation for recycling (Φ_{evap}), and energy requirement due to solvent loss (Φ_{loss}). The energy required for phase separation can be estimated by Equation 5.3-5.6:

$$\Phi_{phase\ separtion} = \Phi_{sep} + \Phi_{evap} + \Phi_{loss}, \tag{5.3}$$

$$\Phi_{sep} = \frac{P_{cent}}{\dot{m}_{TAG} \Delta H^{o}_{c\ biodiesel} \eta_{transest}}, \tag{5.4}$$

$$\Phi_{evap} = \frac{\frac{x_{solv}}{x_{TAG}} \left(\lambda_{solv} + \frac{1}{K} \lambda_{w}\right) (1 - \eta_{energy-rec})}{\Delta H^{o}_{c\ biodiesel} \eta_{transest}}, \tag{5.5}$$

$$\Phi_{loss} = \frac{x_{solv} \phi_{solvent} \Delta H^{o}_{c\ solvent}}{x_{TAG} \Delta H^{O}_{C\ biodiesel} \eta_{transest}}, \tag{5.6}$$

where P_{cent} is the power rate for centrifuge (assumed to be 9800 W [213]), $\dot{m}_{TAG}$is the mass flow rate of TAG flow through the centrifuge, x_{solv} is the solvent concentration, λ_{solv} is the latent heat of solvent, K is the relative volatilization of water to solvent, λ_{w} is the latent heat of water, $\eta_{energy-rec}$ is the recovering efficiency of solvent and water, $\phi_{solvent}$ is the solvent loss ratio (assumed to be 3 kg/tone [212]), and $\Delta H^{o}_{c\ solvent}$ is the combustion heat of solvent. The detail analysis of phase separation energy requirement can be found in elsewhere [210]. The energy required for transesterification has been

estimated elsewhere, and the value of 0.119 $MJ/MJ_{biodiesel}$ are assigned to be used in this analysis [214].

The energy percentage for each step of biodiesel production was shown in Figure 5.2. The two largest energy consumption steps are cultivation (31%) and phase separation (21%). Base on Table 5.1, the total energy requirement for making biodiesel from algae can be saved about 44% by using the proposed method. The total energy required for the biodiesel production is 0.373 $MJ/MJ_{biodiesel}$, which means the whole process is energy positive (energy come out of the product is higher than the energy put into the process). However, if we consider about the combustion efficiency (35% for the internal combustion engine), the energy come out of biodiesel will decrease dramatically. The energy ratio for the process will now become 1.01 $MJ/MJ_{biodiesel}$, which means we cannot generate energy from this process. One should also consider about distribution cost for the biofuel. The energy analysis shows that the process for biodiesel production from algae is still not energy feasible. Therefore, we should keep improving the process.

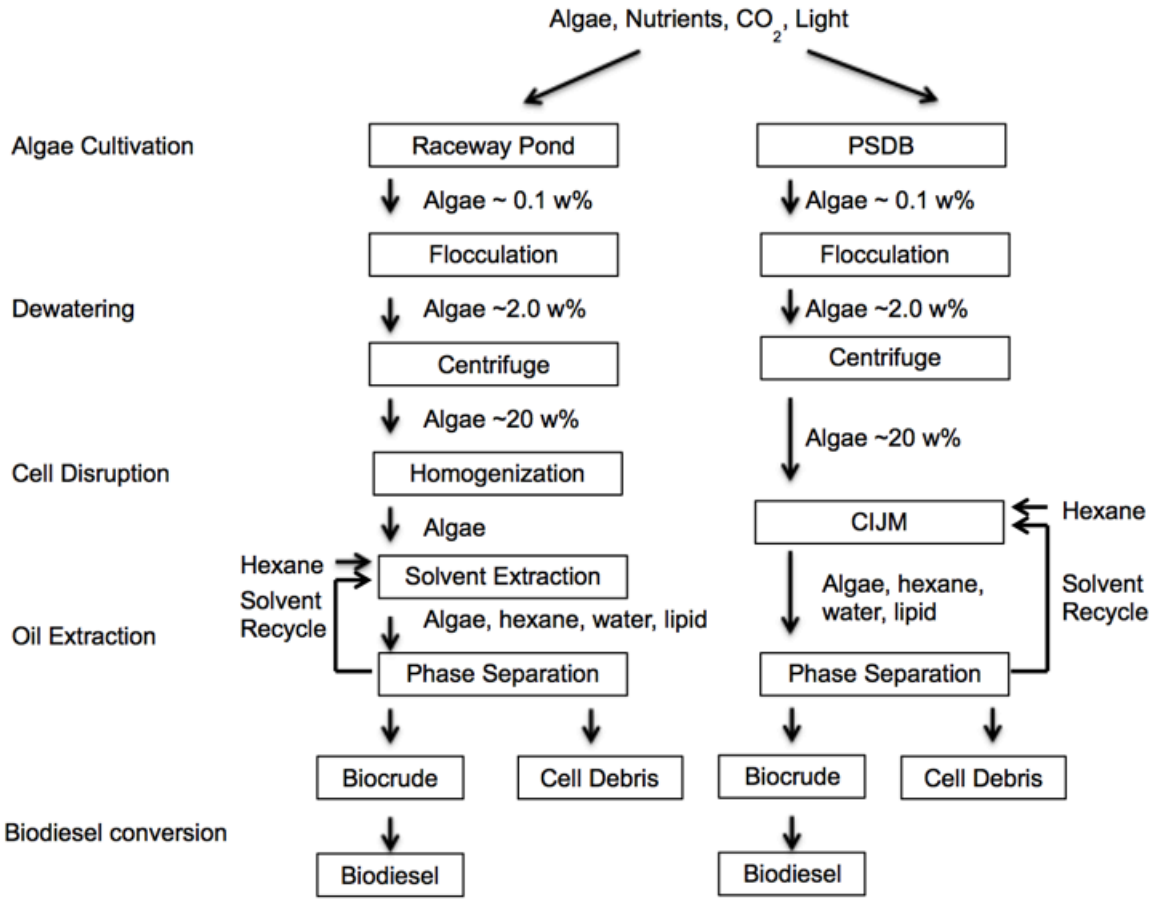

Figure 5.1. The flow chart of biodiesel production from microalgae by traditional method and the proposed method (PSDB+CIJM).

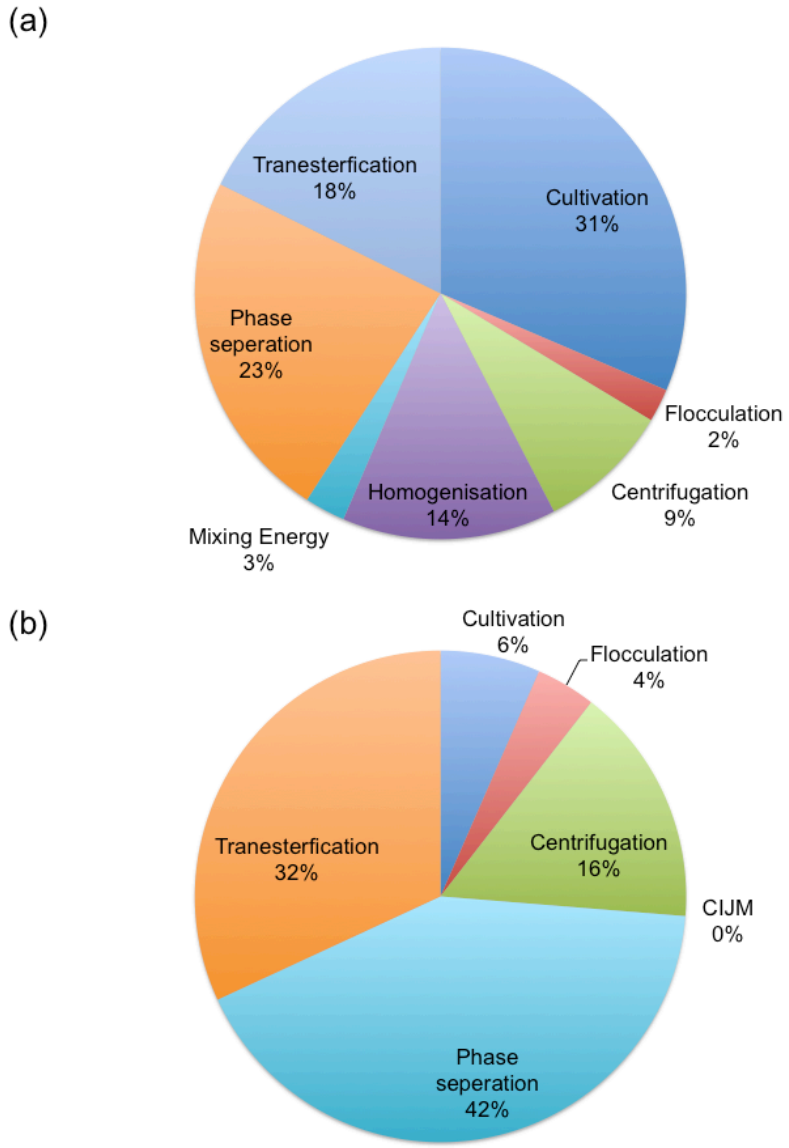

Figure 5.2. (a) The energy percentage for each step of biodiesel production in traditional method. (b) The energy percentage for each step of biodiesel production in proposed method.

Table 5.1. The energy requirement analysis for traditional method and the proposed method (PSDBs and CIJM).

	Traditional Method ($MJ/MJ_{biodiesel}$)	Proposed Method ($MJ/MJ_{biodiesel}$)
Cultivation	0.212	0.025
Flocculation	0.015	0.015
Centrifugation	0.059	0.059
Homogenization	0.095	0.000
Mixing Energy	0.018	$1.27 \cdot 10^{-9}$
Phase Separation	0.156	0.156
Tranesterfication	0.119	0.119
Total Energy	0.673	0.373

Table 5.2. Operation parameters for CIJM

Q(ml/min)	960
Pump Efficiency	0.7
Pipe Length (m)	0.5
Inner Diameter of Pipe (in)	0.25
Solvent to Algae Ratio (V/V)	1

CHAPTER 6

CONCLUSION AND FUTURE WORKS

In this dissertation, we proposed two new technologies and one application for biodiesel production. The idea of PSDBs was inspired by the fluid dynamic technology, which is highly scalable and energy efficient as well. The larger PSDBs were built by assembling the single unit cell reactors, which makes PSDBs fit into any shape of reservoir easily. We have proven that PSDBs can be used for algae cultivation. The three different sized reactors (one-cell, seven-cell, and nineteen-cell) have the same production profiles. Thus, the scalability of PSDBs has been evidenced. The optimal height for a reactor can be predicted from the proposed algae growth model. Based on the theoretical energy analysis, a PSDB is 88.4% energy efficient than the raceway pond system, because the fluid mixing in a PSDB is driven by a pump; however, the raceway pond is powered by a paddle wheel, which is not as efficient as a pump. The cost of the materials for each unit cell of a PSDB decreases when the total cell number increases. The high scalability and energy efficiency of a PSDB allow it to be a competitive candidate for algae cultivation technology.

The CIJM was used to extract algae biocrude and facilitate the biodiesel production. The algae biocrude extraction can be completed in less than a second, which

saves a lot of processing time in comparison with traditional organic solvent extraction method. The wet algae suspension can be directly handled by the CIJM, which saves the energy for dewatering. Due to the high turbulent mixing, the diffusion scale decreases, the algae cell wall breaks up, and the lipids inside the cell wall are released into the liquid phase, which facilitates the lipid diffusion. We also evaluated the multistage extraction, and we found that the optimal stages can be estimated from the proposed model. The CIJM combines the steps of cell disruption and lipid extraction, which occurs in the traditional process, into one single step. The short processing time and wet extraction process of a CIJM allow it to be an alternative technology for algae lipid extraction.

The biodiesel was added into the waxy crude oil (black wax and yellow wax), which was produced in the east Utah. The wax appearance temperature (WAT) was detected by FTIR method. At the 30% weight-mixing ratio (diluent weight/total weight), the WAT of waxy crude oils dropped from 45.1 to 42.4^{o}C for Yellow Wax and from 41.6 to 37.7^{o}C for Black Wax. This result proves that biodiesel can be used as a diluent for waxy crude oil.

Using PSDBs and CIJM for algae biodiesel production can save 44% of energy in comparison with the traditional method. The waxy crude diluent is a new application for the biodiesel. These achievements make algae biodiesel production more feasible and energy favorable. However, the technologies proposed in this dissertation are not perfect yet. The general ideals for PSDB and CIJM optimization are listed in the next section.

Algae Photobioreactor

We already demonstrated the scalability of PSDB in the previous chapter. The next goal for this objective is to optimize the PSDB. Several factors affect the performance of PSDB like algae species, nutrient strategy, CO_2 supply, temperature control, PH control, light intensity, piping system, water recycle, and dilution rate. Since we already proofed the scalability, all the work related to optimization can be done in the single cell reactor.

First, the algae species is the most important parameter that affects the production rate. Some algae grow faster, and some can produce more lipids. To get the maximum production rate, one should test several algae species in PSDB. One can start with the growing condition mention in the previous chapter. Then choose the species with highest production rate to continue the rest optimization.

Once the algae species was selected, the growing condition becomes critical for production rate. The growing conditions include temperature, nutrients, CO_2, and PH. For temperature, algae growth rate should increase when the temperature increase before it hit the optimized temperature. Once it reaches the optimized temperature, the algae growth rate will start to decrease when the temperature increase. Temperature control system can be used to control the temperature of PSDB. Nutrients are another important factor for algae growing. Nitrogen-starving strategy can increase the lipids percentage inside of algae. Two stages of growing strategies can also be used to grow the algae. Carbon dioxide is one of the essential components required for algae growing. The CO_2 supply can come from the gas cylinder in the lab or a power plant outside. One can try to place a small nozzle at the center of the bottom, which can be countercurrent of the

circulation flow. The optimized PH environment should also be determined for the optimized algae species.

After finished the optimization of single unit cell reactor. The large-scale pilot plant should be built in the outdoor environment to evaluate the performance of PSDB in the open environment. The material used to make large-scale PSDB should be made of concrete instead of the current material acrylic.

Confined Impinging Jet Mixer

It was demonstrated that CIJM could facilitate the microalgae lipid extraction. The biocurde extracted by CIJM can be converted into biodiesel by transesterification. The future work of CIJM should focus on the optimization of CIJM, scale-up of CIJM, and try to fit in the biofuel production process.

For CIJM optimization, there are some parameters should be tested just like: different organic solvents, CIJM geometry, and the effect of temperature. Due to the material restriction, there is only hexane been used in this thesis. One should try to make CIJM with chemical resistance material like Teflon, PEEK, or metal. The organic solvent is an important parameter of the lipid extraction. Because hexane is a nonpolar solvent, one can start from some polar solvent like chloroform or the combination of polar and nonpolar like methanol and chloroform. The geometry of CIJM is also one of the parameters that can be evaluated. One can start by changing the angle of inlets or the shape of the mixing chamber. Temperature can facilitate the lipid extraction but will also increase the process cost. One can evaluate the effect of temperature by building CIJM in

temperature resistance material and heating it up with the water bath or just place it on the hot plate.

The cell wall strength should vary with different algae species. Therefore, the optimized flow rate will be different for each algae strain. One should run the CIJM test for several potential algae candidates to establish the optimized flow rate database. Productivity is the key for algae harvesting. Therefore, one can try to build a large scale of CIJM. There are some parameters should be determined just like the geometry ratio between the inlet channel and mixing chamber and the optimized flow rate for each geometry.

To simplify the algae harvesting process, one can test the straight conversion from algae suspension into biodiesel. The algae suspension can be mixed with methanol in a heated CIJM. The small mixing length scale provides by CIJM can facilitate the biodiesel conversion. Since all the reactions happen in such a small region, the energy required to produce biodiesel can be minimized. The time needed for biodiesel conversion can be minimized too.

For algae biodiesel production, there are some parameters need to be determined just like algae suspension concentration (algae dry biomass/algae suspension weight) and TAG concentration in biocrude. The algae suspension concentration for CIJM inlet has been evaluated in Chapter 3, but the maximum inlet concentration has not been determined. There should be a maximum pump able concentration for algae suspension. One should evaluate the biocrude yield for the highest concentration and compare to the results in Chapter 3. The TAG concentration in the biocrude is essential for the biodiesel conversion. The TAG is the target component for biodiesel conversion in the biocrude.

One should know the TAG concentration to estimate the actual production rate for biodiesel.

REFERENCES

[1] Chisti, C. Biodiesel from Microalgae. *Biotechnol. Adv.* **2007**, *25*, 294-306.

[2] Halim, R.; Danquah, M. K.; Webley, P. A. Extraction of Oil from Microalgae for Biodiesel Production: A Review. *Biotechnol. Adv,* **2012**, *30*, 709-732.

[3] Doucha, J.; Straka, F.; Lívanský, K. Utilization of Flue Gas for Cultivation of Microalgae Chlorella Sp. in an Outdoor Open Thin-Layer Photobioreactor. *J. Appl. Phycol.* **2005**, *17*, 403-412.

[4] Negoro, M.; Shioji, N.; Miyamoto, K.; Micira, Y. Growth of Microalgae in High CO_2 Gas and Effects of SO_X and NO_X. *Appl. Biochem. Biotechnol.* **1991**, *28*, 877-886.

[5] Negoro, M.; Shioji, N.; Ikuta, Y.; Makita, T.; Uchiumi, M. Growth Characteristics of Microalgae in High-Concentration CO_2 Gas, Effects of Culture Medium Trace Components, and Impurities Thereon. *Appl. Biochem. Biotechnol.* **1992**, 34, 681-692.

[6] *International Energy Outlook 2014: World Petroleum and Other Liquid Fuels*; U. S. Energy Information Administration, U. S. Government Printing Office: Washington, DC, 2014.

[7] *International Energy Outlook 2013: With Projections To 2040*; U. S. Energy Information Administration, U. S. Government Printing Office: Washington, DC, 2013.

[8] World Population 2012; U. S. Department of Engergy, United Nations, Population Division, 2012.

[9] Widjaja, A.; Chien, C.-C.; Ju, Y.-H. Study of Increasing Lipid Production from Fresh Water Microalgae Chlorella Vulgaris. *J. Taiwan Inst. Chem. Eng.* **2009**, *40*, 13-20.

[10] Dinh, L. T. T.; Guo, Y.; Mannan, M. S.; Sustainability Evaluation of Biodiesel Production Using Multicriteria Decision-Making. *Environ. Prog. Sustain. Energy.* **2009**, *28*, 38-46.

[11] Renaud, S. M.; Zhou, H. C.; Parry, D. L.; Thinh, L. V.; Woo, K. C. Effect of Temperature on the Growth, Total Lipid Content and Fatty Acid Composition of Recently Isolated Tropical Microalgae Isochrysis Sp., Nitzschia Closterium, Nitzschia Paleacea, and Commercial Species Isochrysis Sp. (Clone T.ISO). *J. Appl. Phycol.* **1995**, *7*, 595-602.

[12] Renaud, S. M.; Thinh, L.V.; Lambrinidis, G.; Parry, D. L. Effect of Temperature on Growth, Chemical Composition and Fatty Acid Composition of Tropical Australian Microalgae Grown in Batch Cultures. *Aquaculture.* **2002**, *211*, 195-214.

[13] Gramling, C. As Green as it Gets: Algae Biofuels. *Earth,* **2009**.

[14] Demirbas, A. Biodiesel From Oilgae, Biofixation Of Carbon Dioxide By Microalgae: A Solution to Pollution Problems. *Appl. Energ.* **2011**, *88*, 3541-3547.

[15] Atabani, A. E.; Silitonga, A. S.; Badruddin, I. A.; Mahlia, T. M. I.; Masjuki, H. H.; Mekhilef, S. A Comprehensive Review on Biodiesel as an Alternative Energy Resource and its Characteristics. *Renew. Sust. Energ. Rev.* **2012**, *16*, 2070-2093.

[16] The Washington Post. A Promising Oil Alternative: Algae Energy. http://washingtonpost.com (Accessed Jul 21, 2008).

[17] Sheehan, T. D.; Benemann, J.; Roessler, P. A Look Back At The U.S. Department of Energy's Aquatic Species Program—Biodiesel from Algae. *National Renewable Energy Laboratory,* **1998**.

[18] John, R. P.; Anisha, G. S.; Nampoothiri, K. M.; A. Pandey. Micro and Macroalgal Biomass: A Renewable Source for Bioethanol. *Bioresour. Technol.* **2011**, *102*, 186-193.

[19] Ellis, J. T.; Hengge, N. N.; Sims, R. C.; Miller, C. D. Acetone, Butanol, and Ethanol Production from Wastewater Algae. *Bioresour. Technol.* **2012***, 111*, 491-495.

[20] Demirbas, M. F. Biofuels from Algae for Sustainable Development. *Appl. Energy.* **2011**, *88*, 3473-3480.

[21] Pienkos P. T.; Darzins A. The Promise and Challenges of Microalgal-Derived Biofuels. *Biofuels, Bioprod. Biorefin.* **2009**, *3*, 431-440.

[22] Butterwick, C.; Heaney, S. I.; Talling J. F. Diversity in the Influence of Temperature on the Growth Rates of Freshwater Algae, and its Ecological Relevance. *Freshwater Biol.* **2005**, *50*, 291-300.

[23] Sorgeloos, P.; Lavens. P. *Manual on the Production and Use of Live Food for Aquaculture*; Food and Agriculture Organization of United Nations: Rome, 1996.

[24] Clarens, A. F.; Resurreccion, E. P.; White, M. A.; Colosi, L. M. Environmental Life Cycle Comparison of Algae to other Bioenergy Feedstocks. *Environ. Sci. Technol.* **2010**, *44*, 1813-1819.

[25] Suh I.; Lee, C.-G. Photobioreactor Engineering: Design and Performance," *Biotechnol. Bioprocess Eng.* **2003**, *8*, 313-321.

[26] Prokop, A.; Quinn, M. F.; Fekri, M.; Murad, M.; Ahmed, S. A. Spectral Shifting by Dyes to Enhance Algae Growth. *Biotechnol. Bioeng.* **1984**, *26*, 1313-1322.

[27] Stephen, B. P. Photoinhibition of Photosynthesis Induced by Visible Light. *Ann. Rev. Plant Physiol,* **1984**, *35*, 15-44.

[28] Kodama, M.; Ikemoto, H.; Miyachi, S. A New Species of Highly CO_2 Tolerant Fast Growing Marine Microalga Suitable for High Density Culture. *Mar. Biotechnol.* **1993**, *1*, 21-25.

[29] Ugwu, C. U.; Aoyagi, H.; Uchiyama, H. Photobioreactors for Mass Cultivation of Algae. *Bioresour Technol.* **2008**, *99*, 4021-4028.

[30] Camacho, F. G.; Gómez, A. C.; Sobczuk, T. M.; Grima, E. M. Effects of Mechanical and Hydrodynamic Stress in Agitated, Sparged Cultures of Porphyridium Cruentum. *Process Biochem.* **2000**, *35*, 1045-1050.

[31] Mandalam R. K.; Palsson, B. Elemental Balancing of Biomass and Medium Composition Enhances Growth Capacity in High-Density Chlorella Vulgaris Cultures. *Biotechnol. Bioeng.* **1998**, *59*, 605-611.

[32] Horsman, Y.; Li, M.; Wang, B.; Wu, N.; Lan, C. Effects of Nitrogen Sources on Cell Growth and Lipid Accumulation of Green Alga Neochloris Oleoabundans. *Appl. Microbiol. Biotechnol.* **2008**, *81*, 629-636.

[33] Zhang, Z.; Sachs, J. P.; Marchetti, A. Hydrogen Isotope Fractionation in Freshwater and Marine Algae: II. Temperature and Nitrogen Limited Growth Rate Effects. *Org. Geochem.* **2009**, *40*, 428-439.

[34] Goldman J. C.; Carpenter, E. J. A Kinetic Approach to the Effect of Temperature on Algal Growth. *Limnol. Oceanogr.* **1974**, *19*, 756-766.

[35] Pulz, O. Photobioreactors: Production Systems for Phototrophic Microorganisms. *Appl. Microbiol. Biotechnol.* **2001**, *57*, 287-293.

[36] Lee Y.-K.; Pirt, S. J. CO_2 Absorption Rate in an Algal Culture: Effect of Ph. *J. Chem Technol. Biotechnol. Biotechnology,* **1984**, *34*, 28-32.

[37] Coleman, J. R.; Colman, B. Inorganic Carbon Accumulation and Photosynthesis in a Bluegreen Alga as a Function of External Ph. *Plant Physiol.* **1981**, *67*, 32-899.

[38] Rubio, F. C.; Fernández, F. G. A.; Pérez, J. A. S.; Camacho, F. G. Grima, E. M. Prediction of Dissolved Oxygen and Carbon Dioxide Concentration Profiles in Tubular Photobioreactors for Microalgal Culture. *Biotechnol. Bioeng.* **1999**, *62*, 71-86.

[39] Brennan L.; Owende, P. Biofuels from Microalgae: A Review of Technologies for Production, Processing, and Extractions of Biofuels and Co-Products. *Renew. Sust. Energ. Rev.* **2010**, *14*, 557-577.

[40] Terry K. L.; Raymond, L. P. System Design for the Autotrophic Production of Microalgae. *Enzyme Microb. Technol.* **1985**, *7*, 474-487.

[41] Lee, Y.-K. Microalgal Mass Culture Systems and Methods: Their Limitation and Potential. *J. Appl. Phycol.* **2001**, *13*, 307-315.

[42] Pulz O. Scheibenbogen, K. Photobioreactors: Design and Performance with Respect to Light Energy Input. *Bioproc. Algae Reactor Technol. Apoptosis*. **1998**, *59*, 123-152.

[43] Borowitzka, L. J.; Borowitzka, M. A. Commercial Production of (3-Carotene Bydunaliella Salina in Open Ponds. *Bull. Mar. Sci.* **1990**, *47*, 244-252.

[44] Singh R. N.; Sharma, S. Development of Suitable Photobioreactor for Algae Production: A Review. *Renew. Sust. Energ. Rev.* **2012**, *16*, 2347-2353.

[45] Mata, T. M.; Martins, A. A.; Caetano, N. S. Microalgae for Biodiesel Production and other Applications: A Review. *Renew. Sust. Energ. Rev,* **2010**, *14*, 217-232.

[46] Takano, H.; Takei, R.; Manabe, E.; Burgess, J. G.; Hirano, M.; Matsunaga, T. Increased Coccolith Production by Emiliania Huxleyi Cultures Enriched with Dissolved Inorganic Carbon. *Appl. Microbiol. Biotechnol.* **1995**, *43*, 460-465.

[47] Javanmardian, M.; Palsson, B. O. High-Density Photoautotrophic Algal Cultures: Design, Construction, and Operation of a Novel Photobioreactor System. *Biotechnol. Bioeng.* **1991**, *38*, 1182-1189.

[48] Lee, C. G.; Palsson, B. High-Density Algal Photobioreactors Using Light-Emitting Diodes. *Biorechnol. Bioeng,* **1994**, *44*, 1161-1167.

[49] Suh I. S.; Lee, S. B. A Light Distribution Model for an Internally Radiating Photobioreactor. *Biotechnol. Bioeng.* **2003**, *82*, 180-189.

[50] Csőgör, Z.; Herrenbauer, M.; Schmidt, K. Posten, C. Light Distribution In a Novel Photobioreactor: Modelling for Optimization. *J. Appl. Phycol.* **2001**, *13*, 325-333.

[51] Suh I.; Lee, S. Cultivation of a Cyanobacterium in an Internally Radiating Air-Lift Photobioreactor. *J. Appl. Phycol.* **2001**, *13*, 381-388.

[52] Sánchez Mirón, A.; Contreras Gómez, A. GarcíA Camacho, F.; Molina Grima, E.; Chisti, Y. Comparative Evaluation of Compact Photobioreactors for Large-Scale Monoculture of Microalgae. *J. Biotechnol.* **1999**, *70*, 249-270.

[53] Chisti, Y. Shear Sensitivity. *Encyclop. Bioprocess Technol.: Fermentation, Biocatalysis, Bioseparation,* **1999**, *5*, 2379-2406.

[54] Burlew, J. S. Algal Culture from Laboratory to Pilot Plant. *Carnegie Institution of Washington.* **1953**, *1*, 357.

[55] Milner, H. W. Algal Culture from Laboratory to Pilot Plant. *Carnegie Institution of Washington,* **1953**, *1*, 108.

[56] Slegers, P. M.; Wijffels, R. H.; Straten, G. V.; Boxtel, A. J. B. Design Scenarios for Flat Panel Photobioreactors. *Appl. Energy.* **2011**, *88*, 3342-3353.

[57] Buehner, M. R.; Young, P. M.; Willson, B.; Rausen, D.; Schoonover, R.; Babbitt, G. Microalgae Growth Modeling and Control for a Vertical Flat Panel Photobioreactor. *A. C. C.* **2009**, *1*, 2301-2306.

[58] Sierra, E.; Acién, F. G.; Fernández, J. M.; García, J. L.; González, C.; Molina, E. Characterization of a Flat Plate Photobioreactor for the Production of Microalgae. *Chem. Eng. J.* **2008**, *138*, 136-147.

[59] Barbosa, M. J.; Zijffers, J. W.; Nisworo, A.; Vaes, W.; Schoonhoven, J. V.; Wijffels, R. H. Optimization of Biomass, Vitamins, and Carotenoid Yield on Light Energy in a Flat-Panel Reactor Using the A-Stat Technique. *Biotechnol. Bioeng.* **2005**, *89*, 233-242.

[60] Camacho, F. G.; Rodríguez, J. G.; Mirón, A. S.; García, M. C. C.; Belarbi, E. H.; Chisti, Y. Biotechnological Significance of Toxic Marine Dinoflagellates. *Biotechnol. Adv.* **2007**, *25*, 176-194.

[61] Molina, E.; Fernández, J.; Acién, F. G.; Chisti, Y. Tubular Photobioreactor Design for Algal Cultures. *J. Biotechnol.* **2001**, *92*, 113-131.

[62] Acién Fernández, F. G.; Fernández Sevilla, J. M.; Sánchez Pérez, J. A.; Molina Grima, E.; Chisti, Y. Airlift-Driven External-Loop Tubular Photobioreactors for Outdoor Production of Microalgae: Assessment of Design and Performance. *Chem. Eng. Sci.* **2001**, *56*, 2721-2732.

[63] Molina, E; Acién Fernández, F. G.; García Camacho, F.; Camacho Rubio, F., Chisti, Y. Scale-Up of Tubular Photobioreactors. *J. Appl. Phycol.* **2000**, *12*, 355-368.

[64] MR, T. Bioreactors, Photo. Flickinger MC, Drew SW, Editors. *Encycl. Bioprocess Technol. Fermen. Biocatal. Biosep.* **1999**, *1*, 395-419.

[65] Murray, M.-Y.; Chisti Y, Improve the Performance of Airlift Reactors. *Chem. Eng. Prog.* **1993**, *89*, 38-45.

[66] Chisti, Y. Pneumatically Agitated Bioreactors in Industrial and Environmental Bioprocessing: Hydrodynamics, Hydraulics, and Transport Phenomena. *Appl. Mech. Rev.* **1998**, *51*, 33-112.

[67] Molina Grima, E.; Fernández, F. G. A.; GarcíA Camacho, F.; Chisti, Y. Photobioreactors: Light Regime, Mass Transfer, and Scaleup. *J. Biotechnol.* **1999**, *70*, 231-247.

[68] Kumar, K.; Dasgupta, C. N.; Nayak, B.; Lindblad, P.; Das, D. Development of Suitable Photobioreactors for CO_2 Sequestration Addressing Global Warming Using Green Algae and Cyanobacteria. *Bioresour. Technol.* **2011**, *102*, 4945-4953.

[69] Hoshino, K.; Hamochi, M.; Mitsuhashi, S.; Tanishita, K. Measurements of Oxygen Production Rate in Flowing Spindina Suspension. *Appl. Microbial. Biotechnol.,* 1991, *35*, 89-93.

[70] Mignot, L.; Junter, G. A.; Labbé, M. A New Type of Immobilized-Cell Photobioreactor with Internal Illumination by Pptical Fibres. *Biotechnol. Tech.* **1989**, *3*, 299-304.

[71] Yakunin, A. F.; Tsygankov, A. A.; Gogotov, I. N.; L'vov, N. P. Dependence of the Nitrogenase and Nitrate Reductase Activities on the Molybdenum Concentration in the Medium and Assimilation of Nitrate in Cells of Rhodopseudomonas Capsulata. *Mikrobiologiya.* **1986**, *55*, 564-569.

[72] Muñoz, R.; Köllner, C.; Guieysse, B.; Mattiasson, B. Photosynthetically Oxygenated Salicylate Biodegradation in a Continuous Stirred Tank Photobioreactor. *Biotechnol. Bioeng.* **2004**, *87*, 797-803.

[73] Patrick, E.; Wiley, B. M. Production of Biodiesel and Biogas from Algae: A Review of Process Train Options. *Water Environ. Res.* **2011**, *83*, 326-338.

[74] Teixeira, M. R.; Rosa, M. J. Comparing Dissolved Air Flotation and Conventional Sedimentation to Remove Cyanobacterial Cells of Microcystis Aeruginosa: Part I: The Key Operating Conditions. *Sep. Purif. Technol*. **2006**, *52*, 84-94.

[75] Ebeling, J. M.; Sibrell, P. L.; Ogden, S. R.; Summerfelt, S. T. Evaluation of Chemical Coagulation–Flocculation Aids for the Removal of Suspended Solids and Phosphorus from Intensive Recirculating Aquaculture Effluent Discharge. *Aquacul. Eng.* **2003**, *29*, 23-42.

[76] Molina Grima, E.; Belarbi, E. H.; Acién Fernández, F. G.; Robles Medina, A.; Chisti, Y. Recovery of Microalgal Biomass and Metabolites: Process Options and Economics. *Biotechnol. Adv.* **2003**, *20*, 491-515.

[77] Wiley, P. E.; Brenneman, K. J.; Jacobson, A. E. Improved Algal Harvesting Using Suspended Air Flotation. *Water Environ. Res.* **2009**, *81*, 702-708.

[78] Uduman, N.; Qi, Y.; Danquah, M. K.; Forde, G. M.; Hoadley, A. Dewatering of Microalgal Cultures: A Major Bottleneck to Algae-Based Fuels. *J. Renew. Sus. Energ.* **2010**, *2*, 12-701.

[79] Shelef, G.; Sukenik, A.; Green, M. Microalgae Harvesting and Processing: A Literature Review; Technical Report. U. S. Mar. 1984.

[80] Koopman B.; Lincoln, E. P. Autoflotation Harvesting of Algae from High-Rate Pond Effluents. *Agricul. Wastes,* **1983**, *5*, 231-246.

[81] Al-Shamrani, A. A.; James, A.; Xiao, H. Separation of Oil from Water by Dissolved Air Flotation. *Colloids and Surfaces A: Physicochemical and Engineering Aspects,* **2002**, *209*, 15-26.

[82] Lundh, M.; Jönsson, L.; Dahlquist, J. Experimental Studies of the Fluid Dynamics in the Separation Zone in Dissolved Air Dlotation. *Water Res.* **2000**, *34*, 21-30.

[83] Chung, Y.; Choi, Y. C.; Choi, Y. H.; Kang, H. S. A Demonstration Scaling-Up of the Dissolved Air Flotation. *Water Res.* **2000**, *34*, 817-824.

[84] Féris, L. A.; Rubio, J. Dissolved Air Flotation (DAF) Performance at Low Saturation Pressures. *Filtr. Sep.* **1999**, *36*, 61-65.

[85] French, K.; Guest, R. K.; Finch, G. R.; Haas, C. N. Correlating Cryptosporidium Removal Using Dissolved Air Flotation in Water Treatment. *Water Res.* **2000**, *34*, 4116-4119.

[86] Bailey Green, F.; Bernstone, L. S.; Lundquist, T. J.; Oswald, W. J. Advanced Integrated Wastewater Pond Systems for Nitrogen Removal. *Water Sci. Technol.* **1996**, *33*, 207-217.

[87] Chen, G. Electrochemical Technologies in Wastewater Treatment. *Sep. Purif. Technol.* **2004**, *38*, 11-41.

[88] Jiang, J.-Q.; Graham, N.; André, C.; Kelsall, G. H.; Brandon, N. Laboratory Study of Electro-Coagulation–Flotation for Water Treatment. *Water Res.* **2002**, *36*, 4064-4078.

[89] Mollah, M. Y. A.; Morkovsky, P.; Gomes, J. A. G.; Kesmez, M.; Parga, J.; Cocke, D. L. Fundamentals, Present and Future Perspectives of Electrocoagulation. *J. Hazard. Mater.* **2004**, *114*, 199-210.

[90] Mollah, M. Y. A.; Schennach, R.; Parga, J. R.; Cocke, D. L. Electrocoagulation (EC) — Science and Applications. *J. Hazard. Mater.* **2001**, *84*, 29-41.

[91] Emamjomeh M. M., Sivakumar, M. Review of Pollutants Removed by Electrocoagulation and Electrocoagulation/Flotation Processes. *J. Environ. Manage.* **2009**, *90*, 1663-1679.

[92] Burns, S. E.; Yiacoumi, S.; Tsouris, C. Microbubble Generation for Environmental and Industrial Separations. *Sep. Purif. Technol.* **1997**, *11*, 221-232.

[93] Holt, P. K.; Barton, G. W.; Mitchell, C. A. The Future for Electrocoagulation as a Localised Water Treatment Technology. *Chemosphere.* **2005**, *59*, 355-367.

[94] Golueke, C. G.; Oswald, W. J. Harvesting and Processing Sewage-Grown Planktonic Algae. *J. Water Pollut. Control Fed.* **1965**, *37*, 471-498.

[95] Schenk, P.; Thomas-Hall, S.; Stephens, E.; Marx, U.; Mussgnug, J.; Posten, C. Second Generation Biofuels: High-Efficiency Microalgae for Biodiesel Production. *Bioenerg. Res.* **2008**, *1*, 20-43.

[96] Viessman, W. H. M. *Water Supply and Pollution Control*; Pearson Prentice Hall: Upper Saddle River, **2004**.

[97] Stechemesser, H. D. B. *Coagulation and Flocculation*; CRC Press: Boca Raton, **2005**.

[98] Milledge J.; Heaven, S. A Review of the Harvesting of Micro-Algae for Biofuel Production. *Rev. Environ. Sci. Bio/Technol.* **2013**, *12*, 165-178.

[99] Perrot, P. *A To Z of Thermodynamics*: Oxford University Press, **1998**.

[100] Cordero B.; Voltolina, D. Viability of Mass Algal Cultures Preserved by Freezing and Freeze-Drying. *Aquacul. Eng.* **1997**, *16*, 205-211.

[101] Mubarak, M.; Shaija, A.; Suchithra, T. V. A Review on the Extraction of Lipid from Microalgae for Biodiesel Production. *Algal Res.* **2015**, *7*, 117-123.

[102] Demirbaş, A. Production of Biodiesel from Algae Oils. *Energ. Source. Part A: Recovery, Utilization, Environ. Effects,* **2008**, *31*, 163-168.

[103] Mercer P.; Armenta, R. E. Developments in Oil Extraction from Microalgae. *Eur. J. Lipid Sci. Technol.* **2011**, *113*, 539-547.

[104] K. M, Definition and Classification of Lipids. Techniques of Lipidology Isolation, Analysis, and Identification of Lipids. *Elsevier Science* **1986**.

[105] Volkman JK, J. S.; Nichols, P. D.; Rogers, G. I.; Garland, C. D. Fatty Acid and Lipid Composition of 10 Species of Microalgae Used in Mariculture. *J. Exp.L Mar. Biol. Ecol.* **1989**, *40*, 91.

[106] Khan L. M.; Hanna, M. A. Expression of Oil from Oilseeds—A Review. *J. Agr. Eng. Res.* **1983**, *28*, 495-503.

[107] Niraj, S.; Tapare, S.; Khedka, V.; Chavan, Y. P.; Bhagat, S. L. Extraction of Oil from Algae by Solvent Extraction and Oil Expeeler Method. *Int. J. Chem. Sci,* **2011**, *9*, 1746-1750.

[108] Harun, R.; Singh, M.; Forde, G. M.; Danquah, M. K. Bioprocess Engineering of Microalgae to Produce a Variety of Consumer Products. *Renew. Sus. Energ. Rev.* **2010**, *14*, 1037-1047.

[109] Lee, S.; Yoon, B.-D.; Oh, H. M. Rapid Method for the Determination of Lipid From the Green Alga Botryococcus Braunii. *Biotechnol. Tech.* **1998**, *12*, 553-556.

[110] Wei, F.; Gao, G. Z.; Wang, X. F.; Dong, X. Y.; Li, P. P.; Hua, W. Quantitative Determination of Oil Content in Small Quantity of Oilseed Rape by Ultrasound-Assisted Extraction Combined with Gas Chromatography. *Ultrason. Sonochem.* **2008**, *15*, 938-942.

[111] Iqbal J.; Theegala, C. Microwave Assisted Lipid Extraction from Microalgae Using Biodiesel as Co-Solvent. *Algal Re.* **2013**, *2*, 34-42.

[112] Virot, M.; Tomao, V.; Ginies, C.; Visinoni, F.; Chemat, F. Microwave-Integrated Extraction of Total Fats and Oils. *J. Chromatogr. A.* **2008**, *1196*, 57-64.

[113] Grima, E. M.; Medina, A. R.; Giménez, A. G.; Sánchez Pérez, J. A.; Camacho, F. G.; García Sánchez, J. L. Comparison Between Extraction of Lipids and Fatty Acids from Microalgal Biomass. *J. Am. Oil Chem. Soc.* **1994**, *71*, 955-959.

[114] Fajardo, A. R.; Cerdán, L. E.; Medina, A. R.; Fernández, F. G. A.; Moreno, P. A. G.; Grima, E. M. Lipid Extraction from the Microalga Phaeodactylum Tricornutum. *Eur. J. Lipid Sci. Technol.* **2007**, *109*, 120-126.

[115] Pieber, S.; Schober, S.; Mittelbach, M. Pressurized Fluid Extraction of Polyunsaturated Fatty Acids from the Microalga Nannochloropsis Oculata. *Biomass Bioenerg.,* **2012**, *47*, 474-482.

[116] Folch, J.; Lees, M.; Sloane-Stanley, GH. A Simple Method of Isolation and Purification of Total Lipids from Animal Tissues. *J. Biol. Chem,* **1956**, *1*, 497-509.

[117] Willis, R. M.; Mccurdy, A. T.; Ogborn, M. K.; Wahlen, B. D.; Quinn, J. C.; Pease III, L. F. Improving Energetics of Triacylglyceride Extraction from Wet Oleaginous Microbes. *Bioresource Technol.* **2014**, *167*, 416-424.

[118] Guckert JB, C. K.; Jackson, LL. Lipid Solvent Systems are Not Equivalent for Analysis of Lipid Classes in the Microeukaryotic Green Alga, Chlorella. *J Microbiol. Meth.* **1988**, *49*, 2.

[119] Taylor, L. T. *Supercritical Fluid Extraction*; Wiley: Hoboken, **1996**.

[120] Pourmortazavi S. M.; Hajimirsadeghi, S. S. Supercritical Fluid Extraction in Plant Essential and Volatile Oil Analysis. *J. Chromatogr. A*. **2007**, *1163*, 2-24.

[121] Hu, Q.; Pan, B.; Xu, J.; Sheng, J.; Shi, Y. Effects of Supercritical Carbon Dioxide Extraction Conditions on Yields and Antioxidant Activity of Chlorella Pyrenoidosa Extracts. *J. Food Eng.* **2007**, *80*, 997-1001.

[122] Santana, A.; Jesus, S.; Larrayoz, M. A.; Filho, R. M. Supercritical Carbon Dioxide Extraction of Algal Lipids for the Biodiesel Production. *Procedia Eng.* **2012**, *42*, 1755-1761.

[123] Macías-Sánchez, M. D.; Mantell, C.; Rodríguez, M.; Martínez De La Ossa, E.; Lubián, L. M.; Montero, O. Supercritical Fluid Extraction of Carotenoids and Chlorophyll a from Synechococcus Sp. *J. Supercrit. Fluids.* **2007**, *39*, 323-329.

[124] Young, G.; Nippgen, F.; Titterbrandt, S.; Cooney, M. J. Lipid Extraction from Biomass Using Co-Solvent Mixtures of Ionic Liquids and Polar Covalent Molecules. *Sep. Purif. Technol.* **2010**, *72*, 118-121.

[125] Dzyuba S. V.; Bartsch, R. A. Expanding the Polarity Range of Oonic Liquids. *Tetrahedron Letters.* **2002**, *43*, 4657-4659.

[126] Freire, M. G.; Santos, L. M. N. B. F.; Fernandes, A. M.; Coutinho, J. A. P.; Marrucho, I. M. An Overview of the Mutual Solubilities of Water–Imidazolium-Based Ionic Liquids Systems. *Fluid Phase Equilibria,* **2007**, *261*, 449-454.

[127] Huddleston, J. G.; Visser, A. E.; Reichert, W. M.; Willauer, H. D.; Broker, G. A.; Rogers, R. D. Characterization and Comparison of Hydrophilic and Hydrophobic Room Temperature Ionic Liquids Incorporating the Imidazolium Cation. *Green Chem.* **2001**, *3*, 156-164.

[128] Kim, Y. H.; Choi, Y. K.; Park, J.; Lee, S.; Yang, Y. H.; Kim, H. J. Ionic Liquid-Mediated Extraction of Lipids from Algal Biomass. *Bioresource Technol.* **2012**, *109*, 312-315.

[129] Ahmad, D.; Adlie, K.; Shamsuri, A. Ionic Liquids: Preparations and Limitations. *Makara, Sains.* **2010**, *14*, 101-106.

[130] Ben-Amotz, A.; Tornabene, T. G.; Thomas, W. H. Chemical Profile of Selected Species of Microalgae with Emphasis on Lipids1. *J. Phycol.* **1985**, *21*, 72-81.

[131] Banerjee, A.; Sharma, R.; Chisti, Y.; Banerjee, U. C.; Botryococcus Braunii: A Renewable Source of Hydrocarbons and other Chemicals. *Crit. Rev. Biotechnol.* **2002**, *22*, 245-279.

[132] Metzger P.; Largeau, C. Botryococcus Braunii: A Rich Source for Hydrocarbons and Related Ether Lipids. *Appl. Microbiol. Biotechnol.* **2005**, *66*, 486-496.

[133] Kishimoto, M.;. Okakura, T; Nagashima, H.; Minowa, T.; Yokoyama, S. Y.; Yamaberi, K. CO_2 Fixation and Oil Production Using Micro-Algae," *J. Ferment. Bioeng.* **1994**, *78*, 479-482.

[134] Tsukahara K., Sawayama, S. Liquid Fuel Production Using Microalgae. *J. Jap. Pet. Inst.* **2005**, *48*, 251-259.

[135] Valenzuela-Espinozaa, E.; Millan-Nunez, R.; Filiberto, N. Protein, Carbohydrate, Lipid and Chlorophyllacontent Inisochrysis Aff. Galbana (Clone T-Iso) Cultured with a Low Cost Alternative to the F/2 Medium. *Aquacul. Eng.* **2002**, *25*, 207-216.

[136] Hu, Q.; Sommerfeld, M.; Jarvis, E.; Ghirardi, M.; Posewitz, M.; Seibert M. Microalgal Triacylglycerols as Feedstocks for Biofuel Production: Perspectives and Advances. *The Plant Journal.* **2008**, *54*, 621-639.

[137] Kyle, D. J.; Gladue, R. Eicosapentaenoic Acids and Methods for their Production. Editor: Google Patents, **1993**.

[138] Chini Zittelli, G.; Rodolfi, L.; Biondi, N.; Tredici, M. R. Productivity and Photosynthetic Efficiency of Outdoor Cultures of Tetraselmis Suecica in Annular Columns. *Aquaculture.* **2006**, *261*, 932-943.

[139] Brown, M. R.; Dunstan, G. A.; Norwood, S. J.; Miller, K. A. Effects of Harvest Stage and Light on the Biochemical Composition of the Diatom Thalassiosira Pseudonana1. *J. Phycol.* **1996**, *32*, 64-73.

[140] Setlik I, V. S.; Malek I. Dual Purpose Open Circulation Units for Large Scale Culture of Algae in Temperate Zones. I. Basic Design Considerations and Scheme of a Pilot Plant. *Algologie Studies (Trebon).* **1970**, *1*, 111-164.

[141] Doucha J.; Lívanský, K.; Productivity, CO_2/O_2 Exchange and Hydraulics in Outdoor Open High Density Microalgal (Chlorella Sp.) Photobioreactors Operated in a Middle and Southern European Climate. *J. Appl. Phycol.* **2006**, *18*, 811-826.

[142] Richmond, A.; Lichtenberg, E.; Stahl, B.; Vonshak, A. Quantitative Assessment of the Major Limitations on Productivity Ofspirulina Platensis in Open Raceways. *J. Appl. Phycol.* **1990**, *2*, 195-206.

[143] Jiménez, C.; CossíO, B. R.; Labella, D.; Xavier Niell, F. The Feasibility of Industrial Production of Spirulina (Arthrospira) in Southern Spain. *Aquaculture.* **2003**, *217*, 179-190.

[144] Eriksen, N. Production of Phycocyanin: A Pigment with Applications in Biology, Biotechnology, Foods and Medicine. *Appl. Microbiol. Biotechnol.* **2008**, *80*, 1-14.

[145] Huntley M.; Redalje, D. CO_2 Mitigation and Renewable Oil from Photosynthetic Microbes: A New Appraisal. *Mitigation and Adaptation Strategies for Global Change.* **2007**, *12*, 573-608.

[146] Weissman JC, T. D. Design and Operation of Outdoor Microalgae Test Facility. in: Brown LM, Sprague S, Editors. Aquatic Species Report; NREL/MP-232-4174. *National Renewable Energy Laboratory,* **1992**, 32-57.

[147] Pushparaj, B.; Pelosi, E.; Tredici, M.; Pinzani, E.; Materassi, R. As Integrated Culture System for Outdoor Production of Microalgae and Cyanobacteria. *J. Appl. Phycol.* **1997**, *9*, 113-119.

[148] Moreno, J.; Vargas, M. Á.; Guez, H. Outdoor Cultivation of a Nitrogen-Fixing Marine Cyanobacterium, Anabaena Sp. ATCC 33047. *Biomol. Eng.* **2003**, *20*, 191-197.

[149] Ugwu, C.; Ogbonna, J.; Tanaka, H. Improvement of Mass Transfer Characteristics and Productivities of Inclined Tubular Photobioreactors by Installation of Internal Static Mixers. *Appl. Microbiol. Biotechnol.* **2002**, *58*, 600-607.

[150] Carlozzi, P. Dilution of Solar Radiation Through "Culture" Lamination in Photobioreactor Rows Facing South–North: A Way to Improve the Efficiency of Light Utilization by Cyanobacteria (Arthrospira Platensis). *Biotechnol. Bioeng.* **2003**, *81*, 305-315.

[151] Hall, D. O.; Acién Fernández, F. G.; Guerrero, E. C.; Rao, K. K.; Grima, E. M. Outdoor Helical Tubular Photobioreactors for Microalgal Production: Modeling of Fluid-Dynamics and Mass Transfer and Assessment of Biomass Productivity. *Biotechnol. Bioeng.* **2003**, *82*, 62-73.

[152] Olaizola, M. Commercial Production of Astaxanthin from Haematococcus Pluvialis Using 25,000-Liter Outdoor Photobioreactors. *J. Appl. Phycol.* **2000**, *12*, 499-506.

[153] López, M. C. G.-M.; Sánchez, E. D. R.; López, J. L. C.; Fernández, F. G. A.; Sevilla, J. M. F.; Rivas, J. Comparative Analysis of the Outdoor Culture of Haematococcus Pluvialis in Tubular and Bubble Column Photobioreactors. *J. Biotechnol.* **2006**, *123*, 329-342.

[154] Cheng-Wu, Z.; Zmora, O.; Kopel, R.; Richmond, A. An Industrial-Size Flat Plate Glass Reactor for Mass Production of Nannochloropsis Sp. (Eustigmatophyceae). *Aquaculture.* **2001**, *195*, 35-49.

[155] Converti, A.; Lodi, A.; Del Borghi, A.; Solisio, C. Cultivation of Spirulina Platensis in a Combined Airlift-Tubular Reactor System. *Biochem. Eng. J.* **2006**, *32*, 13-18.

[156] Carlozzi, P. Hydrodynamic Aspects and Arthrospira Growth in Two Outdoor Tubular Undulating Row Photobioreactors. *Appl. Microbiol. Biotechnol.* **2000**, *54*, 14-22.

[157] Sato, T.; Usui, S.; Tsuchiya, Y.; Kondo, Y. Invention of Outdoor Closed Type Photobioreactor for Microalgae. *Energy Convers. Manage.* **2006**, *47*, 791-799.

[158] Chandrasekhar, S. *Hydrodynamic and Hydromagnetic Stability*: Courier Corporation, **2013**.

[159] Wu, N.; Pease, L. F.; Russel, W. B. Electric-Field-Induced Patterns in Thin Polymer Films: Weakly Nonlinear and Fully Nonlinear Evolution. *Langmuir,* **2005**, *21*, 12290-12302.

[160] Wu, N.; Pease, L. F.; Russel, W. B. Toward Large‐Scale Alignment of Electrohydrodynamic Patterning of Thin Polymer Films. *Adv. Funct. Mat.* **2006**, *16*, 1992-1999.

[161] Park, J. B. K.; Craggs, R. J.; Shilton, A. N. Wastewater Treatment High Rate Algal Ponds for Biofuel Production. *Bioresour. Technol.* **2011**, *102*, 35-42.

[162] Hase, R.; Oikawa, H.; Sasao, C.; Morita, M.; Watanabe, Y. Photosynthetic Production of Microalgal Biomass in a Raceway System Under Greenhouse Conditions in Sendai City. *J. Biosci. Bioeng.* **2000**, *89*, 157-163.

[163] Lin Q.; Lin, J. Effects of Nitrogen Source and Concentration on Biomass and Oil Production of a Scenedesmus Rubescens Like Microalga. *Bioresour. Technol.* **2011**, *102*, 1615-1621.

[164] Chinnasamy, S.; Bhatnagar, A.; Claxton, R.; Das, K. C. Biomass and Bioenergy Production Potential of Microalgae Consortium in Open and Closed Bioreactors Using Untreated Carpet Industry Effluent as Growth Medium. *Bioresour. Technol.* **2010**, *101*, 6751-6760.

[165] Hu, Q.; Westerhoff, P.; Vermaas, W.; Removal of Nitrate from Groundwater by Cyanobacteria: Quantitative Assessment of Factors Influencing Nitrate Uptake. *Appl. Environ. Microbiol.* **2000**, *66*, 133-139.

[166] Yang, J.; Rasa, E.; Tantayotai, P.; Scow, K. M.; Yuan, H.; Hristova, K. R. Mathematical Model of Chlorella Minutissima UTEX2341 Growth and Lipid Production Under Photoheterotrophic Fermentation Conditions. *Bioresour. Technol.* **2011**, *102*, 3077-3082.

[167] Stephenson, A. L.; Kazamia, E.; Dennis, J. S.; Howe, C. J.; Scott, S. A.; Smith, A. G. Life-Cycle Assessment of Potential Algal Biodiesel Production in the United Kingdom: A Comparison of Raceways and Air-Lift Tubular Bioreactors. *Energy Fuels,* **2010**, *24*, 4062-4077.

[168] Colebrook, C.; White, C. Experiments with Fluid Friction in Roughened Pipes. *Proceedings of the Royal Society of London. Series A, Mathematical and Physical Sciences,* **1937**, 367-381.

[169] Colebrook, C. F.; Blench, T.; Chatley, H.; Essex, E.; Finniecome, J.; Lacey, G. "Correspondence. Turbulent Flow in Pipes, with Particular Reference to the Transition Region Between the Smooth and Rough Pipe Laws.(Includes Plates). *J. Inst. Civil Eng.* **1939**, *12*, 393-422.

[170] Howell, T. A.; Barinas, F. A. Pressure Losses Across Trickle Irrigation Fittings and Emitters. *Transactions of the ASAE,* **1980**, *23*, 928-0933.

[171] Engineeringtoolbox.com Home Page. http://www.Engineeringtoolbox.Com/-Resistance-Equivalent-Length-D_192.html (Accessed Apr 13, 2016).

[172] Beltaos, S.; Rajaratnam, N. Impingement of Axisymmetric Developing Jets. *J. Hydr. Res.* **1977**, *15*, 311-326.

[173] Beltaos, S. Oblique Impingement of Circular Turbulent Jets. *J. Hydr. Res.* **1976**, *14*, 17-36.

[174] Dw, H. *Water Treatment Unit Processes, Physical and Chemical*: Crc Press, **2006**.

[175] H, R. *Elementary Mechanics of Fluids*. New York: John Willey and Sons, **1946**.

[176] Saltzman, B. Finite Amplitude Free Convection as an Initial Value Problem-I. *J. Atmos. Sci.* **1962**, *19*, 329-341.

[177] Manneville, P. Rayleigh-Bénard Convection: Thirty Years of Experimental, Theoretical, and Modeling Work. in *Dynamics of Spatio-Temporal Cellular Structures*. Springer, **2006**, *207*. 41-65.

[178] Deng, Y.; Wang, Q.; Yuan, Y.; Huang, J. Vividly Colorful Hybrid Perovskite Solar Cells by Doctor-Blade Coating with Perovskite Photonic Nanostructures. *Mater. Horiz.* **2015**, *2*, 578-583.

[179] Engineeringtoolbox Home Page. Http://Www.Engineeringtoolbox.Com/Surface-Roughness-Ventilation-Ducts-D_209.Html (Accessed Apr 13, 2016).

[180] Wiley, P. E. C.; Elliott, J.; Brandi, M. Production of Biodiesel and Biogas from Algae: A Review of Process Train Options. *Water Environ. Fed.* **2011**, *83*, 326-338.

[181] Johnson, B. K.; Prud'homme, R. K. Chemical Processing and Micromixing in Confined Impinging Jets. *AICHE J.* **2003**, *49*, 2264-2282.

[182] Sultan, M. A.; Krupa, K.; Fonte, C. P.; Nunes, M. I.; Dias, M. M.; Lopes, J. C. B. High-Throughput T-Jets Mixers: An Innovative Scale-Up Concept. *Chem. Eng. Technol.* **2013**, *36*, 323-331.

[183] Siddiqui, S. W.; Zhao, Y.; Kukukova, A.; Kresta, S. M. Characteristics of a Confined Impinging Jet Reactor: Energy Dissipation, Homogeneous and Heterogeneous Reaction Products, and Effect of Unequal Flow. *Ind. Eng. Chem. Res.* **2009**, *48*, 7945-7958.

[184] Baldyga, J.; Bourne, J. A Fluid Mechanical Approach to Turbulent Mixing and Chemical Reaction Part II Micromixing in the Light of Turbulence Theory. *Chem. Eng. Commun.* **1984**, *28*, 243-258.

[185] Liu, Y.; Fox, R. O. CFD Predictions for Chemical Processing in a Confined Impinging-Jets Reactor. *AICHE J.* **2006**, *52*, 731-744.

[186] Chiou, H.; Chan, H. K.; Heng, D.; Prud'homme, R. K.; Raper, J. A. A Novel Production Method for Inhalable Cyclosporine a Powders by Confined Liquid Impinging Jet Precipitation. *J. Aerosol Sci.* **2008**, *39*, 500-509.

[187] Valente, I.; Celasco, E.; Marchisio, D.; Barresi, A. Nanoprecipitation in Confined Impinging Jets Mixers: Production, Characterization and Scale-Up of Pegylated Nanospheres and Nanocapsules for Pharmaceutical Use. *Chem. Eng. Sci.* **2012**, *77*, 217-227.

[188] Prud' Homme, R. K. Personal Communication 2016.

[189] Willis, R. M.; Mccurdy, A. T.; Ogborn, M. K.; Wahlen, B. D.; Quinn, J. C.; Pease, L. F. Improving Energetics of Triacylglyceride Extraction from Wet Oleaginous Microbes. *Bioresour. Technol.* **2014**, *167*, 416-424.

[190] Zhu, M.; Zhou, P.; Yu, L. Extraction of Lipids from Mortierella Alpina and Enrichment of Arachidonic Acid from the Fungal Lipids. *Bioresour. Technol.* **2002**, *84*, 93-95.

[191] Lee, J. Y.; Yoo, C.; Jun, S. Y.; Ahn, C. Y.; Oh, H. M. Comparison of Several Methods for Effective Lipid Extraction from Microalgae. *Bioresour. Technol.* **2010**, *101*, 75-77.

[192] Karam, H.; Bellinger, J. Deformation and Breakup of Liquid Droplets in a Simple Shear Field. *Ind. Eng. Chem. Fundam.* **1968**, *7*, 576-581.

[193] Poon, W. C.; Andelman, D. *Soft Condensed Matter Physics in Molecular and Cell Biology*: CRC Press, 2006.

[194] Michels, M. H. A.; Van Der Goot, A. J.; Norsker, N. H.; Wijffels, R. H. Effects of Shear Stress on the Microalgae Chaetoceros Muelleri. *Bioprocess Biosystems Eng.* **2010**, *33*, 921-927.

[195] Cheng, Y.; Zhou, W.; Gao, C.; Lan, K.; Gao, Y.; Wu, Q. Biodiesel Production from Jerusalem Artichoke (Helianthus Tuberosus L.) Tuber by Heterotrophic Microalgae Chlorella Protothecoides. *J. Chem. Technol. Biotechnol.* **2009**, *84*, 777-781.

[196] Xiong, W.; Li, X.; Xiang, J.; Wu, Q. High-Density Fermentation of Microalga Chlorella Protothecoides in Bioreactor for Microbio-Diesel Production. *Appl. Microbiol. Biotechnol.* **2008**, *78*, 29-36.

[197] Chen, C. Y.; Yeh, K. L.; Aisyah, R.; Lee, D. J.; Chang, J. S. Cultivation, Photobioreactor Design and Harvesting of Microalgae for Biodiesel Production: a Critical Review. *Bioresour. Technol.* **2011**, *102*, 71-81.

[198] Hoekman, S. K.; Broch, A.; Robbins, C.; Ceniceros, E.; Natarajan, M. Review of Biodiesel Composition, Properties, and Specifications. *Renew. Sustain. Energy Rev.* **2012**, *16*, 143-169.

[199] Henley, E. J.; Seader, J. D.; Roper, D. K. *Separation Process Principles*: Wiley New York, 2011.

[200] Beal, C. M.; Hebner, R. E.; Webber, M. E.; Ruoff, R. S.; Seibert, A. F. The Energy Return on Investment for Algal Biocrude: Results for a Research Production Facility. *Bioenergy Res.* **2012**, *5*, 341-362.

[201] Beal, C. M.; Stillwell, A. S.; King, C. W.; Cohen, S. M.; Berberoglu, H.; Bhattarai, R. P. Energy Return on Investment for Algal Biofuel Production Coupled with Wastewater Treatment. *Water Environ. Res.* **2012**, *84*, 692-710.

[202] Mcmillan, J. R.; Watson, I. A.; Ali, M.; Jaafar, W. Evaluation and Comparison of Algal Cell Disruption Methods: Microwave, Waterbath, Blender, Ultrasonic and Laser Treatment. *Appl. Energy.* **2013**, *103*, 128-134.

[203] Adam, F.; Abert-Vian, M.; Peltier, G.; Chemat, F. Solvent-Free" Ultrasound-Assisted Extraction of Lipids from Fresh Microalgae Cells: A Green, Clean and Scalable Process. *Bioresour. Technol.* **2012**, *114*, 457-465.

[204] Keris-Sen, U. D.; Sen, U.; Soydemir, G.; Gurol, M. D. An Investigation of Ultrasound Effect on Microalgal Cell Integrity and Lipid Extraction Efficiency. *Bioresour. Technol.* **2014**, *152*, 407-413.

[205] Deen, W. M. *Analysis of Transport Phenomena (Topics In Chemical Engineering)* Oxford University Press, New York, **1998**, 3.

[206] Mashaghi, A.; Partovi-Azar, P.; Jadidi, T.; Nafari, N.; Maass, P.; Tabar, M. R. R. Hydration Strongly Affects the Molecular and Electronic Structure of Membrane Phospholipids. *J. Chem. Phys,* **2012**, *136*, 114-709.

[207] Fox, M. A.; Whitesell, J. K. *Organische Chemie: Grundlagen, Mechanismen, Bioorganische Anwendungen*: Spektrum Akad. Verlag, 1995.

[208] Roy, M. M.; Wang, W.; Bujold, J. Biodiesel Production and Comparison of Emissions of a DI Diesel Engine Fueled by Biodiesel–Diesel and Canola Oil–Diesel Blends at High Idling Operations. *Appl. Energy.* **2013**, *106*, 198-208.

[209] Davis, R.; Aden, A.; Pienkos, P. T. Techno-Economic Analysis of Autotrophic Microalgae for Fuel Production. *Appl. Energy,* **2011**, *88*, 3524-3531.

[210] Martin, G. J.; Energy Requirements for Wet Solvent Extraction of Lipids from Microalgal Biomass. *Bioresour. Technol.* **2016**, *205*, 40-47.

[211] Quinn J. C.; Davis, R. The Potentials and Challenges of Algae Based Biofuels: A Review of the Techno-Economic, Life Cycle, and Resource Assessment Modeling. *Bioresour. Technol.* **2015**, *184*, 444-452.

[212] Yap, B. H.; Dumsday, G. J.; Scales, P. J.; Martin, G. J. Energy Evaluation of Algal Cell Disruption by High Pressure Homogenisation. *Bioresour. Technol.* **2015**, *184*, 280-285.

[213] Brar, S. K.; Verma, M.; Tyagi, R. D.; Valéro, J. R.; Surampalli, R. Y. Efficient Centrifugal Recovery of Bacillus Thuringiensis Biopesticides from Fermented Wastewater and Wastewater Sludge. *Water Res.* **2006**, *40*, 1310-1320.

[214] Orfield, N. D.; Levine, R. B.; Keoleian, G. A.; Miller, S. A.; Savage, P. E. Growing Algae for Biodiesel on Direct Sunlight or Sugars: A Comparative Life Cycle Assessment. *Sustain. Chem. Eng.* 2015, *3*, 386-395.

[215] Utah Energy Research Triangle Project: *Characterization of Waxy Crude Deposition in Pipelines*; 2014-2015 Final Report; State of Utah, Office of Energy Development; March 2015.

[216] Roehner, R.; Hanson, F. Measurement of Wax Precipitation Temperature and Estimation of Weight Percent Precipitated Solid versus Temperature for Crude Oils Using FT-IR Spectroscopy. *Energy & Fuels,* **2001***, 15*, 756-763.

[217] Fangrui. M.; Milford, A.; Hanna. Biodiesel production: a review. *Bioresour. Technol*. **1999**, *70*, 1-15.

[218] Pedersen, K.; Christensen, P. Phase Behavior of Petroleum Reservoir Fluids. CRC Taylor & Francis Group. Chapter 11 Wax Formation. 2007.

[219] ASTM D7169-11, Standard Test Method for Boiling Point Distribution of Samples with Residues Such as Crude Oils and Atmospheric and Vacuum Residues by High Temperature Gas Chromatography.

[220] ASTM D5853-11, Standard Test for Pour Point of Crude Oils.